Science
AAAS

Supplementary Materials for

Global rise in forest fire emissions linked to climate change in the extratropics

Matthew W. Jones *et al*.

Corresponding author: Matthew W. Jones, matthew.w.jones@uea.ac.uk

Science **386**, eadl5889 (2024)
DOI: 10.1126/science.adl5889

The PDF file includes:

Materials and Methods

Forest Ecoregions

We defined forest ecoregions by filtering the Olson/WWF terrestrial ecoregions of the world *(57)* dataset for tropical, temperate and boreal forest biomes (including broadleaf, coniferous or mixed forest types) plus ecoregions within the Mediterranean forest, woodlands and scrub biome whose names featured the keywords "forest" or "woodland". We excluded ecoregions where the mean annual forest burned area (BA) fell below 0.01% of total forested area of the ecoregion based on MODIS BA data. 414 forest ecoregions were selected by these criteria. Abatzoglou et al. (ref. *(54)*) previously assessed the drivers of fire on an ecoregion level based on correlation analyses involving a subset of the variables used in our current study.

Burned Area and Fire Emissions

The burned area (BA) data used in the current study derive from the MODIS BA produced (MCD64A1 collection 6.1) at 500 m spatial resolution *(58)*. The fire C emissions data derive from the global dataset of 500 m estimates of fire C emissions from van Wees et al. (ref. *(59)*), updated with BA driving data *(58)* through the year 2022.. These emissions estimates are in line with the Global Fire Emissions Database version 4.1s (ref. *(134)*) but better calibrated and available at far higher resolution *(59)*, and also fully consistent with the BA dataset used in this work *(58)*.

Forest BA and forest fire C emissions were isolated from the total BA and total fire C emissions datasets using 250 m tree cover fractions from the MODIS vegetation continuous field product (MOD44B, collection 6.0) *(67, 135)*, aggregated by spatial averaging from its native 250 m resolution to 500m resolution. Forest cells were defined by a tree cover threshold of 30%, which includes woody savannahs, woodlands and forests in the University of Maryland scheme *(136)* and has been among the most widely-used thresholds in previous work *(95, 96, 137)*.

Various satellite sensors and definitions of forest have been used to monitor change in forest cover globally, resulting in notable disagreements in the direction or magnitude of forest cover change between forest cover products *(95–97)*. We note that the Global Forest Change product *(138)*, based on Landsat data at 30m resolution, shows a net decline in forest cover across much of the northern extratropics, in contrast to the increased forest cover in the MODIS MOD44B product for extratropical pyromes (**Table S1**; note that the tree cover threshold for forests is 30% in the Global Forest Change product, as in the current study). Discrepancies between MODIS- and Landsat- based trends in forest cover have been noted in prior research spanning tropical, temperate and high-latitude regions *(95–97)*. Hence, our study consistently uses MODIS observations for forest BA, forest C emissions, and forest burnable area as well as the trends in these variables. It will become possible to conduct similar work with a fully compatible suite of Landsat products once global Landsat-based fire products with global coverage reach maturity (*139*).

Values of ecoregion or pyrome-level annual BA (km^2 $year^{-1}$) or fire C emissions (kg C $year^{-1}$) were calculated by spatially and temporally aggregating across months and within each spatial domain. The BA data cover years 2001-2023, while the fire C emissions data cover years 2002-2022. We extrapolated the ecoregion- and pyrome- level fire C emissions data to years 2001 and 2023 by multiplying the annual BA (km^2 $year^{-1}$) in 2001 and 2023 with the trendline-tracking values of fire C combustion rate (g C km^{-2} burned) for those years.

Total burned area fraction (BAF) was calculated as the total BA divided by total burnable area, where burnable area excluded cells that are water bodies in the MODIS MCD64A1 product. Forest BAF was calculated as the forest BA divided by forest area (cells with >30% tree cover). Non-forest BAF was calculated as the non-forest BA divided by non-forest area (non-water cells with <30% tree cover).

Total fire C combustion rate (g C m^{-2} burned) was calculated as total fire C emissions divided by BA, and forest fire C combustion rate (g C m^{-2} burned) was calculated as forest fire C emissions divided by forest BA.

Trendlines were fitted to the time series of BA, BAF, fire C emissions, fire C combustion rate time series using Theil-Sen regression. Absolute changes during 2001-2023 were calculated by subtracting the trendline values in 2001 from trendline values in 2023. Relative changes were calculated conservatively as the absolute change divided by the period mean value, in line with prior work *(6, 15)*.

Fire Season and Growing Season Definitions

We defined the fire season months for each ecoregion in a manner that accounts for fire seasons spanning two calendar years, as is often the case in the southern extratropics. Fire season months were defined as the 5-month period centred around the climatological peak in BA during 2001-2023, but excluding any months with BA below 10% of the month with maximum BA in the climatology. Fire seasons that initiated in one year (e.g. November 2019) but extended into a second year (e.g. through March 2020) were associated with the primary year (2019 in the given example).

We similarly defined the growing season months for each ecoregion based on normalised difference vegetation index (NDVI) data from MODIS MOD13A3 *(65)*, collection 6.1. Growing season months were defined as the 5 months centred around the climatological peak in NDVI during 2000-2023. The growing season is not constrained to calendar years and so respects the seasonal cycle of vegetation growth even if seasons span two calendar years.

We matched fire seasons with prior growing seasons as follows. In cases where the climatological peak of BA occurs after or contemporaneously with the climatological peak of NDVI, we treat the growing season of the same year as the prior growing season. In cases where the climatological peak of BA precedes the climatological peak of NDVI, we treat the growing season of the year prior as the prior growing season (including NDVI data from the year 2000 for the growing season prior to 2001).

Correlations between Burned Area and the Predictors

Principles behind the Adopted Correlation Structures

Each variable addressed in the sections that follow is treated as a predictor of forest BA in each ecoregion. Its influence on forest BA in each ecoregion is measured by correlation analysis, though the correlations take a variety of structural forms depending on whether the predictor co-varies with forest BA across inter-annual fire seasons, across fire season months, or across space. The structure of each correlation analysis was chosen to capture the cause-and-effect relationship between the variables. We also operated within the limitations of the predictor datasets. For example, if the gridded data represented a single point in time then it was not possible to analyse a temporal correlation. The correlation structures applied to various groups of variables are detailed below.

- **Fire weather, atmospheric instability, and lightning activity:** correlations with forest BA relate to the co-variation across all fire season months during 2001-2021 at the ecoregion level (i.e. up to five data values per year). This formulation is appropriate because the listed meteorological factors have contemporaneous controls on the potential for fire ignition and spread. Our approach is akin to that of Jones et al. (ref. *(6)*), but restricted to fire season months.
- **Soil moisture:** correlations with forest BA relate to the inter-annual co-variation across fire seasons during 2001-2021 at the ecoregion level (i.e. one data value per year). This formulation

is chosen because soil moisture tracks seasonal water surpluses or deficit (drought), whose effects on landscape flammability are cumulative across the fire season. Our approach is akin to that of Abatzoglou et al. (ref. *(54)*).

- **Vegetation productivity (NDVI):** correlations with forest BA relate to the productivity during each prior growing season during 2001-2021 and the forest BA during the following fire season at the ecoregion level (i.e. one data value per year). Productivity is represented in our analysis by the mean NDVI value during the prior growing season. This formulation is chosen because the cumulative production of biomass, particularly herbaceous and soft plant tissues, during the growing season impacts the quantity of fuels available to burn during the following fire season. Our approach is akin to that of Abatzoglou et al. (ref. *(54)*), though we focus directly on a proxy for vegetation productivity (NDVI) rather than on precipitation in the growing season.
- **Human factors (population, cropland cover, pasture cover and road density):** correlations with forest BA relate to the mean annual value of forest BA for each 0.05° cell in each ecoregion, and values representing the density of the variable in each 0.05° cell. The formulation is chosen because fire ignition and suppression related to human activities can be expected to follow the densities of those activities. Our approach is akin to that of Andela et al. (ref. *(15)*), though we work at a higher spatial resolution.
- **Other landscape factors (potential fuel loads and terrain ruggedness):** correlations with forest BA relate to the mean annual value of forest BA for each 0.05° cell in each ecoregion, and values representing the potential fuel loads and terrain ruggedness in each 0.05° cell. The formulation is chosen because continuous time series of gridded values for these predictors were not available. Our spatial correlation approach is akin to that of Andela et al. (ref. *(15)*).

In all cases, Spearman's rank correlation coefficients are preferred to Pearson's correlation coefficients as these are less sensitive to nonlinearities such as exponential relationships between BA and a predictor.

We used BA as the target variable throughout our correlation analyses, and other observable fire properties were not considered. Previous research on classifying pyromes according to traits of the fire regime has included a wider collection of variables, such as fire counts from active fire products and mean fire sizes based on 'fire atlas' products (e.g. *(72–75)*). BA is among the most widely-studied aspects of fire regimes globally. As it is the product of fire counts and fire mean size, BA usefully integrates information from two of the other metrics that have been used most widely for delineating pyromes and we thus viewed BA as the first priority for the novel disaggregation of the pyromes by fire drivers presented here. A clustering analysis which includes observed relationships between fire predictors and individual fire characteristics would be a significant undertaking and may introduce challenges such as collinearity where fire counts (or other characteristics) correlate with burned area.

Fire Weather Index

The Canadian fire weather index (FWI) is one of several indices used internationally to rate overall fire danger *(4)*. Its value is affected by variability in surface-level meteorological conditions (temperature, humidity, wind speed and 24-hour precipitation) and its variability is designed to represent the changing potential for fire to ignite, spread and consume fuel if an ignition occurred. FWI decreases with fuel moisture levels and increases with dry fuel availability. Variability in FWI often correlates with burned area in forest ecoregions and hence the FWI has proven to be a useful tool in anticipating and responding to elevated wildfire potential *(6, 53)*. FWI has also been used as a metric of the potential for fires to spread upon ignition in various studies of climate change impacts on forest wildfire potential *(6, 31)*.

For each ecoregion, we calculated the correlation between the monthly mean values of FWI *(4, 31)* and monthly forest BA across all fire season months during 2001-2021. FWI data were collected from the ERA5 meteorological reanalysis FWI product at daily 0.25° spatial resolution *(61)*. The monthly mean FWI for each ecoregion was calculated by first averaging the daily FWI values of each cell, and second averaging across all cells in the ecoregion. Monthly forest BA for each ecoregion was calculated by summing across all cells within the ecoregion.

Atmospheric Instability (C-Haines Index)

While fire weather relates to the potential for fire spread amongst a fuelbed due to surface-level meteorology, atmospheric instability relates to the potential for erratic fire behaviour caused by deep and turbulent convection, which enhances fire spread, limits potential for suppression, and presents opportunities for neighbouring fire ignitions *(35, 140–142)*. The continuous Haines index (CHI) rates the potential for extreme fire behaviour by accounting for lower tropospheric instability and dryness *(35, 140–142)*. Higher values of the CHI indicate greater atmospheric instability and potential for vertical updrafts and extreme fire spread behaviour. Updrafts can also cause the uplift and redistribution of embers or firebrands with potential to ignite additional spotting fires. The most extreme manifestation of atmospheric instability is the formation of pyrocumulonimbus (PyroCb), which can generate dry lightning with potential to ignite additional fires.

For each ecoregion, we calculated correlations between the monthly mean values of CHI and monthly forest BA across all fire season months during 2001-2021. 3-hourly CHI values were calculated at 0.25° spatial resolution using the 3-hourly data for temperature and dewpoint temperature at the 700 and 850 hPa pressure levels from the ERA5 reanalysis *(143)*, and following the equations provided in refs. *(35, 140)*. The monthly mean CHI for each ecoregion was calculated by first averaging the 3-hourly CHI values of each cell, and second averaging across all cells in the ecoregion. Monthly burned area for each ecoregion was calculated by summing across all cells within the ecoregion.

Lightning Frequency

Although human activities are the dominant ignition source in most locations occupied by humans, lightning can be an important ignition source in lesser-occupied areas and the dominant ignition source in remote locations *(34, 44)*. Hence there is a clear connection between the prevalence of lightning and fire that is expected to strengthen with remoteness.

We analysed the seasonal correlation between lightning flash count and monthly forest BA data across all fire season months during 2010-2021. Lightning observations derive from the Worldwide Lightning Location Network (WWLLN) *(63)* and include cloud-to-ground and cloud-to-cloud lightning flashes. Cloud-to-ground lightning strikes are relevant for fire ignitions and have been found to scale with total lightning flashes in prior work *(144)*. Lightning flash data were collected in vector format with spatial accuracy of around 5 km and a temporal accuracy on the scale of microseconds *(63)*. Monthly lightning flash count was calculated by summing binning vector observations into cells within 0.25 degree cells. As the number of detectors in the WWLLN network has grown through time since 2010, the detection efficiency (DE) of lightning has increased and an increase in the number of lightning flashes has occurred *(63)*. The WWLLN provides gridded detection efficiencies as a unitless fraction of the probability of detection in the current network *(145)*. We corrected lightning flash counts using the average value of DE in that month.

Monthly lightning flash counts for each ecoregion were calculated by summing across all cells within the ecoregion. Monthly forest BA for each ecoregion was calculated by summing across all cells within the ecoregion.

Soil Moisture

Soil moisture responds to seasonal balance of precipitation and evapotranspiration, increasing during periods of surplus precipitation and decreasing during periods of water deficit. Droughts or unusually dry periods during the fire season can place vegetation under moisture stress and eventually inhibit the vascular functioning of plants. The senescence and mortality of plants under drought stress leads to soft plant tissues (standing or debris) that are not supplied with water by the vascular system. These components can become particularly dry and flammable, especially towards the end of the fire season. Low soil moisture is used here as a proxy for the impacts of variability in seasonal water deficit or drought on the susceptibility of landscapes to fire.

For each ecoregion, we calculated correlations between the mean soil moisture and burned area during the fire season. We collected monthly mean volumetric soil moisture content for the subsurface depth interval (7-28 cm) at 0.1° spatial resolution from the ERA5-Land dataset *(62)*. Annual mean soil moisture values for each ecoregion were calculated by first averaging the soil moisture across fire season months in each cell, and second averaging all cells in the ecoregion. Annual forest BA during the fire season was calculated for each ecoregion by summing forest BA values across months and cells within the ecoregion.

Vegetation Productivity

It is well established that vegetation productivity and the build-up of biomass during the growing season influences fuel availability during subsequent fire seasons. While the effect is particularly noted in savannah grasslands *(54, 146)*, variation in vegetation productivity has also been found to imprint on forest fire activity during subsequent fire seasons in some regions (*147*, *148*). Here, we used the normalised difference vegetation index (NDVI) to evaluate how vegetation vitality during the growing season influences fire in the following fire season. NDVI increases with leaf area and photosynthetic capacity and has been used widely as a proxy for vegetation greenness (*149*).

For each ecoregion, we calculated correlations between the annual mean NDVI during growing season months and annual total burned area during the following fire season months. We collected NDVI data from the MODIS MOD13A3 (*65*), collection 6.1, at 1 km resolution with a monthly timestep. We calculated the annual mean growing season NDVI for each ecoregion by first averaging the monthly NDVI values across growing season months in each forested cell, and second averaging across all forested cells in the ecoregion. Annual forest BA during the fire season was calculated for each ecoregion by summing forest BA values across months and cells within the ecoregion.

Potential Fuel Loads

While NDVI is useful for tracking variability in the productivity of vegetation, fuel loads are also subject to biogeographical component of variation in fuel availability given the types of vegetation that grow in different climates and environmental settings. Here, we use data representing the potential fuel loads in each fuelbed stratum from a global fuel dataset *(51)*. The Global Fuel Dataset is an extension of the US-based Fuel Characteristic Classification System (FCCS) *(150)* to include fuel loads for six fuelbed strata in each land cover category of each Olson biome. For natural land covers, potential fuel loads are the baseline quantities of fuel stored in various fuelbed strata in the climax community of any given land cover following all stages of vegetation succession. For croplands and managed grasslands, potential fuel loads are the baseline quantities of fuel stored at the typical point of burning. Spatial variability in fuel loads reflects the biogeographical component of variation in fuel availability in relation to land cover and biome. The data were constructed for use

in global fire emissions models and fire behaviour models, but they were used in previous work to establish the relationship between forest BA and fuel availability alongside metrics of temporal variability in vegetation productivity (such as NDVI) *(53)*.

For each ecoregion, we calculated the spatial correlation between potential fuel loads and mean annual forest BA during the fire season for three classes of fuel: surface fuels, shrub fuels, and ladder/canopy fuels. Potential fuel load data were collected in tabular format from the global fuel dataset *(52)*, spatially joined to ecoregion and land cover combinations, and gridded with spatial averaging to 0.05° cells (the resolution used in all spatial correlation analyses included in the current work). We considered surface fuel loads to be the sum of leaf litter, woody debris and herbaceous fuel classes of the global fuels dataset. Mean annual forest BA during the fire season was calculated by first summing forest BA within each 0.05° cell for each fire season, and second averaging across all fire seasons 2001-2021. The spatial correlations represent the co-variation of fuel load and forest BA across all 0.05° cells that occupy each ecoregion.

Cropland and Pasture Cover

Agricultural land use is known to have ranging impacts on fire prevalence in different parts of the world. In tropical forests, the incursion of agriculture tends to increase fire activity in otherwise inflammable landscapes by adding deforestation fires, pasture maintenance burns, crop residue burns, and escaped fires from unintentional or wanton ignitions *(151)*. Elsewhere, agricultural land use has been associated with reduced forest fire activity due to incentives or legal obligations to protect high-value farmland, involvement of landowners in forest fire avoidance and suppression *(152, 153)*. Here, we sought to capture spatial variability in the relationships between land use and fire using cropland and pasture data.

For each ecoregion, we calculated the spatial correlation between cropland cover fraction and mean annual fire season BA. Cropland and grassland cover fraction data were collected from the MODIS MCD12Q1 product *(67)*, collection 6.1, at 250m resolution with an annual time step. To convert grassland cover fraction to pasture cover fraction, we collected data from the Gridded Livestock of the World dataset *(154)*, version 3, and created a mask for areas with livestock density over 1 livestock unit per km^2. We followed guidelines from the Eurostat agency of the European Commission to standardise the stocking density of different livestock species *(155)*. Grasslands with more than 1 livestock unit per km^2 were treated as pastures. Mean annual cropland and pasture cover fractions were calculated by averaging the cover fractions of each 250m cell over the years 2001-2021. The cropland and pasture cover fraction data were then resampled to 0.05° to match all spatial correlation analyses included in this work. Mean annual forest BA during the fire season was calculated by first summing forest BA within each 0.05° cell for each fire season, and second averaging across all fire seasons 2001-2021. The spatial correlations represent the co-variation of each land cover and forest BA across all 0.05° cells that occupy each ecoregion.

Forest Continuity

We conceptually refer to forest continuity as the inverse of fragmentation in forests. In tropical forests, forest fragmentation has been shown to increase fire due to increased forest edge length, which can enhance ventilation and rates of fuel drying while also increasing exposure to potential ignition sources from neighbouring land covers such as agriculture *(48, 49)*. In dry or fire-tolerant forests, it is conceivable that fragmentation has the opposite effect on fire, as seen in savannahs where the discontinuity of naturally fire-prone vegetation fuels can leads to slower fire spread or early extinction such as annual BA reduces in more fragmented areas *(49)*.

The forest continuity metric used in this work is the Forest Area Index (FAD) *(156, 157)*, a landscape morphological index based on the proportion of forest pixels within a neighbourhood area.

This algorithm uses a moving window to classify each pixel (at their original spatial resolution) of forest between 0% and 100% according to their density in relation to the neighbourhood pixels (non-forest pixels). The index for continuity is inversely proportional to the landscape fragmentation. For example, forest pixels with >90% forest cover are highly continuous forests largely free of fragmentation (e.g., forests fully connected or core areas), and forest pixels assigned as <10% are highly fragmented forests in the highly fragmented landscape (e.g., forest fragments that are disconnected from other forest fragments). FAD has been used in recent work to assess the links between fragmentation and fire in the tropics *(49)*.

The forest mask used to run the FAD index in this study was based on the MOD44B (collection 6.0) product at 250m spatial resolution for the year 2010. Since the input image for the FAD index needs to be binary (forest foreground and fragmentation background) we used a threshold of 30% of forest cover from MOD44B to create a mask of forest and non-forest pixels. The FAD index was then applied to this mask with a moving window of 27 x 27 pixels of 250m using the GUIDOS Toolbox workbench module available at SEPAL (System for Earth Observation Data Access, Processing and Analysis for Land Monitoring) cloud-computing platform.

Population

People can either increase the number of unintentional or wanton fire ignitions on the landscape or reduce the extent of fires through ignition avoidance, modification of land cover, fuel management, and active firefighting. The balance of these effects varies according to societal and cultural relationships with fire, however in general fire prevalence increases with population at low population densities (in relatively undisturbed environments) and reduces with population at high populations densities (in heavily modified environments where there are efforts to protect homes, capital, and infrastructure) *(53, 158)*. Here, we sought to capture spatial differences in the relationships between people and fire using population density data.

For each ecoregion, we calculated the spatial correlation between population density and mean annual fire season BA. Population data for years 2005, 2010, 2015 and 2020 were collected from the Gridded Population of the World (GPW) dataset *(159)*, version 4, at 1 km resolution. The population data were then resampled to 0.05° to match all spatial correlation analyses included in this work. Mean population density was calculated by averaging the population density of each 0.05° cell across the available years, matching the resolution of all spatial correlation analyses included in this work. Mean annual forest BA during the fire season was calculated by first summing forest BA within each 0.05° cell for each fire season, and second averaging across all fire seasons 2001-2021. The spatial correlations represent the co-variation of population density and forest BA across all 0.05° cells that occupy each ecoregion.

Road Density

Roads offer important access points to vegetated landscapes and so it is common for fire ignition locations to cluster along roads *(160, 161)*. Ignitions related to the improper disposal of cigarette butts, contact with hot vehicle components or flammable substances, and deforestation or arson are generally concentrated along transport routes. On the other hand, roads can inhibit the spread of fires by forming a barrier in the landscape and disrupting fuel continuity *(162)*. Here, we sought to capture spatial differences in the relationships between landscape accessibility and fire using road density data.

For each ecoregion, we calculated the spatial correlation between road density and mean annual fire season BA. Road location data were collected from the Global Roads Inventory Project dataset *(69)*, version 4 (GRIP4). The GRIP4 database includes mapped roads from various state, open source, and commercial products up to the year 2018. The vector data from GRIP4 was used to

calculate road density (km of road per km^2 of grid cell area) on a grid with a spatial resolution of 0.05°, to match all spatial correlation analyses included in this work. Mean annual forest BA during the fire season was calculated by first summing forest BA within each 0.05° cell for each fire season, and second averaging across all fire seasons 2001-2021. The spatial correlations represent the co-variation of road density and forest BA across all 0.05° cells that occupy each ecoregion.

Terrain Ruggedness

Field observations and models of fluid dynamics show that fires spread upslope more rapidly and intensely than on flat or downslope segments *(163, 164)*. In addition, channelling of wind along terrain corridors can fan the flames and enhance the intensity and spread of fires *(165)*. Here, we use terrain ruggedness index (TRI) data from the Geomorpho90m dataset *(70)* to study the impact of terrain on fire. TRI is calculated as the sum of the absolute differences in elevation between a focal cell and each of its eight neighbours and replicated over a moving window of 3x3 cells. Values can range from zero on flat land to over 500 m in mountainous areas.

For each ecoregion, we calculated the spatial correlation between the TRI and mean annual fire season BA. TRI values were collected from the Geomorpho90m dataset *(70)* at 90 m resolution. Geomorpho90m uses observations from the Monitoring of Earth Rotation and Intercomparison of the Techniques (MERIT) digital elevation model (DEM). The TRI data were resampled to 0.05° to match all spatial correlation analyses included in this work. Mean annual forest BA during the fire season was calculated by first summing forest BA within each 0.05° cell for each fire season, and second averaging across all fire seasons 2001-2021. The spatial correlations represent the co-variation of population and forest BA across all 0.05° cells that occupy each ecoregion.

Delineating the Global Pyromes

We used k-means clustering to group the forest ecoregions that share a similar set of correlations with the variables discussed above. The input data to the k-means algorithm were the correlation values between forest BA and each variable for each of the 414 forest ecoregions. K-means clustering is an unsupervised machine learning algorithm that iteratively partitions a dataset of cases into k clusters. Across iterations, each observation tends towards a nearest centroid in hyperdimensional space. The algorithm operates by minimising the distances between case values and cluster centroid values across all predictors variables. In this study, the clusters derived from k-means clustering are termed pyromes, and the cases are ecoregions. All analyses were performed in *R Statistics* and relied principally on the packages *NbClust*, *caret* and *cluster* (available from the Comprehensive R Archive Network, CRAN, https://cran.r-project.org/).

Preparation Steps

Prior to performing the k-means clustering, we verified that excessive multicollinearity was not present amongst the input variables to ensure that the impact of certain variable sets on clustering outcomes was not inflated **(Fig. S18)**.

We used the *caret* package to transform the input correlations for each variable to a scale range of 0 to 1 using equation (1).

$$(1)\ x' = \frac{xx}{x\,x}$$

The transformation ensures that distances between cases are similar in all input variables and thus gives all variables a similar potential to influence the distance measures that are used by the clustering algorithm to calculate distance between cases to cluster centroids. This step was practical

in our study because correlations between forest BA and meteorological variables tended to occupy a wider range of values than the various spatial correlations; without scaling, meteorological variables would have greater influence on the clustering outcomes than others, and a portion of the uneven influence could relate to differences in correlation structure.

Clustering Analysis for Pyrome Delineation

Although k-means clustering is an unsupervised approach, the number of clusters (k) must be user-defined. Numerous quantitative ratings and heuristic tests have been devised to aid in the selection of the optimal value of k, though none is considered a gold standard. We tested 27 common methods for identifying the optimal k using the NbClust package, which returns an optimal k for each method. We used majority rule across the 27 methods as the basis for selecting k=12. The clustering procedure itself was performed using the *cluster* package, which underpins the pyromes map shown in **Fig. 1**.

Significant Differences in Fire Controls Across Pyromes

After distinguishing the pyromes using k-means clustering, we conducted a statistical evaluation of the differences in the set of correlations exhibited by different pyromes. We plotted the distribution of correlations between forest BA and each predictor for each pyrome (**Fig. 2**). We also conducted analysis of variance (ANOVA) tests for significant differences in the correlation between forest BA and each fire driver across the pyromes. We observed significant differences across pyromes in the correlation between forest BA and all predictors variables.

ANOVA tests were supplemented with Tukey Honest Significant Difference (Tukey HSD) post hoc tests for significant difference in the correlation between forest BA and each fire driver between all possible pairs of pyromes. A 95% confidence level was adopted in all tests. Significant differences in correlation were observed in 58% of pairwise comparisons, where each pairwise comparison is a comparison of the correlations between forest BA and a variable across two pyromes (Fig. S19).

We also visualised differences between the components in a reduced number of dimensions using principal component analysis. Fig. S20 shows the separation of the pyromes along three principal components that explained the majority of the hyperdimensional variance of the dataset used in the k-means clustering analysis. Generally speaking, the pyromes show minimal overlap along at least one axis of the principal components.

Propagation of Uncertainties through the Clustering Analysis

Correlations between the predictors and BA underpin our derivation of the clusters. We note that uncertainties in the predictors and BA do not propagate formally through our correlation analyses to the fitting of pyromes using k-means clustering because uncertainties are incompletely characterised in most input datasets or uncertainty metrics are incompatible and cannot be combined. The key implication is that the set of correlation values observed across the 414 forest ecoregions contain random error stemming from uncertainties in both the predictor variables and BA and may vary spatially, with potential to spuriously influence some of the cluster assignments without formal uncertainty quantification. Below, we summarise the sources and magnitude of uncertainties for predictor variables especially where they may vary spatially, providing key uncertainty metrics wherever possible and otherwise qualitatively summarise the key sources of uncertainties. Uncertainties in BA are also discussed in following sections (see “Uncertainties in Burned Area and Carbon Emissions”) so as to provide a characterisation of all uncertainties that might influence our correlation analyses and therefore contribute to artefacts in the assignment of ecoregions to clusters.

In spite of the uncertainties identified below, we note that these datasets have been routinely used in empirical and machine learning studies that focus on the prediction of BA and identified as effective predictors of fire on regional to global scales.

- Fire Weather Index: Uncertainties in the ERA reanalysis process are only partially quantified. No formal quantification of FWI uncertainties was presented for the global product by Vitolo et al. *(61)*. A multi-member ensemble is available for uncertainty analysis via the Copernicus data store, but those have only been used to assess uncertainty in FWI values for select regions *(166)*.
- Vegetation Productivity (NDVI): Uncertainties in NDVI are only partially characterised *(64, 167)*. Reflectance calibration uncertainty is estimated at ±0.01 VI units for NDVI under normal atmospheric conditions (visibility ≥ 20 km) with a 2% reflectance calibration uncertainty. To achieve desired VI accuracy levels, required calibration uncertainties are 1.9% for NDVI for ±0.01 VI units, and 3.8% for ±0.02 VI units. Additionally, a 2 nm center wavelength shift results in an error of ±0.01 VI units for NDVI. For band-to-band coregistration error, a 20% error results in uncertainties of ±0.01 VI units for NDVI. No specific variation in these uncertainties across forest environments is highlighted in the Algorithm Theoretical Basis Document (ATBD) *(167)*.
- Atmospheric Instability (C-Haines Index): We calculated C-Haines Index values based on the ERA5 reanalysis data. No formal quantification of FWI uncertainties was presented for the global product by Vitolo et al. *(61)*. In this work, we did not calculate the C-Haines Index for all members of the ERA5 ensemble and so uncertainty across the ensemble is not quantified.
- Lightning Frequency: Lightning detection efficiency in the WWLLN depends on the detection of very low frequency waves by ground stations. Detection is affected by assumptions in calibrating attenuation rates and modelling ionospheric rebound *(168)*. Detection efficiency varies globally, being lower in regions such as Africa where ground stations are sparse and higher VLF signal attenuates, resulting in fewer detected low-powered strokes. Spatial accuracy of the network varies from approximately 5-10 km, affecting the gridding of flashes at 0.25 degree resolution (see ref. *(169)*). Additionally, cloud-to-cloud and cloud-to-ground strokes are not disaggregated by the WWLLN and so our analysis does not specifically consider the ground-striking lightning relevant for fire ignitions nor spatial variation in the cloud-to-ground fraction.
- Soil Moisture: Uncertainties in the ERA-Land reanalysis process are only partially quantified. As in ERA5, characterisation of uncertainties in ERA5-Land is possible via outputs from a multi-member ensemble, however the ensemble has not been used to quantify uncertainties in global-scale applications. ERA5-Land has shown high skill relative to other reanlysis products in representing field data from international soil moisture network mostly containing data from the northern mid-latitudes *(170)*. In the case of ERA5-Land, uncertainties in the land surface model are not yet included in the multi-member ensemble (only the uncertainties in atmospheric parameters are represented) *(62)*.
- Cropland and Pasture Cover: Uncertainty in the MODIS Land Cover products (including MCD12Q1) arises from a range of preprocessing errors, persistent cloud cover, geolocation inaccuracies, topographic data errors, and algorithmic misclassifications *(171)*. Persistent cloud cover can lead to data gaps, particularly over tropical forests, generating regional variation in uncertainty. Algorithmic misclassifications cause errors of omission and commission, varying by region, with challenges in heterogeneous landscapes. Validation accuracy typically reaches around 0.97 but varies regionally, with dense reference data like North America and Europe leading to higher performance than in other world regions.
- Forest Continuity: Uncertainties in FAD, a proxy for forest continuity, are not formally quantified by the algorithm of ref. *(156)* and were not quantified by Rosan et al. *(49)*. A key

methodological choice is the selection of the number of pixels in the neighbourhood used to evaluate the density of forest cells at each cell location *(49)*. Our choice of a 27 x 27 neighbourhood follows previous work *(49)* and means that forest cover within ~6.25 km of a cell influences that cell's FAD value; this was the option most consistent with the sub-grid spatial resolution of 0.05° adopted across all of our spatial correlation analyses. Other choices of neighbourhood size would influence FAD values and introduce uncertainty. An additional source of uncertainty in FAD is the forest cover layer used as input, which is based on MODIS land cover products (see discussion of uncertainties in the MODIS land cover products above).

- Potential Fuel Loads: Uncertainties in fuel load could not be formally quantified by ref. *(52)* due to poor reference data, however key sources were discussed. The uncertainties in underlying datasets for generating fuelbeds and creating a global fuel map stem from multiple sources. These include using GlobCover and other land cover products with varying resolutions and accuracies. GlobCover in particular does not distinguish between certain forest types, necessitating additional regional sources that may be inconsistent with GlobCover. The application of FCCS typology to global settings adds uncertainty due to challenges in assigning an existing FCCS fuelbed to ecosystems beyond North America *(150)*.
- Population: Uncertainties in the GPW dataset were not formally quantified by ref. *(159)*. National-level census data are not collected via a standardised protocol, challenging the process of integrating census data across jurisdictions. Therefore, GPW version 4 population grids are limited by the availability and quality of census data. The disaggregation of census jurisdictional units (e.g. counties) to grid cells is another potential source of uncertainty in GPW version 4. The disaggregation method adopted by the dataset, aerial-weighting, follows the assumption that the population of a grid cell is a function of the urban area within that cell *(159)*.
- Road Density: Road lengths vary across geospatial datasets of road locations such as GRIP (21.6 million km globally) and national statistical databases (e.g. the World Road Statistics database has a total road length of 32 million km) *(69)*. This indicates that the coverage of GRIP could be improved, especially focusing on the better representation of local, unplanned, and unofficial roads *(69)*. GRIP has good coverage in developed regions but underestimates road length and density in developing regions *(69)*.
- Terrain Ruggedness: Uncertainties in Geomorpho90m were not quantified by ref. *(70)*, but they rely on three aspects: (i) computing the geomorphometric variables under distinct projections - WGS84 datum underestimates slope in the subarctic zone; (ii) the divergence among the most common geomorphometric layers obtained from Digital Elevation Models (MERIT-DEM and 3DEP-1) - differences are largest close to peak areas and smallest close to valley areas; and (iii) bias associated with the removal of tree height to calculate the Digital Terrain Model – the denser the vegetation, the higher the bias *(70)*.

Overall, the datasets used in our study and across many fields of climate and environmental sciences contain uncertainties that are rarely quantified. An attempt at full quantification of errors across all input datasets and propagation of those errors through our analysis is out of the scope of this study. We highlight that improved quantification of errors across these datasets would enable downpipe studies such as ours to better characterise their uncertainties, especially if uncertainties were expressed in a spatially-explicit manner.

Uncertainties in Burned Area and Carbon Emissions

Uncertainty in the C6 MCD64A1 product stems from regional differences in environmental conditions, the distribution and quality of reference data, the ability of the algorithm to apply to diverse landscapes, and specific challenges such as cloud cover, vegetation density, and mixed land cover types *(58, 172)*. The primary measures of uncertainty magnitude are summarised through several metrics derived from confusion matrices, including overall accuracy (OA), omission error ratio (OE), and commission error ratio (CE). The sixth collection of MCD64A1 product shows an OA of 0.97, OE of 0.37, CE of 0.40 globally, improving on earlier collections *(58)*. Regions with dense vegetation cover or persistent cloud cover experience higher omission errors due to challenges in detecting smaller or less intense fires (for example, low-intensity surface fires in forests). CE is generally greater in regions in which similar spectral characteristics are shared between burned and unburned areas, such as in the case of peatlands where dark surfaces and charred surfaces appear similar. The MCD64A1 BA product shows higher OA and lower OE in boreal forests, where burned areas are detectable for extended periods, than in tropical forest regions where high canopy cover often intersects with high cloud cover.

Uncertainties in GFED 500 m *(173)* emissions estimates are a function of uncertainties in the satellite detection of fires and estimates of carbon consumed per unit area, both of which are resolution-dependent *(134, 173, 174)*. Monte Carlo simulations revealed uncertainties of ±20–25% at 1 standard deviation at global, annual carbon emissions in an earlier version of GFED (GFED3) *(174)*. Uncertainty in a later versions of GFED (GFED4s) are considered to be on the same order as those of GFED3, with uncertainties in fuel consumption reduced by improved fuel consumption constraints from field data *(175)*, but new uncertainties introduced by the addition of small fire detections that are challenging to validate due to sparse field data *(174, 176)*. The GFED-500 m dataset further resolved key uncertainties in the GFED framework stemming from the spatial aggregation (to coarser resolution) of BA and other Earth Observations that drive GFED's fuel model, primarily by reducing mismatch between field measurements and modelled values *(177, 59)*. Various field studies of fire emissions have been used to validate the GFED modelling framework (e.g. *(178, 179)*).

Supplementary Text 1: Assessment of Confidence in Cluster Assignment

The case-level silhouette width statistic *(180)*, a unitless measure of the similarity of a case to the observations in its own cluster (pyrome) relative to the observations in other clusters (pyromes), was used to quantify the ambiguity of the pyrome assignment for each ecoregion. The higher the silhouette width, the lesser ambiguity in the attribution of an ecoregion to a pyrome. Fig. S21 shows maps of the ecoregions whose silhouette widths were in the bottom 20% of all ecoregions signifying that they were clustered least robustly and Fig. S22 shows a confusion matrix for the same ecoregions. The confusion matrix also helps to identify the pyromes that are most regularly confused with one another.

Forest ecoregions with the lowest silhouette widths are generally scattered across world regions. All continents feature ecoregions with ambiguous cluster assignment, and there is not a strong tendency for ambiguously-clustered regions to concentrate in particular world regions aside from their somewhat lower presence in Africa and Australia (Fig. S21). This suggests that the k-means clustering algorithm did not introduce severe regional bias in its cluster assignment, with broadly even levels of ambiguity in the clustering across continents.

One exception to the above is the Iberian peninsula, where low silhouette widths were consistently observed, suggesting that forest ecoregions in this region showed relatively low parity with other ecoregions of the world. The forest ecoregion spanning most of Spain (Iberian sclerophyllous and semi-deciduous forests) was assigned to pyrome ExTrop3, but the ambiguity in

cluster assignment suggests that pyrome ExTropF1 may also be an appropriate assignment. In northern Spain, an ecoregion assigned to ExTropF1 (Cantabrian mixed forests) might rather be assigned to SubTropF2. A forest ecoregion in Southern Portugal (Southwest Iberian Mediterranean sclerophyllous and mixed forests) was assigned to pyrome SupZoF2, but might rather be assigned to SubTropF3.

Amongst the pyromes, clustering ambiguity was greatest in pyromes SubTropF3, SupZoF1 and SupZoF2 (Fig. S22) and lowest in Pyromes ExTropF1 and TropF1. The ambiguously-clustered ecoregions in pyrome SupZoF2 would most often be alternatively assigned to pyrome ExTropF1 or SubTropF3, while ecoregions of ecoregion SupZoF1 would most often be alternatively assigned to pyromes ExTropF1, ExTropF2 or ExTropF4. These patterns indicate that the ambiguously-clustered ecoregions of suppression zones could otherwise be placed in extratropical forest pyromes or dry forest where BA is most sensitive to bioclimatic controls. The ambiguously-clustered ecoregions of Pyrome SubTropF3 could otherwise be assigned to clusters ExTropF1 or ExTrop3, suggesting a level of confusion between the most climate-sensitive subtropical pyrome and with extratropical forests where BA shows varying degrees of sensitivity to climatic factors.

Supplementary Text 2: Further Discussion of Pyrome Geography and Traits

Pyromes in Extratropical Forests

Pyromes ExTropF1 and ExTropF2 cover North American and Eurasian boreal forests, as well as some temperate forests and high-altitude parts of the tropics (Fig. 1). Forest BA correlates positively with fire weather and atmospheric instability and negatively with seasonal soil moisture, whereas forest BA does not correlate with population density, agricultural land cover, and road density (Fig. 2, Fig. S1). Hence, climatic factors primarily govern forest fire extent in pyromes ExTropF1 and ExTropF2, with human activities having a relatively weak impact compared to other pyromes.

Pyrome ExTropF1 dominates in North American extratropics. A distinguishing trait of pyrome ExTropF1 is that forest BA positively correlates with lightning flash density (Fig. 2), indicating that lightning is an important ignition source in these areas *(33, 34, 40, 106)*. Pyrome ExTropF2 prevails in the Eurasian extratropics. BA correlates positively with NDVI from the prior growing season (Fig. 2), suggesting that climatic conditions that enhance vegetation growth during the prior growing season can later influence fire extent by providing additional fine fuels to burn *(76, 77)*.

Two other extratropical forest pyromes, ExTropF3 and ExTropF4, include boreal forests in Scandinavia and western Russia and temperate or subtropical forests in parts of North America, Europe, and China (Fig. 1). Forest BA correlates positively with fire weather in ExTropF3 and ExTropF4, although far less strongly than in pyrome ExTropF1 or ExTropF2 (especially in the case of ExTropF4; Fig. 2). In addition, no correlation is observed between forest BA and soil moisture in ExTropF4 (Fig. 2), indicating that fires are overall not sensitive to water deficits accumulated over the fire season and only weakly related to periods of fire weather. The general weakness of correlations between forest BA and the explanatory variables in pyromes ExTropF3 and ExTropF4 may relate to infrequent burning in these typically stable humid climates (Fig. S7, Table S1), which leads to low statistical power to detect relationships over a relatively short observational period of two decades.

Pyromes in Tropical Forests

Pyromes TropF1 and TropF2 are widespread in the tropical deforestation zones of Amazonia, the Congo, and equatorial islands of southeast Asia (Fig. 1). In both pyromes, forest BA is positively correlated with population density, road density, and the extent of agricultural land covers, while negatively correlated with forest continuity (Fig. 2). Forest BA also correlates positively with fire weather and negatively with soil moisture, highlighting the dependence of deforestation and

degradation fires on appropriate meteorological conditions *(78, 181)*. These relationships are consistent with a concentration of deforestation and degradation fires at forest edges near existing human land use, with peaks during drier parts of the fire season and during drought years *(48, 79)*.

Pyrome TropF1 is mainly found in Amazonia and the Congo (Fig. 1). It shows a particularly strong correlation between forest BA and pasture cover (Fig. 2), consistent with the pattern of forest loss in Amazonia whereby the expansion of cattle ranching typically drives initial forest clearing and cash crop agriculture later establishes on pasture land *(80, 81)*. Meanwhile, pyrome TropF2 prevails in Sumatra, Kalimantan, Borneo, and the Guianas. In pyrome TropF2, correlations between forest BA and soil moisture are notably stronger than in pyrome TropF1, whereas correlations with population, roads, and pasture cover are weaker (Fig. 2). These differences suggest a more constrained window for fire in TropF2, consistent with the role of drought conditions in enabling peak fire activity in the peat forests of southeast Asia *(79, 82)*. Outside of the tropics, pyrome TropF2 includes several forest ecoregions in southeast Russia (Fig. 1), a known global hotspot of extratropical forest fires linked to forestry operations *(83)*.

Pyrome TropF3 commonly maps to older deforestation frontiers in moist tropical forest ecoregions (Fig. 1), including in the Atlantic forests of Southeast Brazil, Veracruz forests of eastern Mexico, Guinean forests of West Africa, and the northern islands of southeast Asia (Fig. 1). Today, these forests are heavily fragmented, their human populations are high and agricultural land cover is extensive *(83–85, 182)*. Forest BA correlates positively with fire weather and negatively with soil moisture, similar to pyromes TropF1 and TropF2. Despite the density of human ignition sources in TropF3, forest BA does not show a strong correlation with the densities of population or agriculture (Fig. 2), possibly due to a saturation of ignition sources in the pyrome.

Pyromes in Subtropical Forests

Pyromes SubTropF1, SubTropF2 and SubTropF3 are commonly placed in subtropical or dry tropical forest ecoregions (Fig. 1), including in northern Colombia, western Madagascar, northeast India, parts of mainland southeast Asia, Sri Lanka, the East African coastal mosaic, and interior parts of the Brazilian Atlantic forests. Forest BA correlates with forest continuity and potential fuel stocks (Fig. 2), consistent with limitations to fire spread caused by fragmentation or discontinuity in fire-prone land covers such as savannahs and dry forests (*15, 49*).

In pyromes SubTropF1 and SubTropF2, negative correlations are observed between forest BA and population density, cropland cover, and road density. These correlations, which are particularly strong in pyrome SubTropF2, suggest that the presence of agriculture and infrastructure in fire-prone landscapes reduces fire activity in fragmented areas of SubTropF1. In contrast, forest BA does not correlate with human activities in pyrome SubTropF3, suggesting that natural landscape factors affecting forest continuity, such as hillslope position with respect to the water table, may play a more significant role in limiting fire spread (*15, 49*).

Pyromes SubTropF1, SubTropF2 and SubTropF3 exhibit positive correlations between forest BA and meteorological factors, indicating that fire is constrained to specific fire-prone weather conditions. However, the windows of opportunity differ between the two pyromes. In SubTropF1 and SubTropF2, forest BA correlates positively with fire weather and negatively with soil moisture, suggesting that fires are enabled by both seasonal-scale moisture deficits and shorter periods of elevated fire weather. On the other hand, forest BA in SubTropF3 correlates only with fire weather, indicating a sensitivity to fire-prone weather spells but not to seasonal-scale moisture deficits. Forest BA shows a positive correlation with lightning frequency in pyrome SubTropF2, suggesting that lightning is an important ignition source in this pyrome.

Pyromes in Zones of Fire Suppression

The final two pyromes, SupZoF1 and SupZoF2, are found in various forest ecoregions of the tropics, subtropics, and temperate climate zones (Fig. 1). Negative correlations are observed between

forest BA and population density, road density, and agriculture (Fig. 2), indicating that the presence of people and human activities dampens forest fire extent in these pyromes (*46, 86*). Land management practices influencing forest continuity and fire spread may also play a role, as indicated by positive correlations between forest BA and forest continuity and fire spread (Fig. 2). Moreover, positive correlations between forest BA and topographical complexity suggest that fires tend to occur in upland landscapes with fewer human activities, making them logistically challenging to suppress and of lower priority for suppression efforts (*46, 87*).

Pyromes SupZoF1 and SupZoF2 prevail in many parts of the world where there are substantial budgets for wildland fire management and efforts to suppress forest fires, including the southeast US (SupZoF1), western US (SupZoF2), southeast Australia (SupZoF1 and SupZoF2), western Australia (SupZoF1), and parts of Iberia (SupZoF2). A range of practices contribute to the reduction of forest fire extent in these regions, including the suppression of active fires, management of fuel loads, and community programs aimed at reducing accidental ignitions and arson (*46, 88*).

Correlations are observed between forest BA and both fire weather and seasonal soil moisture in pyromes SupZoF1 and SupZoF2, though these are notably stronger in pyrome SupZoF2 (Fig. 2). These correlations indicate that forest fires can emerge during periods of fire-prone weather, which can occur despite efforts to suppress fire (*37, 89*). In pyrome SupZoF1, forest BA shows a positive correlation with lightning frequency, highlighting the importance of natural ignitions as observed in some of its ecoregions, such as in southeast Australia (*91*). Also in pyrome SupZoF1, a distinctive correlation is observed between forest BA and vegetation productivity during the prior growing season, emphasizing the role of fuel production as a control on fire extent (*9, 42, 91*).

Supplementary Figures

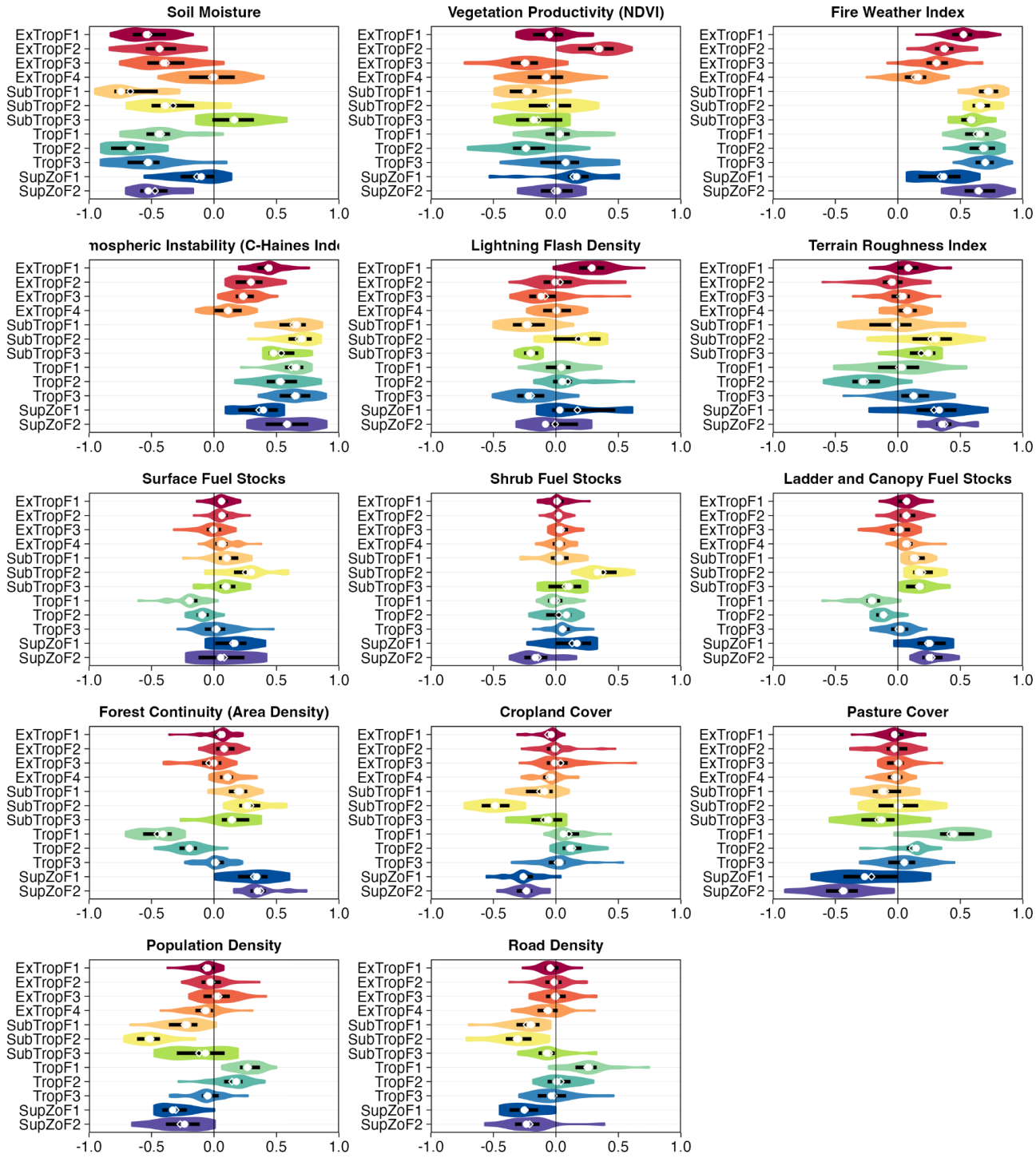

Figure S1: Variation in the relationship between forest burned area (BA) and all predictors across the global forest pyromes. The violins plot the kernel density distribution of correlations values (spearman's ρ) for each predictor amongst the constituent ecoregions of each pyrome. White dots mark the median correlation value for the ecoregions of a pyrome, black line ranges mark the interquartile range, and open diamonds mark the mean value. See Methods for a description of all correlation analyses and the motivation for including each predictor. Correlations are mapped for each forest ecoregion in Fig. S2.

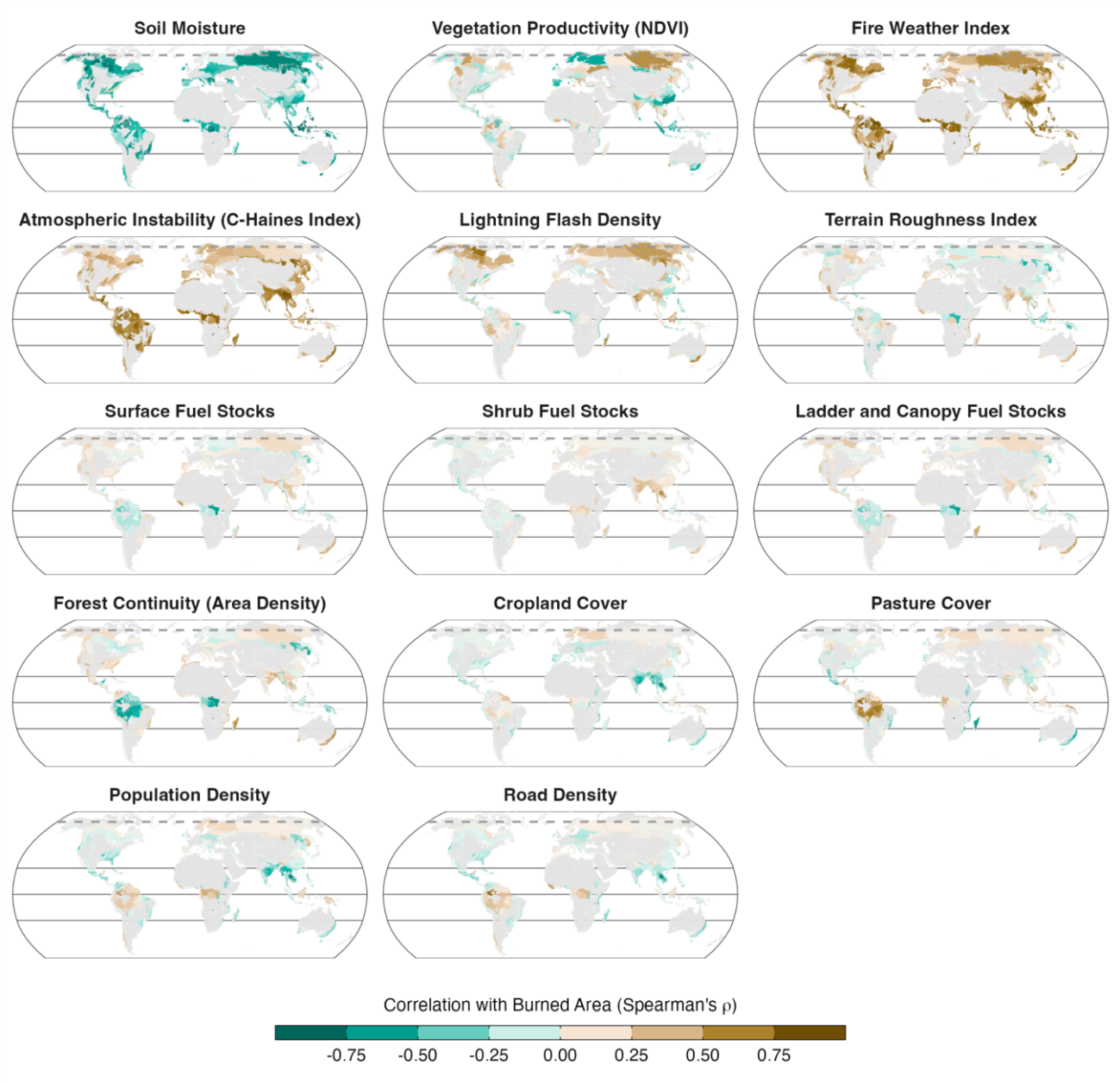

Figure S2: Spearman's correlation (ρ) values between forest burned area (BA) and 14 predictors contributing to variability in forest BA for all forest ecoregions of the world. The predictors are each included as indicators of the meteorological, human and bioclimatic controls on fire activity. See **Methods** for a description of all correlation analyses and the motivation for including each predictor. The distribution of correlations amongst the ecoregions of each pyrome are mapped in **Fig. 2**.

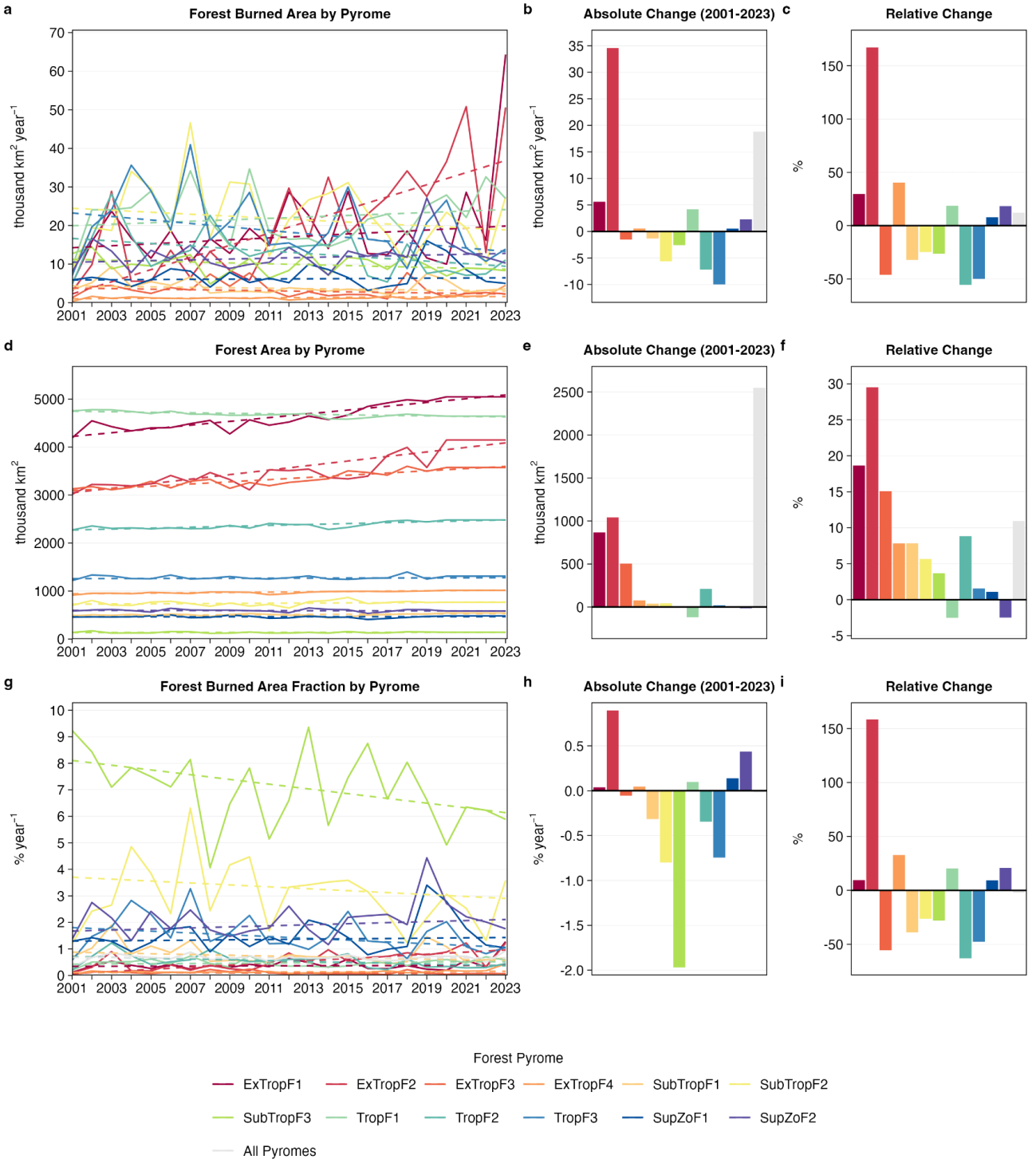

Figure S3: Changes in forest burned area (BA), forest area (spatial extent), and burned area fraction in forests for each pyrome during 2001-2023. Changes in forest area can partially contribute to increases in the forest BA via increased area available to burn. Increases in burned area fraction in forests indicate that increases in forest BA are proportionally larger than the increases in forest area. Forest BA corresponds to burned areas in cells where tree cover exceeds 30% at a spatial resolution of 500m (see **Methods**).

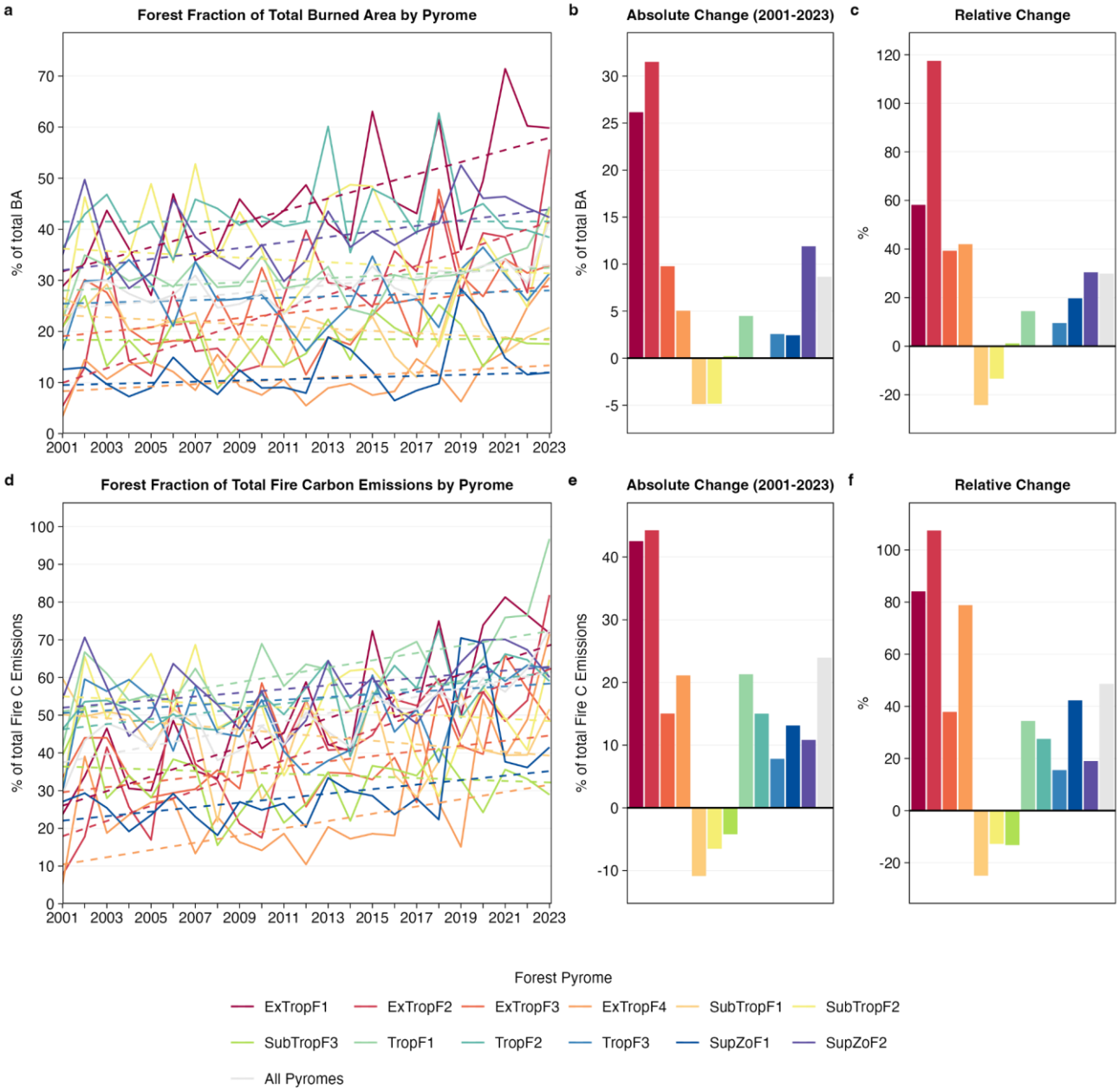

Figure S4: Changes to the forest fraction of total (forest + non-forest) burned area (BA) and the forest fraction of total fire carbon (C) emissions during 2001-2023.

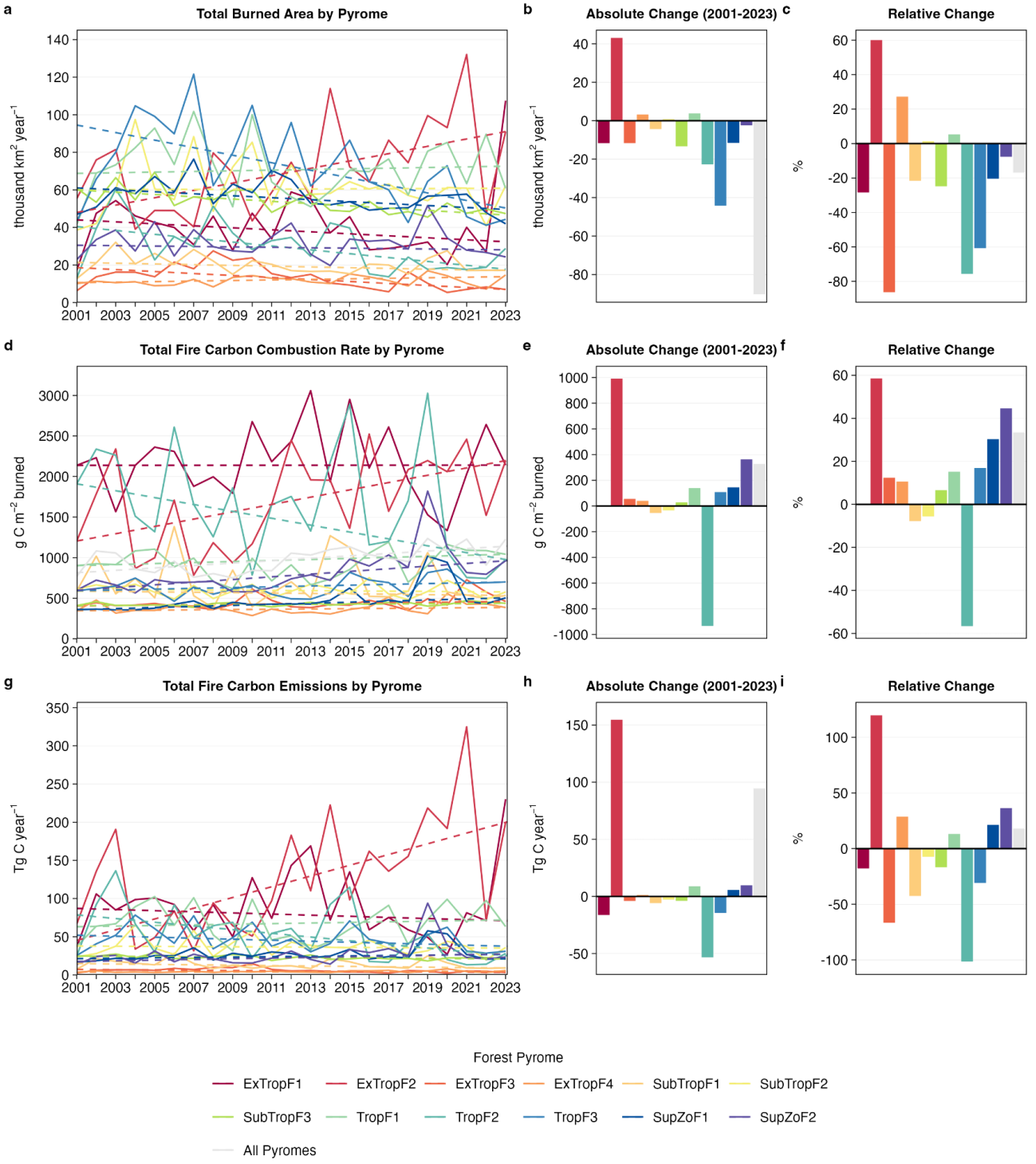

Figure S5: Changes in the total (forest + non-forest) burned area (BA) and associated fire carbon (C) emissions during 2001-2023. The figure replicates **Fig. 3**, but with data relating to total BA and C emissions. See caption of **Fig. 3** for panel-specific information.

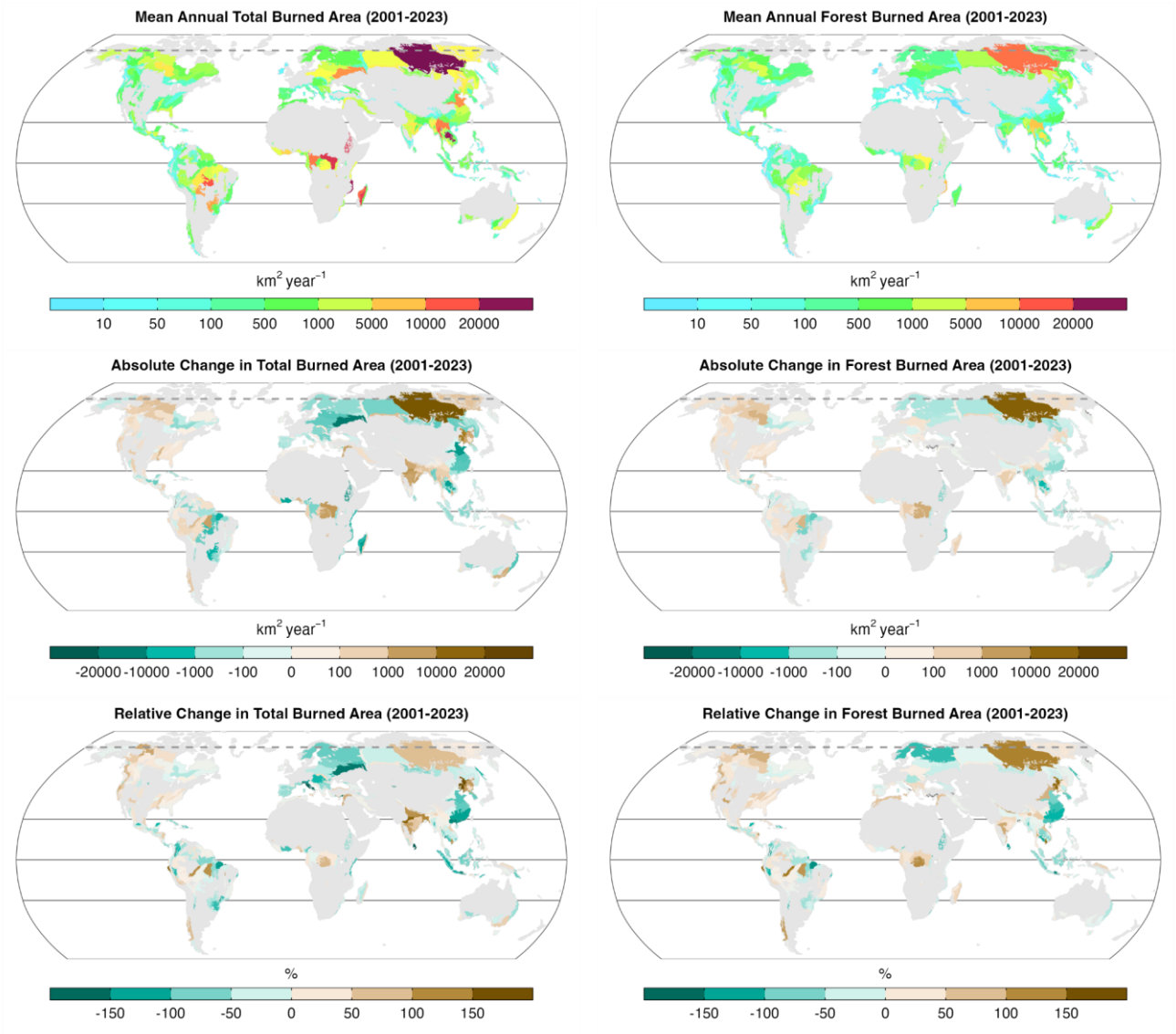

Figure S6: Average values of and changes in total (forest + non-forest) burned area and forest burned area for each ecoregion during the period 2001-2023.

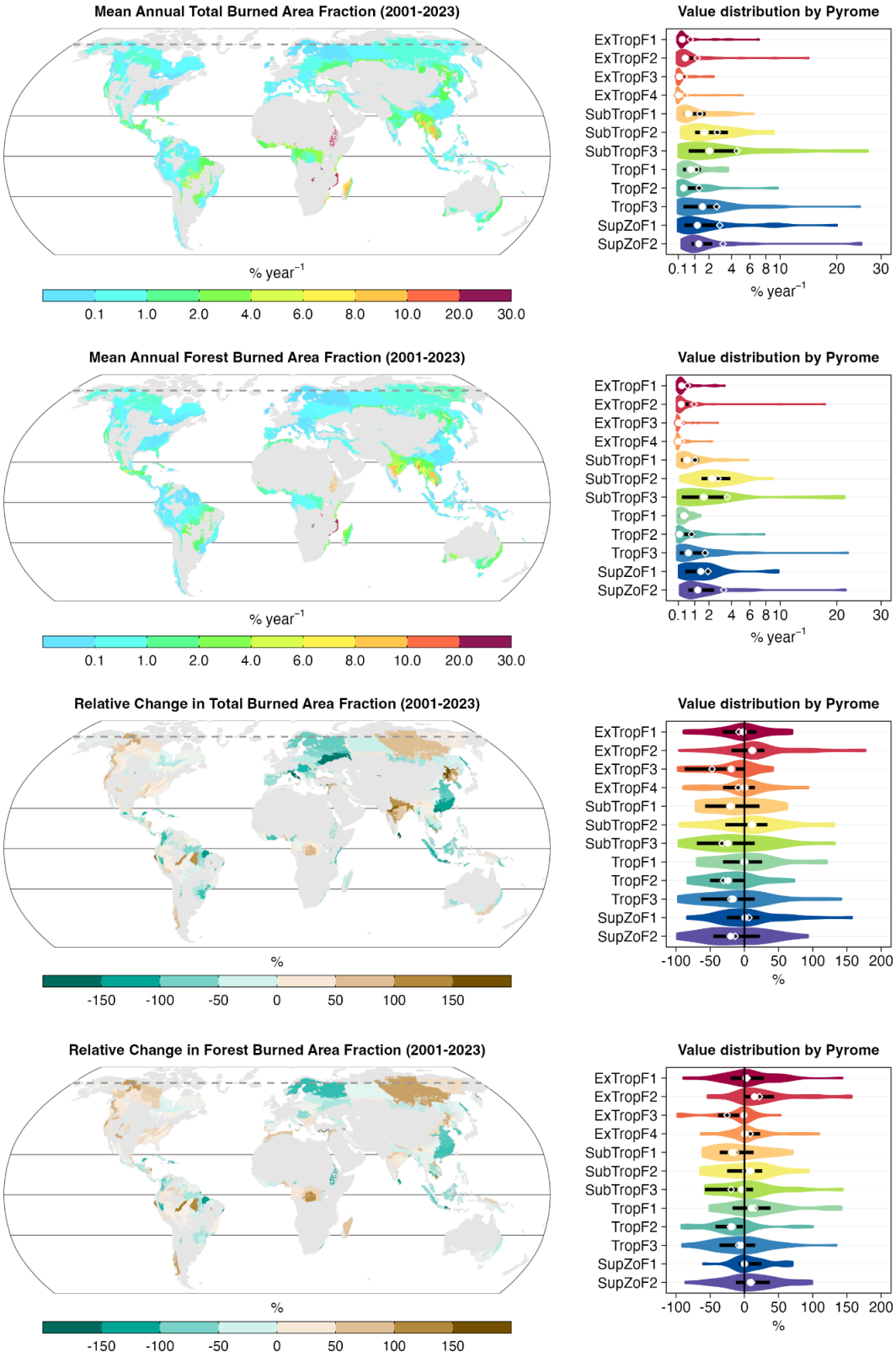

Figure S7: Average values of total (forest + non-forest) burned area fraction (BAF) and forest BAF for each ecoregion during the period 2001-2023, alongside a breakdown of values by pyrome. The violins represent the kernel density of the ecoregion count at each correlation value. White dots mark the median value for the ecoregions of a pyrome, while black line ranges mark the interquartile range and open diamonds mark the mean value.

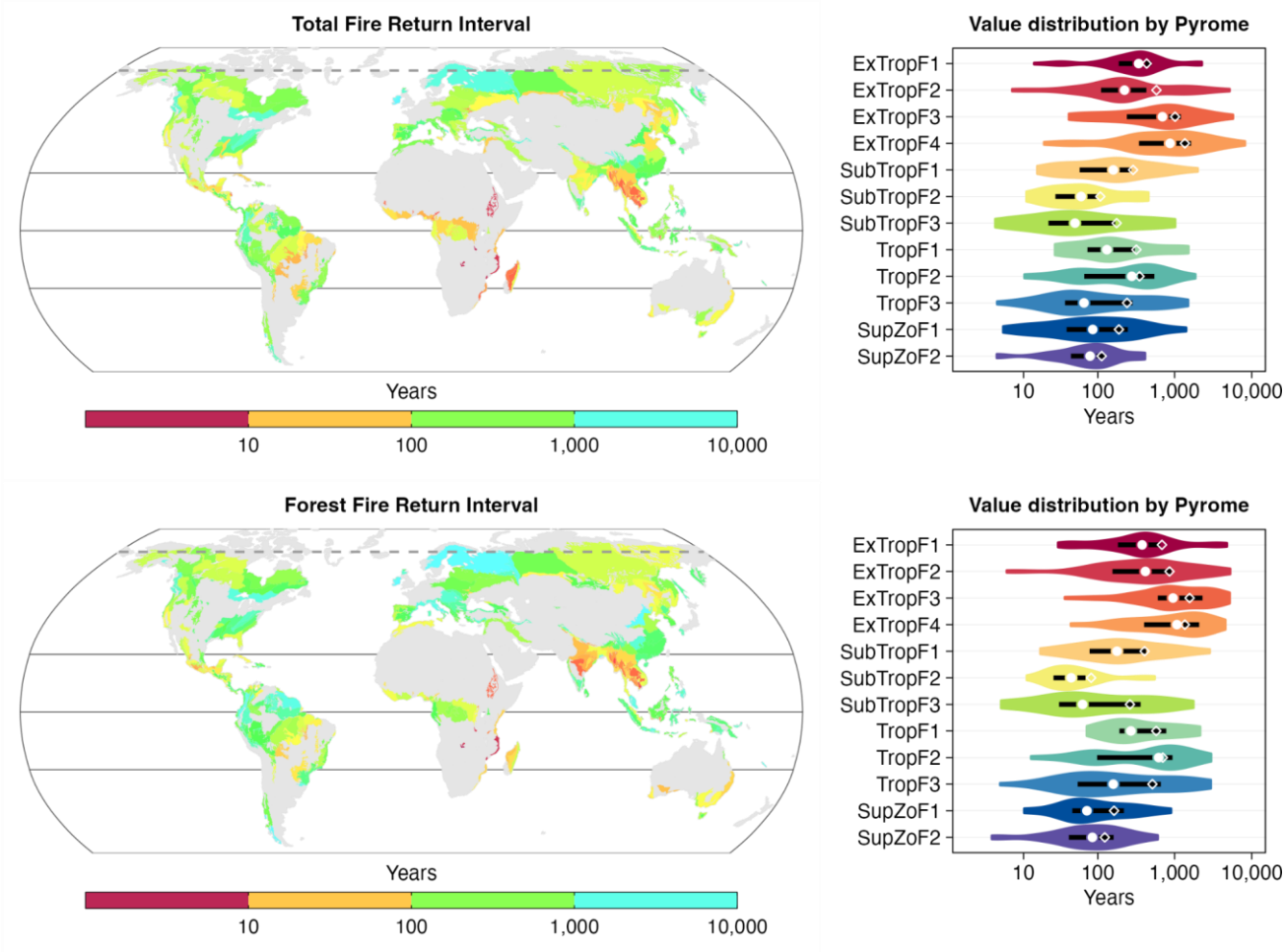

Figure S8: Average values of fire return interval (FRI) for total fires (forest + non-forest) and forest fires for each ecoregion during the period 2001-2023, alongside a breakdown of values by pyrome. Fire return interval is calculated as the inverse of burned area fraction (Fig. S7). The violins represent the kernel density of the ecoregion count at each correlation value. White dots mark the median value for the ecoregions of a pyrome, while black line ranges mark the interquartile range and open diamonds mark the mean value.

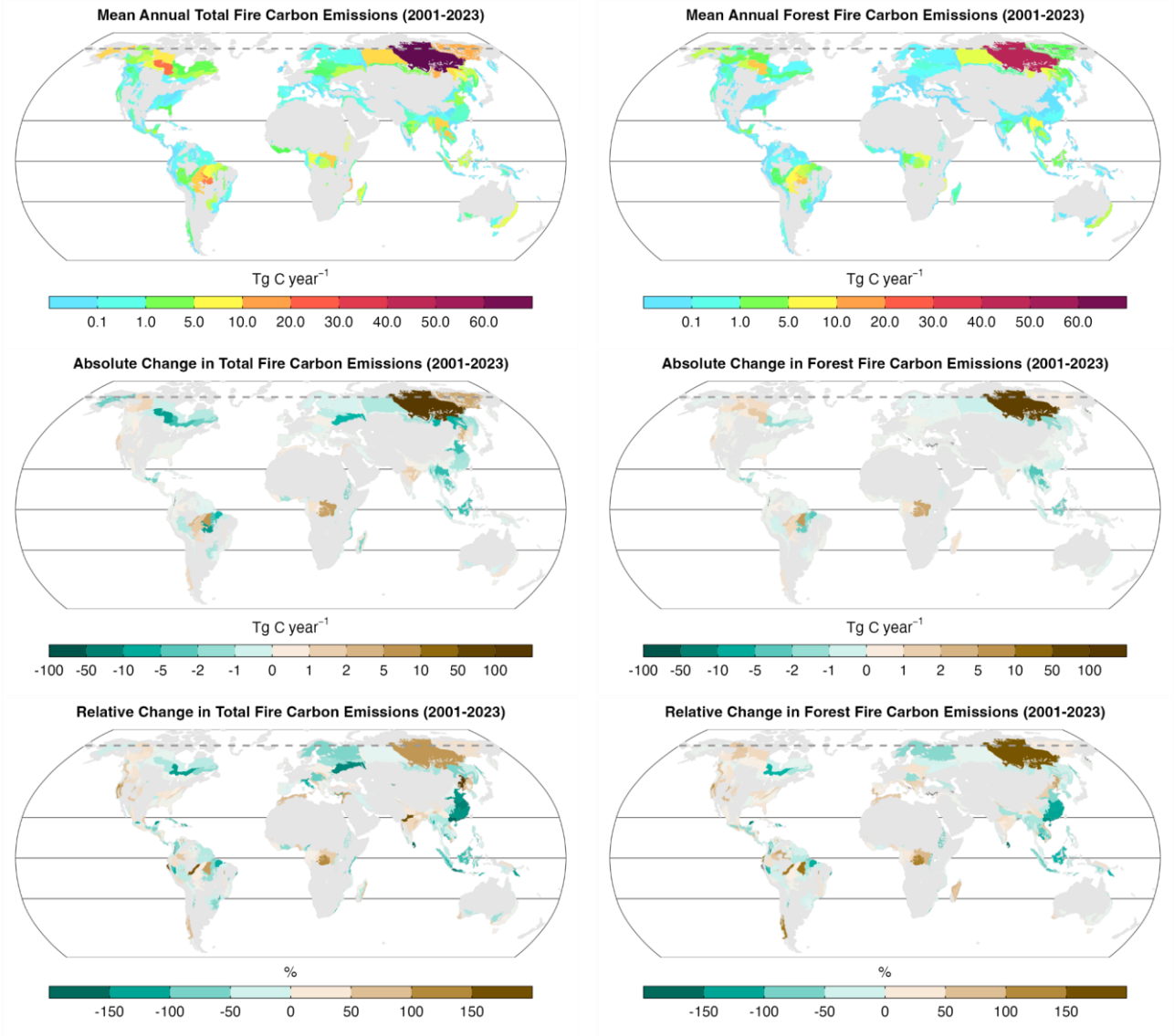

Figure S9: Average values of and changes in total (forest + non-forest) fire carbon (C) emissions and forest fire C emissions for each ecoregion during the period 2001-2023.

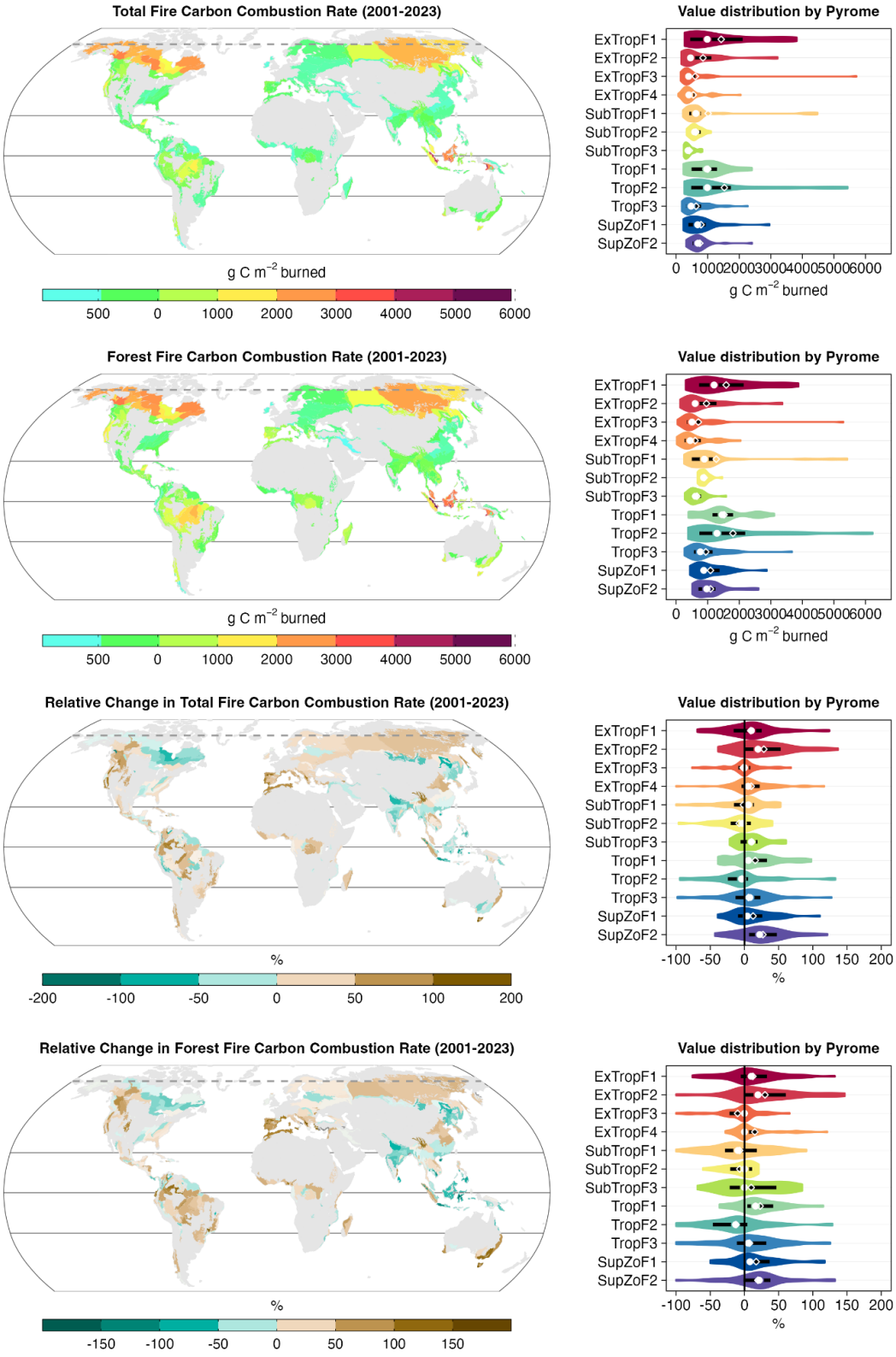

Figure S10: Average values and change in the total (forest + non-forest) fire carbon (C) emissions and forest fire C emissions per unit burned area for each ecoregion during the period 2001-2023, alongside a breakdown of values by pyrome. The violins represent the kernel density of the ecoregion count at each correlation value. White dots mark the median value for the ecoregions of a pyrome, while black line ranges mark the interquartile range and open diamonds mark the mean value.

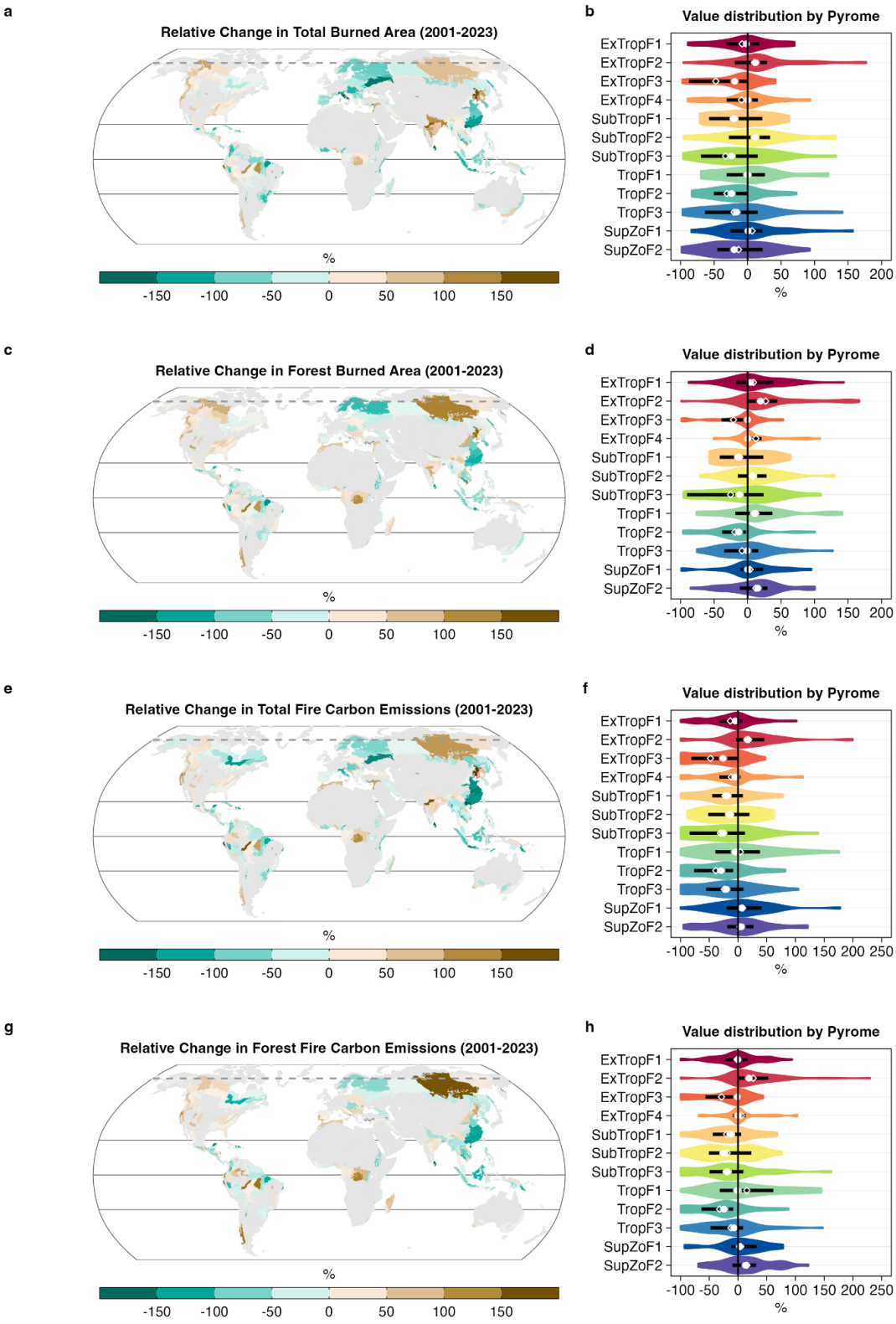

Figure S11: Relative changes in total (forest + non-forest) burned area (BA), forest BA, total fire carbon (C) emissions and forest fire C emissions during 2001-2023, alongside a breakdown of values by pyrome. The violins represent the kernel density of the ecoregion count at each correlation value. White dots mark the median value for the ecoregions of a pyrome, while black line ranges mark the interquartile range and open diamonds mark the mean value.

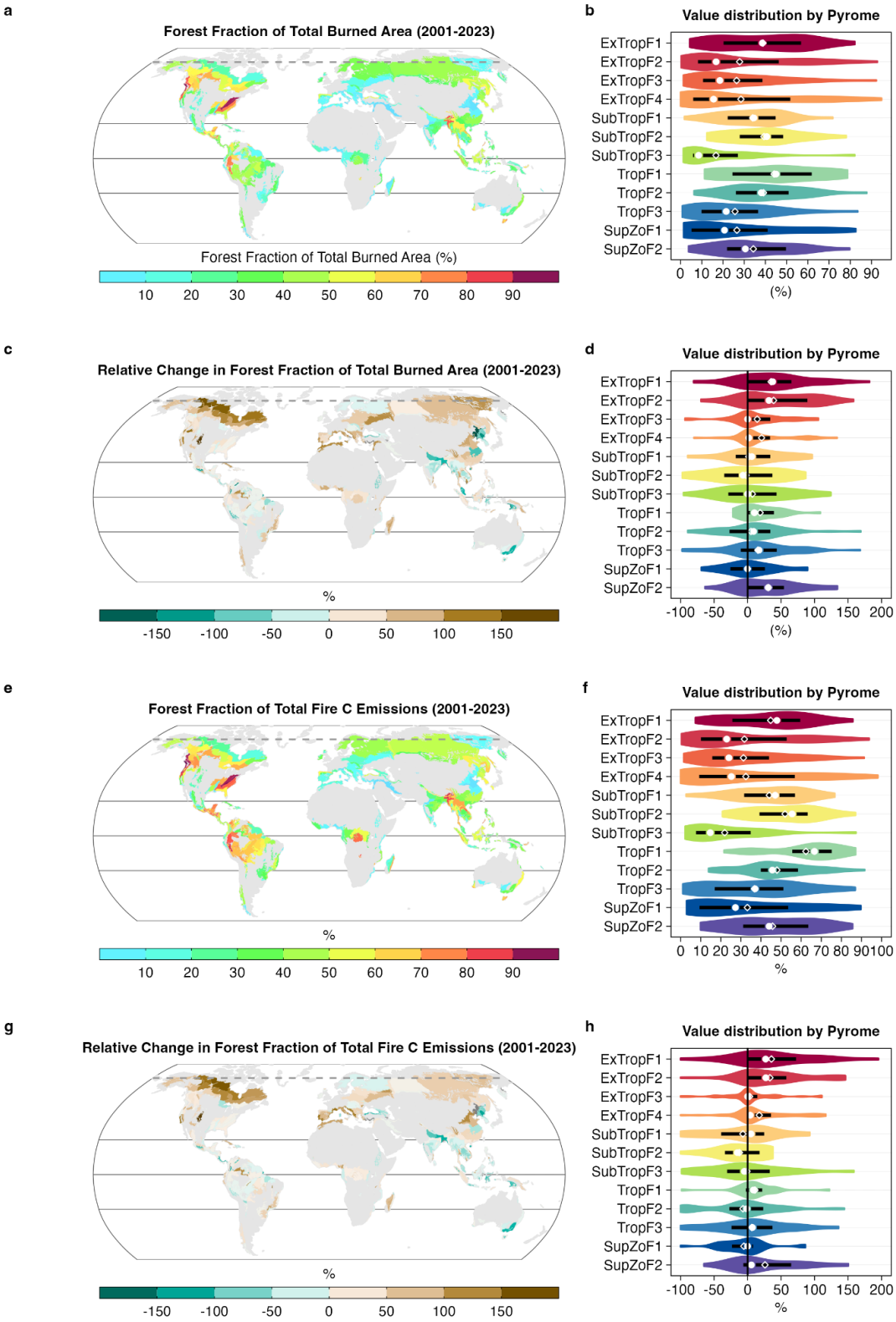

Figure S12: Average values and change in the forest fraction of total (forest + non-forest) burned area (BA) and total fire carbon (C) emissions for each ecoregion during the period 2001-2023, alongside a breakdown of values by pyrome. The violins represent the kernel density of the ecoregion count at each correlation value. White dots mark the median value for the ecoregions of a pyrome, while black line ranges mark the interquartile range and open diamonds mark the mean value.

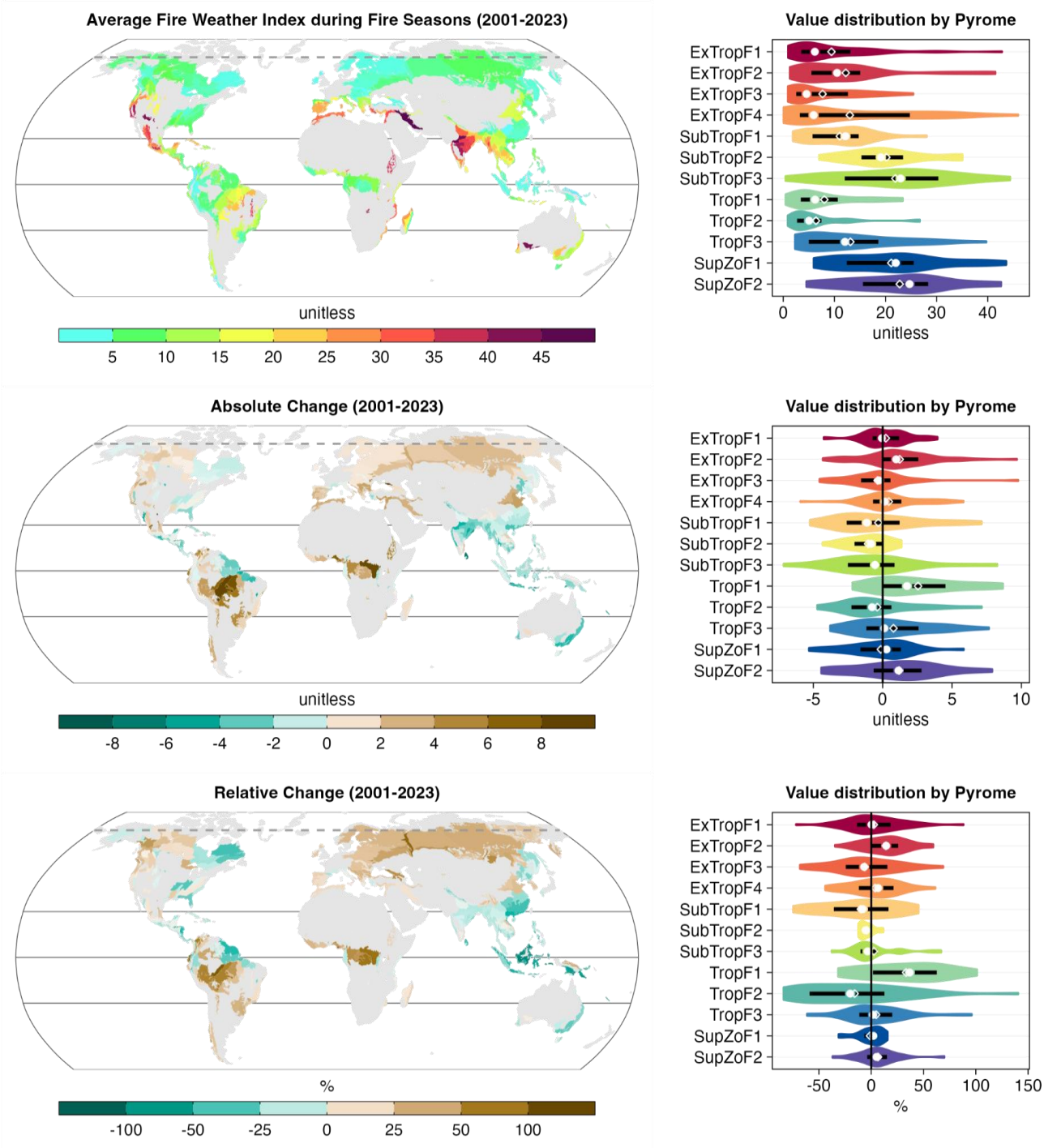

Figure S13: Average values and change in fire weather index (FWI) during fire seasons for each ecoregion during the period 2001-2023, alongside a breakdown of values by pyrome. The FWI value of individual fire seasons is calculated as the mean value during fire season months; the average values shown are the mean across multiple fire seasons. The violins represent the kernel density of the ecoregion count at each correlation value. White dots mark the median value for the ecoregions of a pyrome, while black line ranges mark the interquartile range and open diamonds mark the mean value.

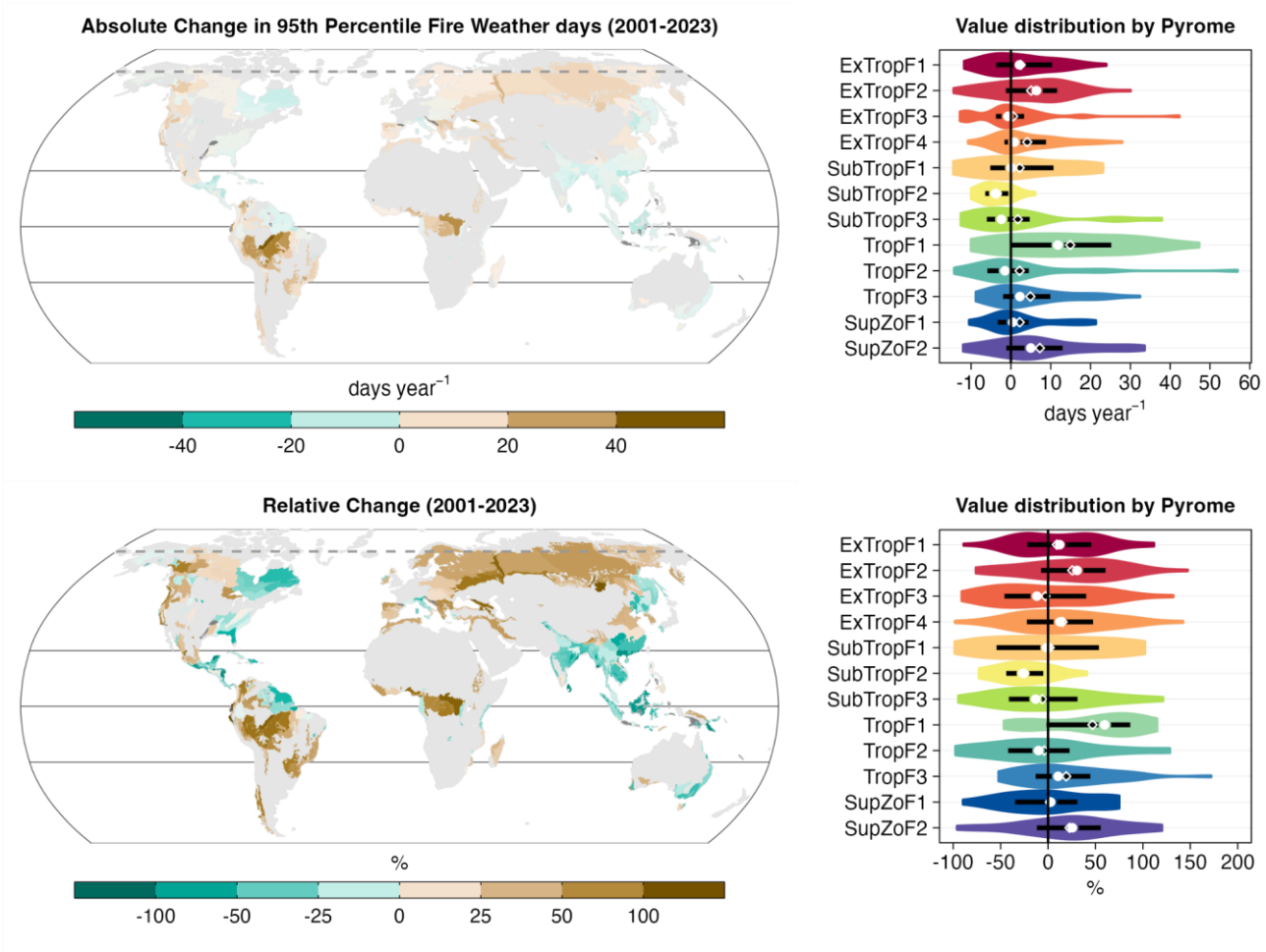

Figure S14: Average values and change in fire season days with 95th percentile fire weather for each ecoregion during the period 2001-2023, alongside a breakdown of values by pyrome. Fire season days with 95th percentile fire weather are those days exceeding the 95th percentile value of all days during 1980-2009. The violins represent the kernel density of the ecoregion count at each correlation value. White dots mark the median value for the ecoregions of a pyrome, while black line ranges mark the interquartile range and open diamonds mark the mean value.

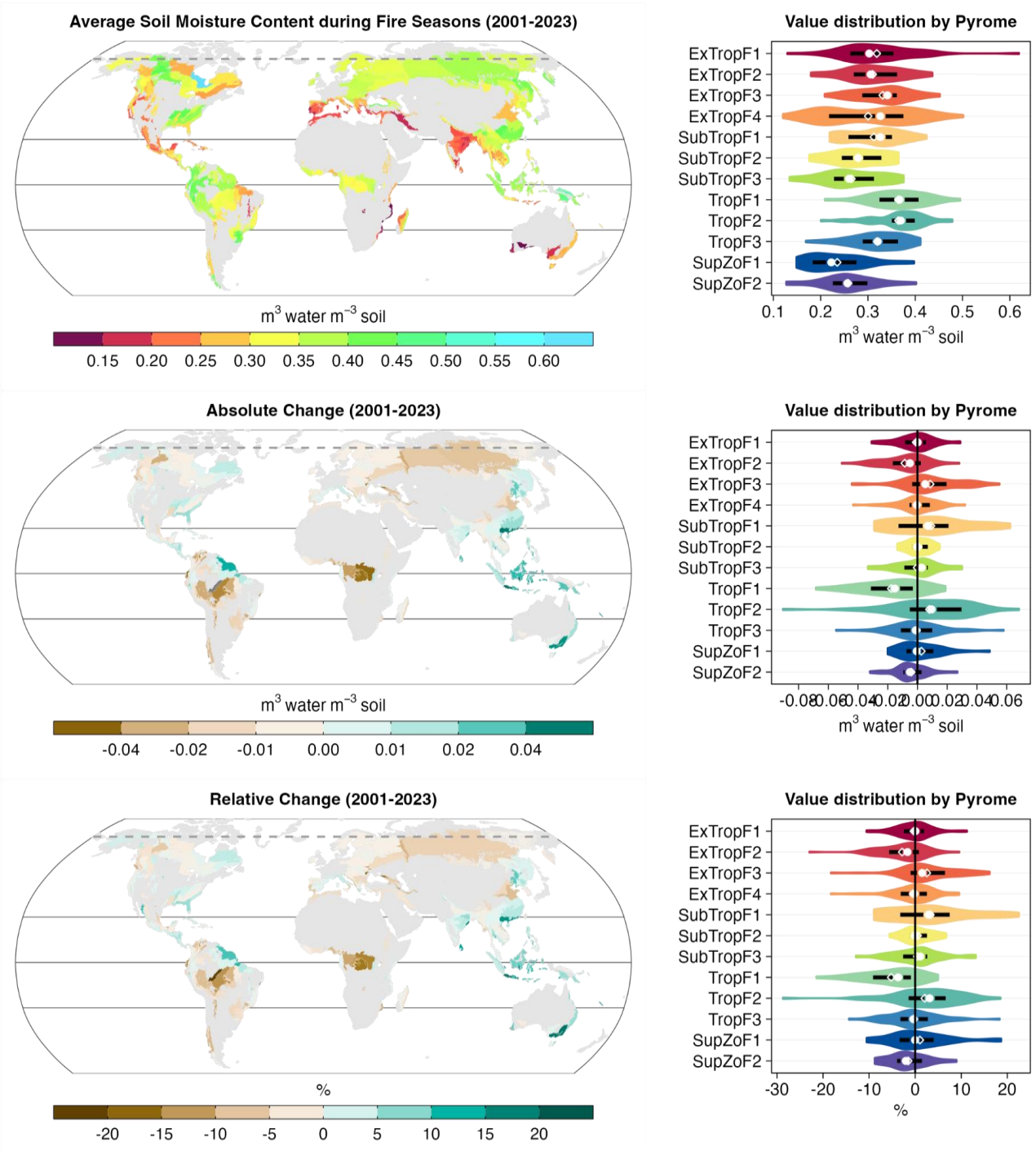

Figure S15: Average values and change in soil moisture content during fire seasons for each ecoregion during the period 2001-2023, alongside a breakdown of values by pyrome. The soil moisture value of individual fire seasons is calculated as the mean value during fire season months; the average values shown are the mean across multiple fire seasons. The violins represent the kernel density of the ecoregion count at each correlation value. White dots mark the median value for the ecoregions of a pyrome, while black line ranges mark the interquartile range and open diamonds mark the mean value.

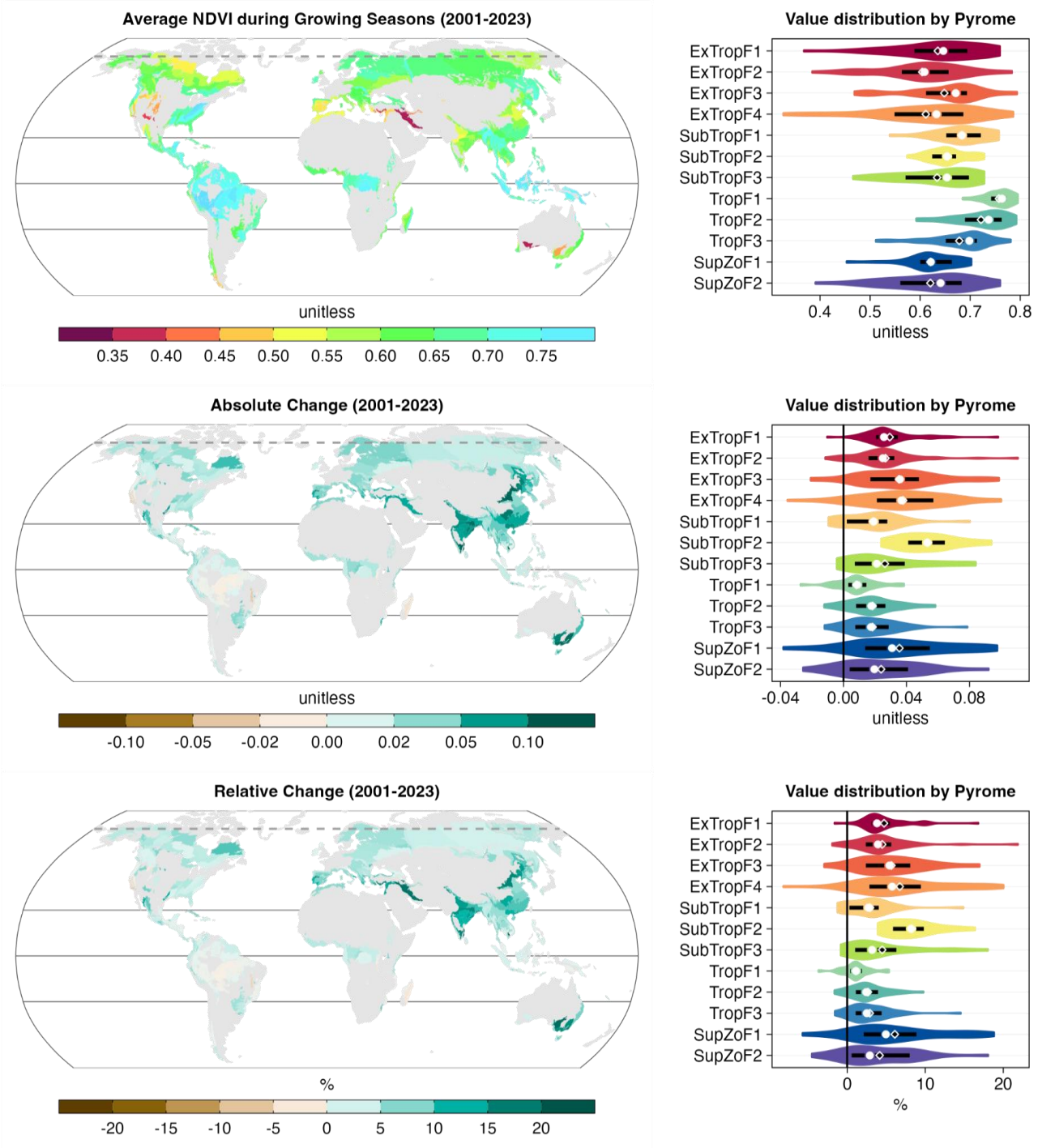

Figure S16: Average values and change in normalised difference vegetation index (NDVI) during prior growing seasons for each ecoregion during the period 2001-2023, alongside a breakdown of values by pyrome. The NDVI of individual fire seasons is calculated as the mean value during fire season months; the average values shown are the mean across multiple fire seasons. The violins represent the kernel density of the ecoregion count at each correlation value. White dots mark the median value for the ecoregions of a pyrome, while black line ranges mark the interquartile range and open diamonds mark the mean value.

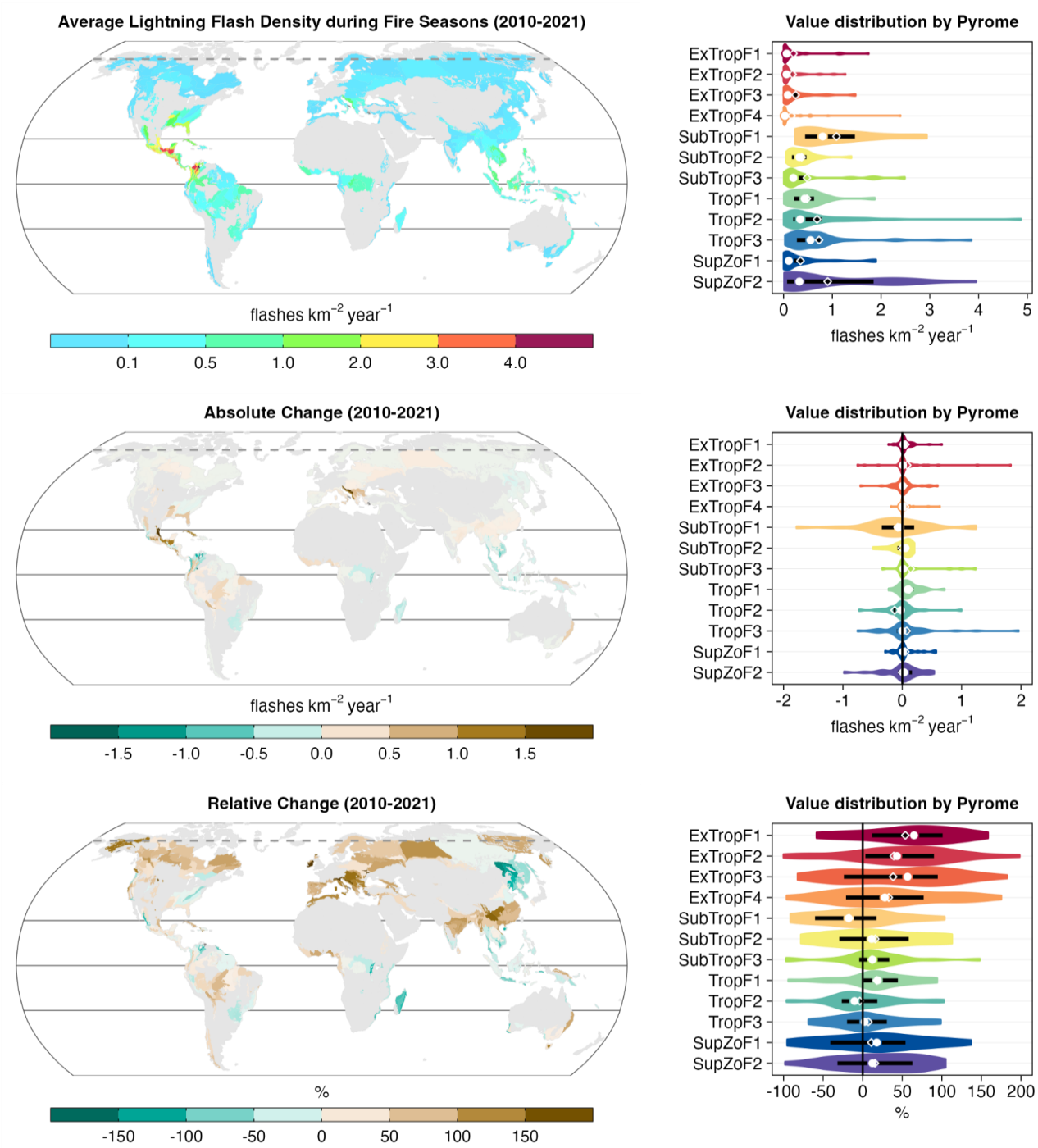

Figure S17: Average values and change in lightning flash density during the fire season for each ecoregion during the period 2010-2021, alongside a breakdown of values by pyrome. The violins represent the kernel density of the ecoregion count at each correlation value. White dots mark the median value for the ecoregions of a pyrome, while black line ranges mark the interquartile range and open diamonds mark the mean value.

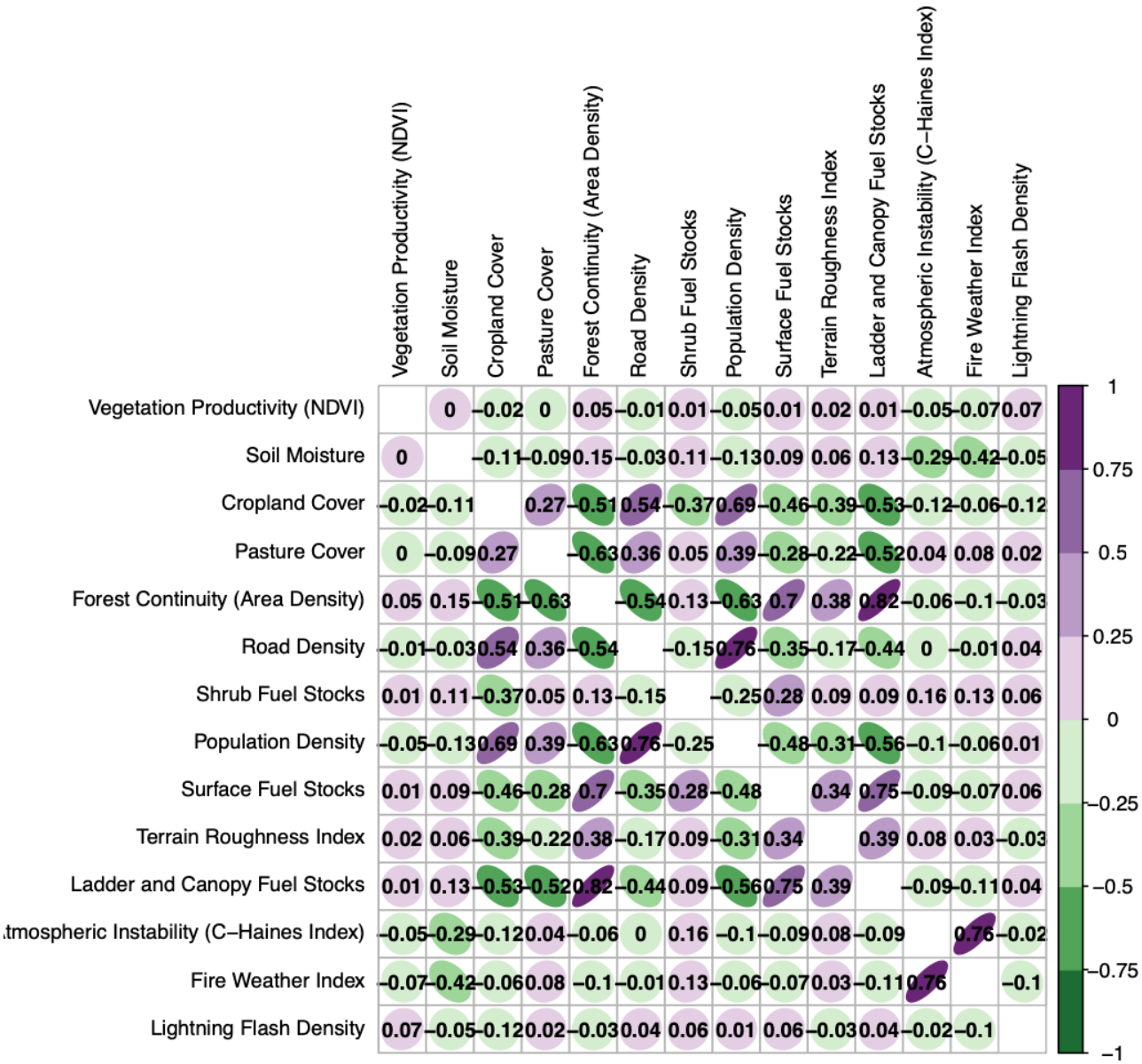

Figure S18: Covariance matrix of the variables used as input to the k-means clustering algorithm.

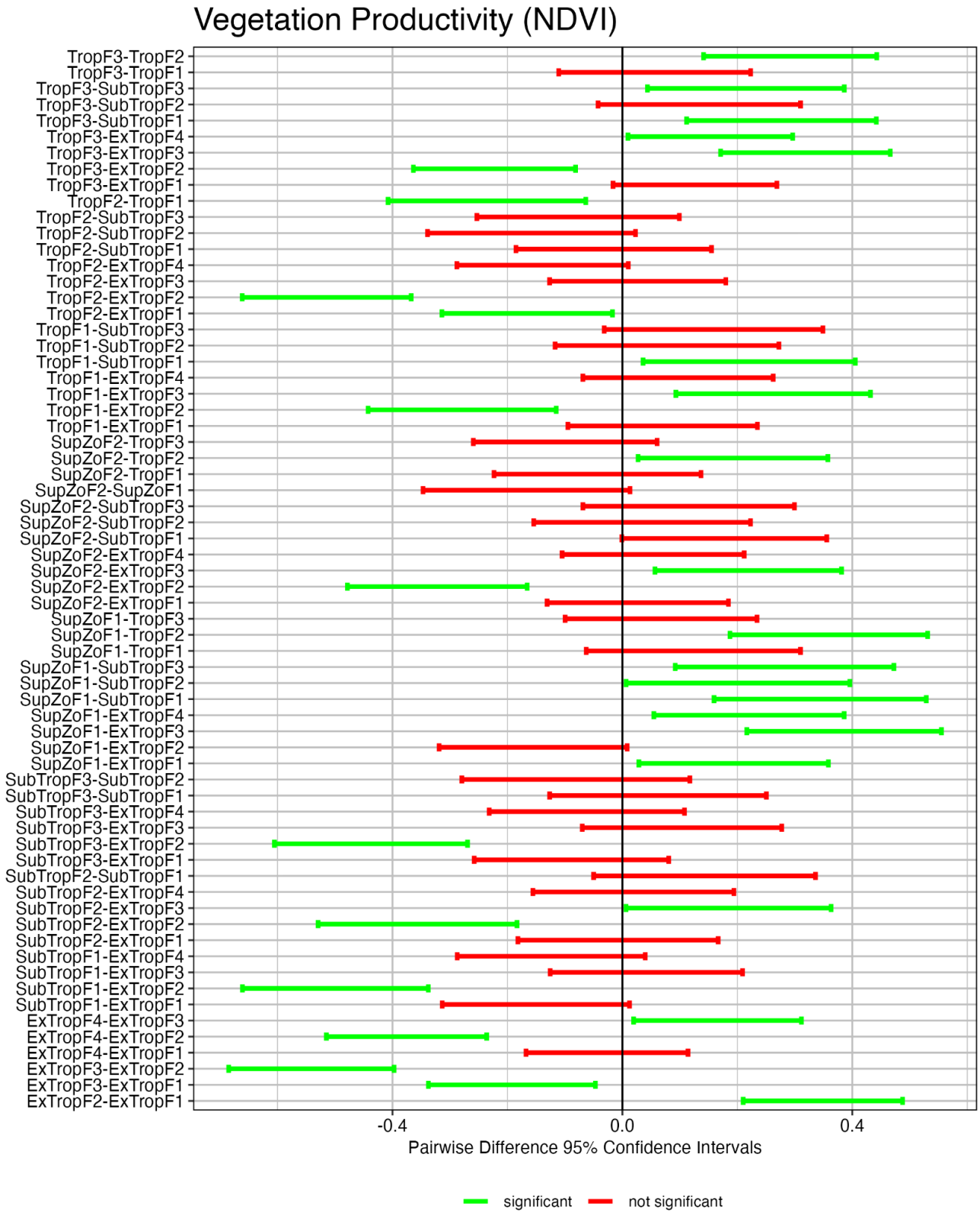

Figure S19: Pairwise differences in the value of each variable used in the k-mean clustering by pyrome, based on the distribution of values in the constituent ecoregions of each pyrome. Each panel shows one variable as indicated at the top of the page. Significant differences ($p<0.05$) are identified according to Tukey HSD posthoc tests. ANOVA tests revealed significant differences across the pyromes for all variables ($p<0.05$).

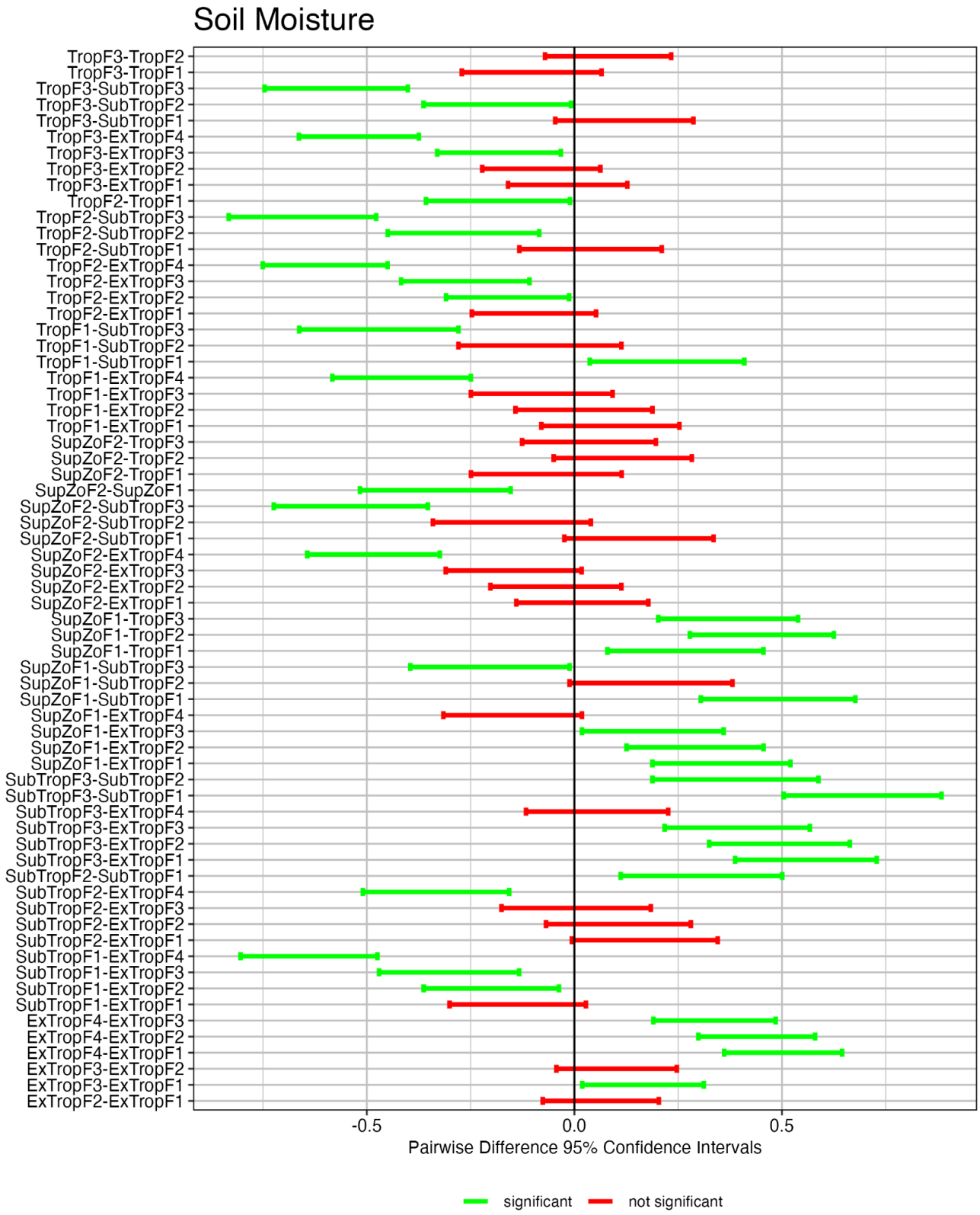

Figure S19 (cont).

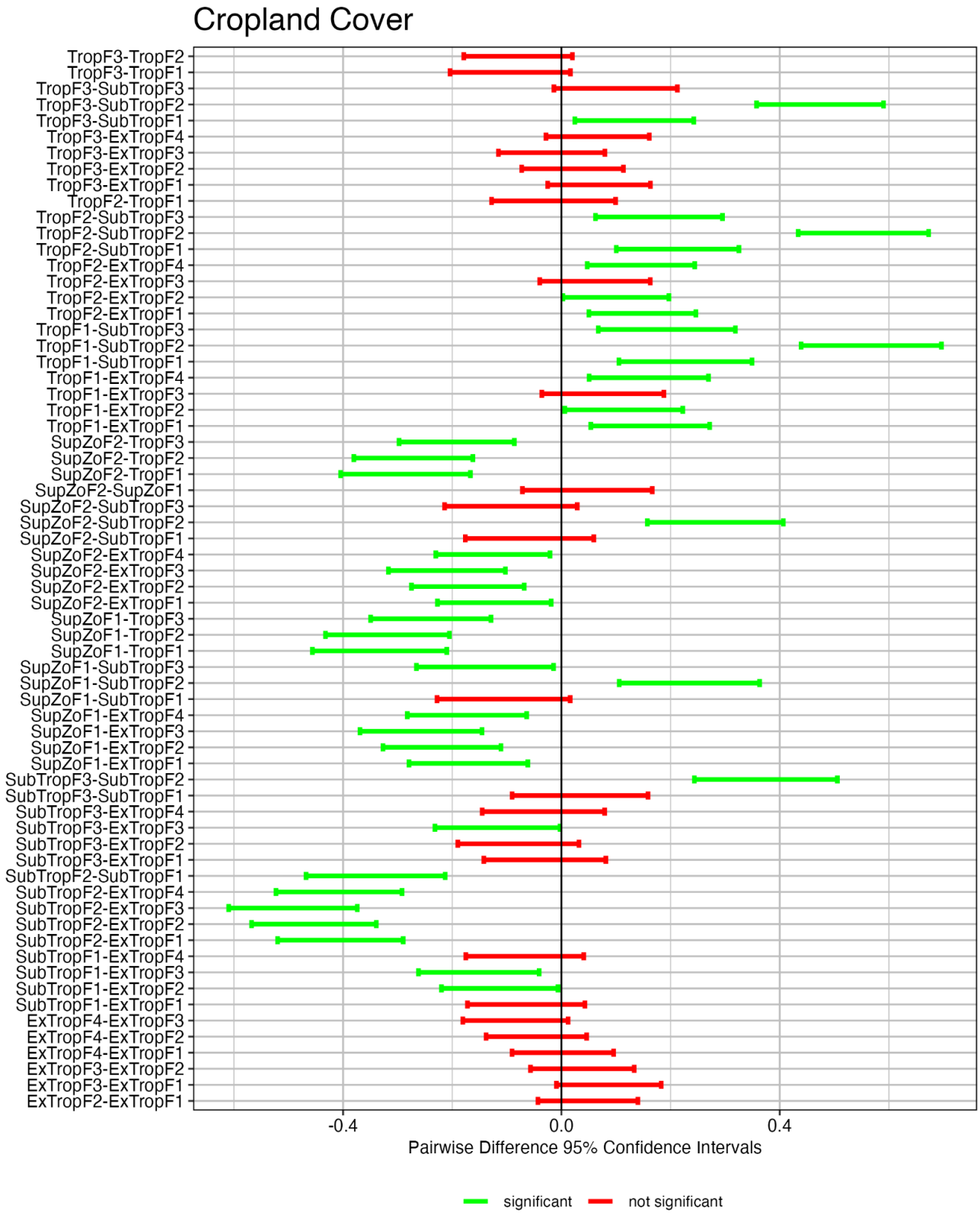

Figure S19 (cont).

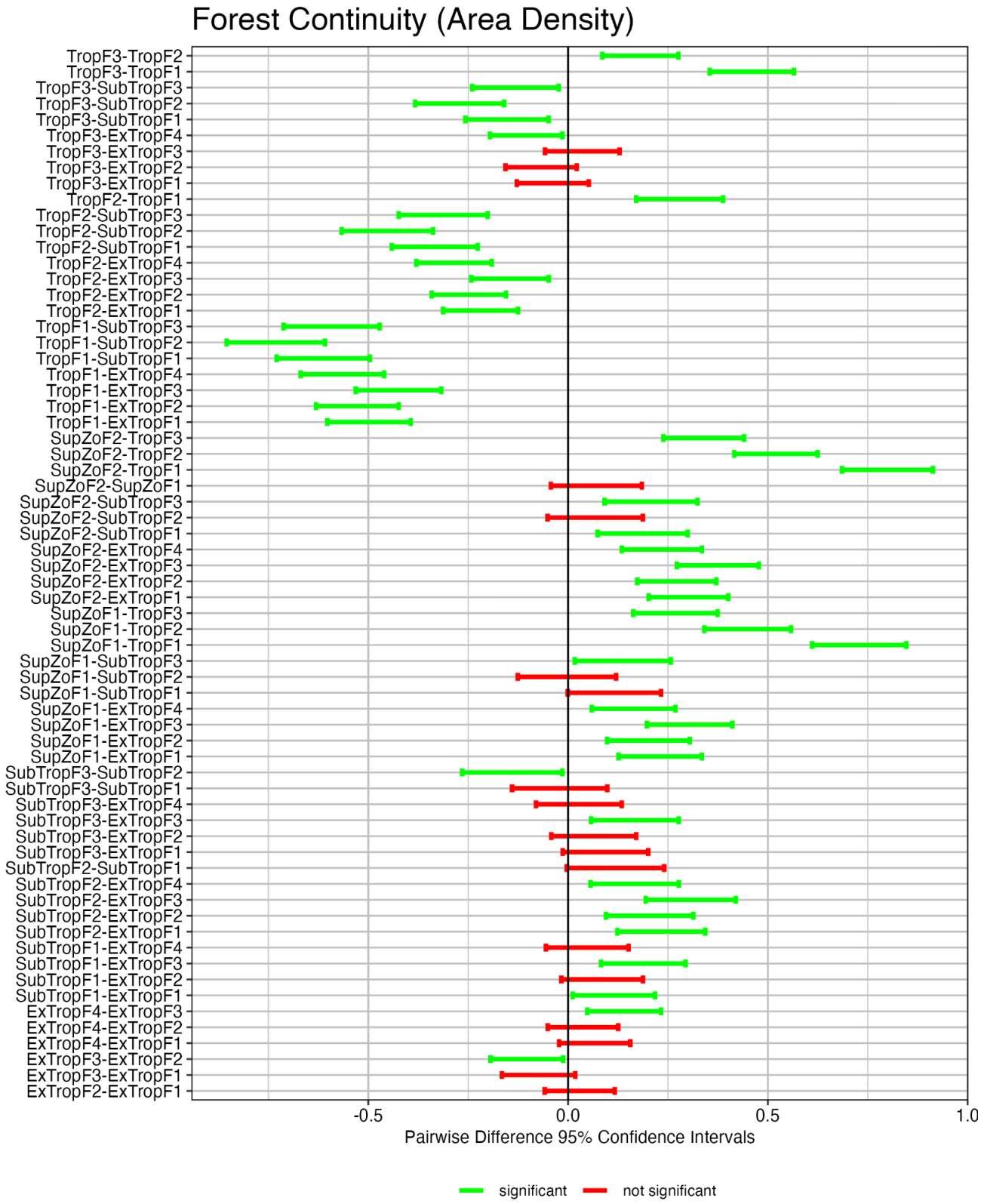

Figure S19 (cont).

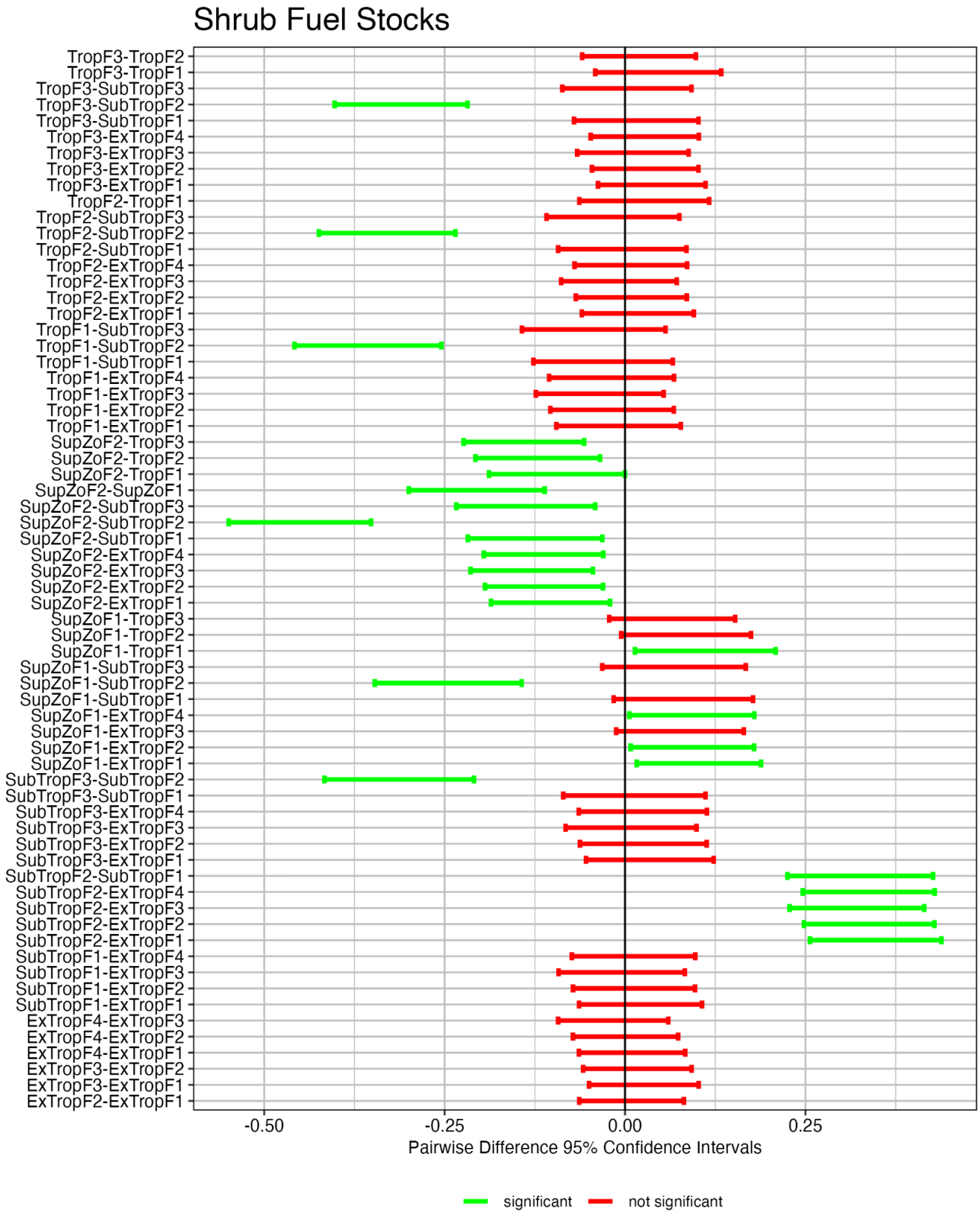

Figure S19 (cont).

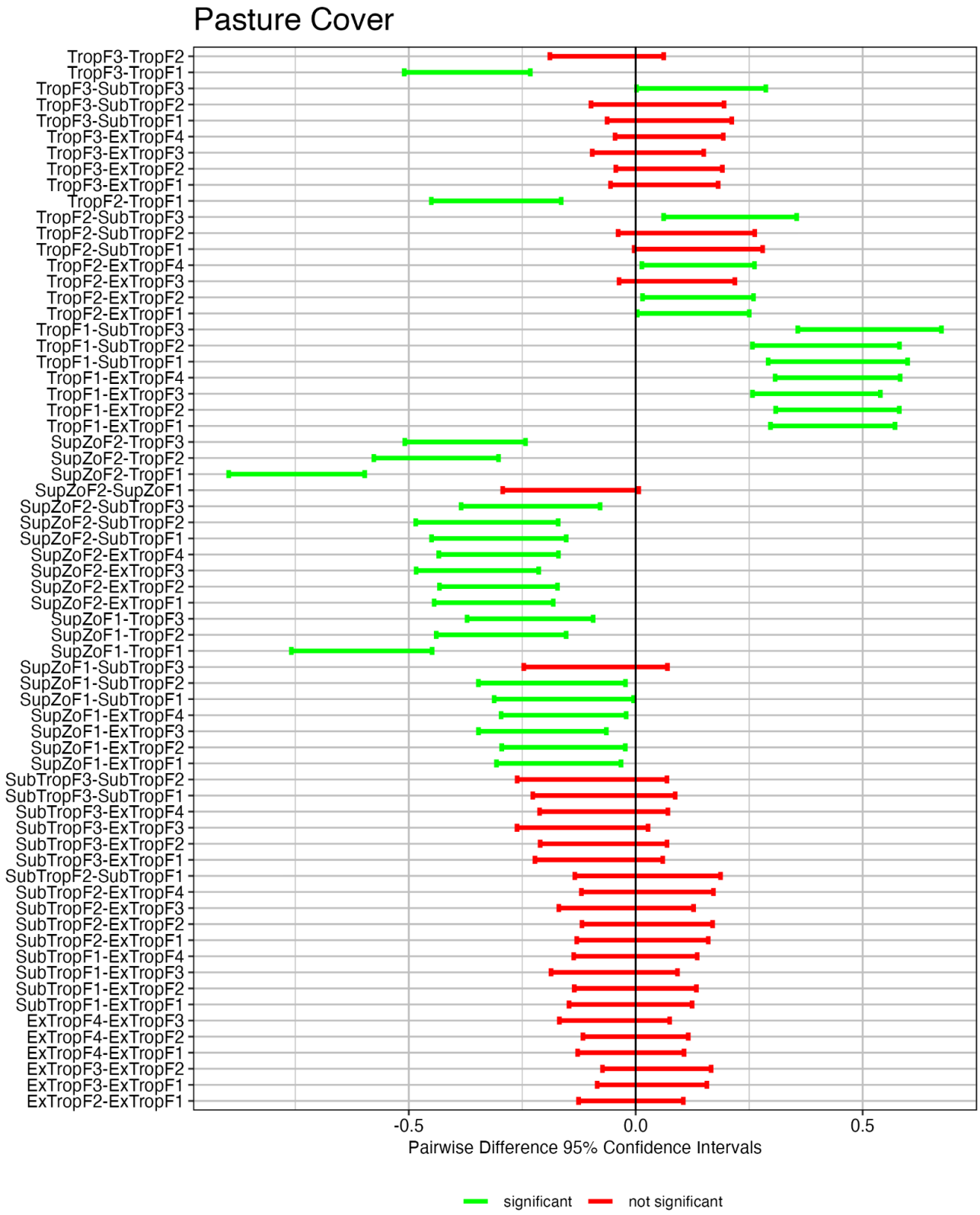

Figure S19 (cont).

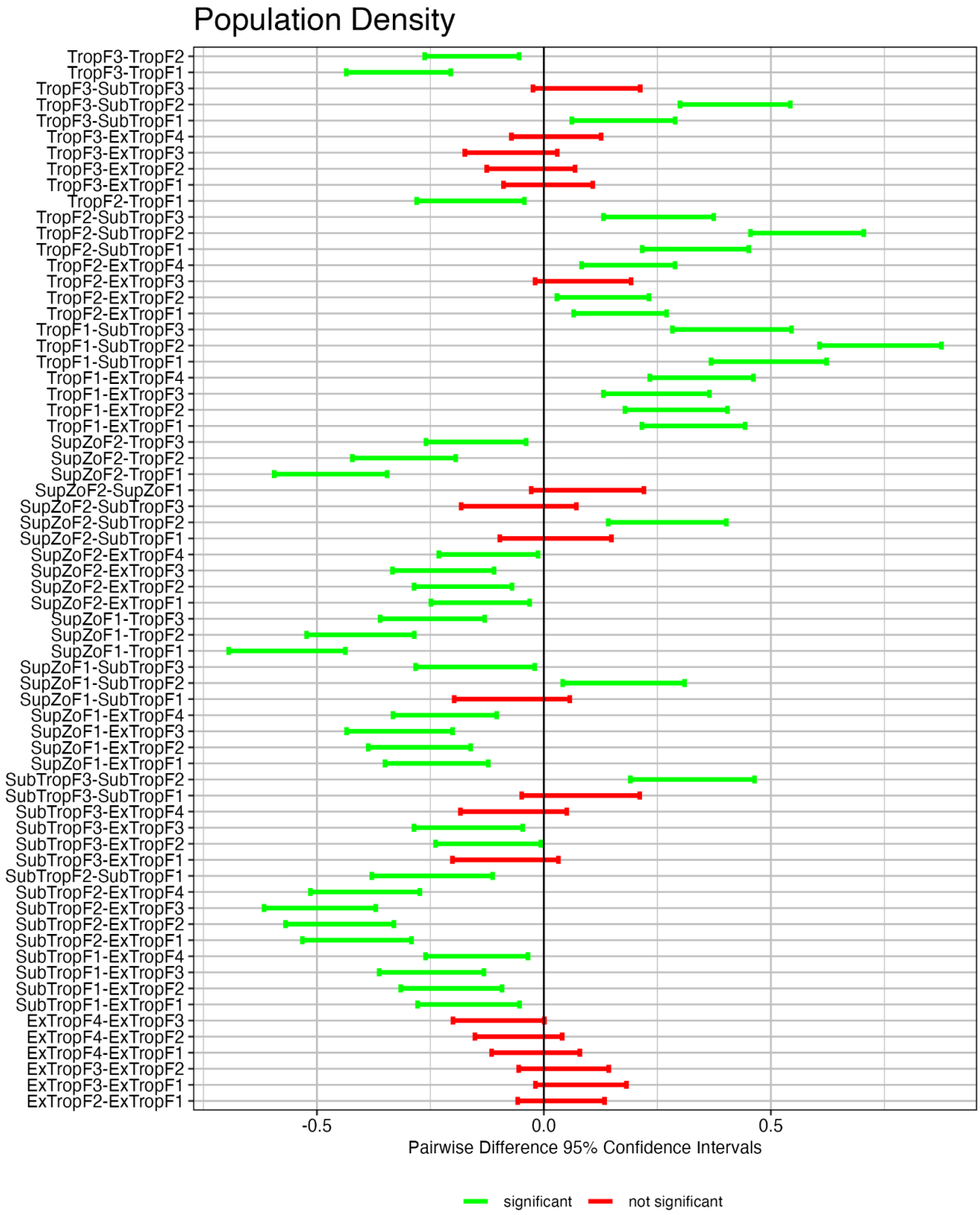

Figure S19 (cont).

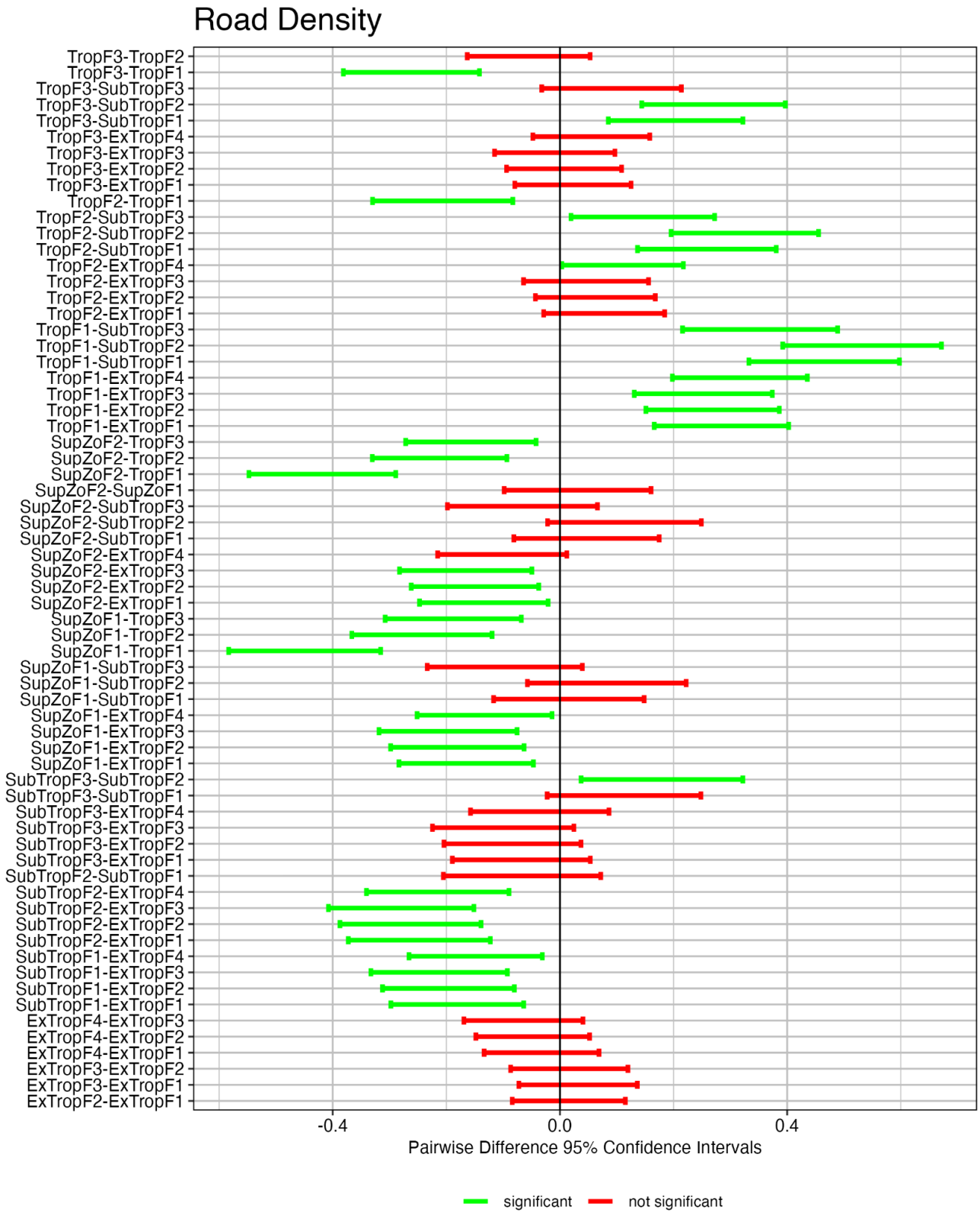

Figure S19 (cont).

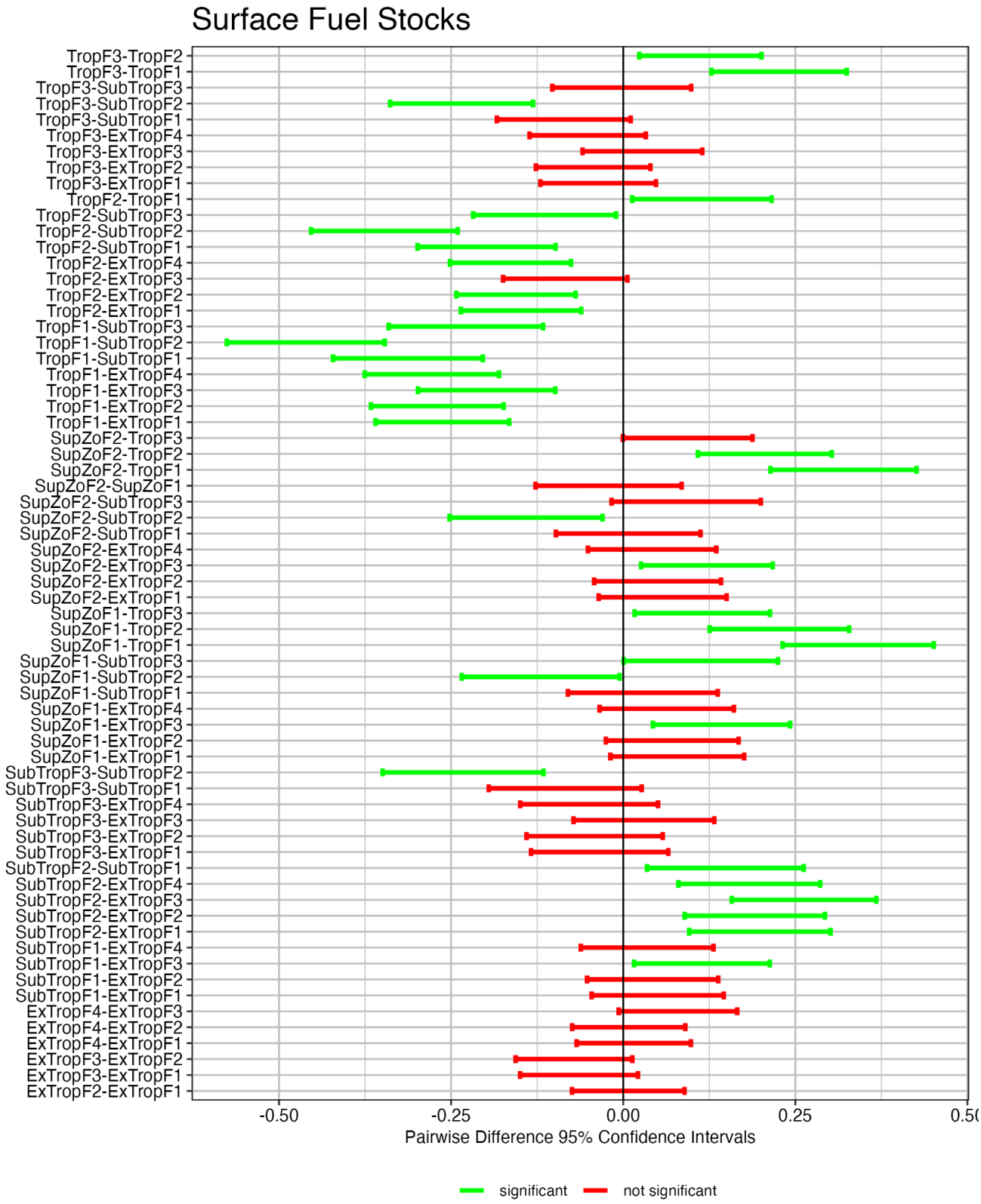

Figure S19 (cont).

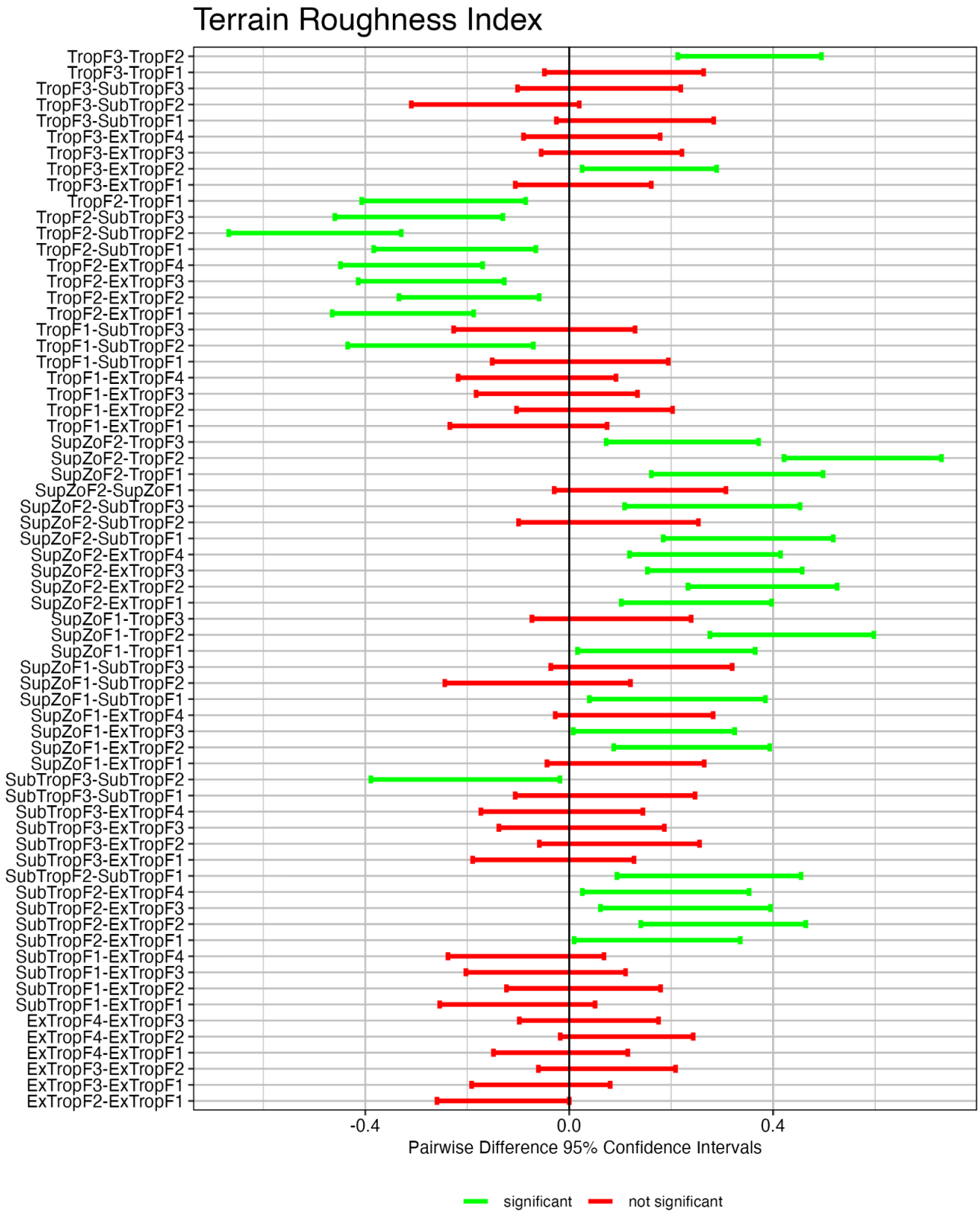

Figure S19 (cont).

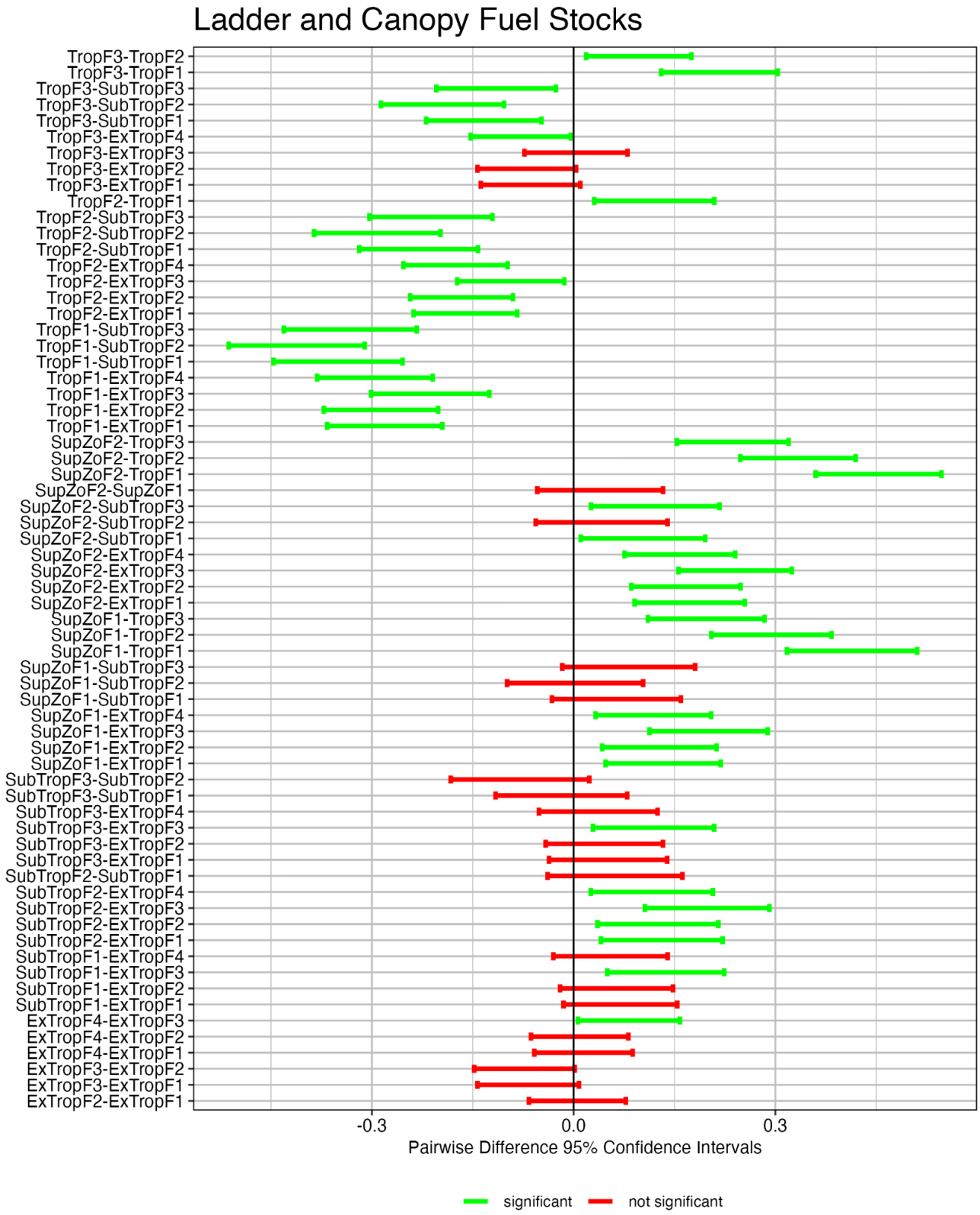

Figure S19 (cont).

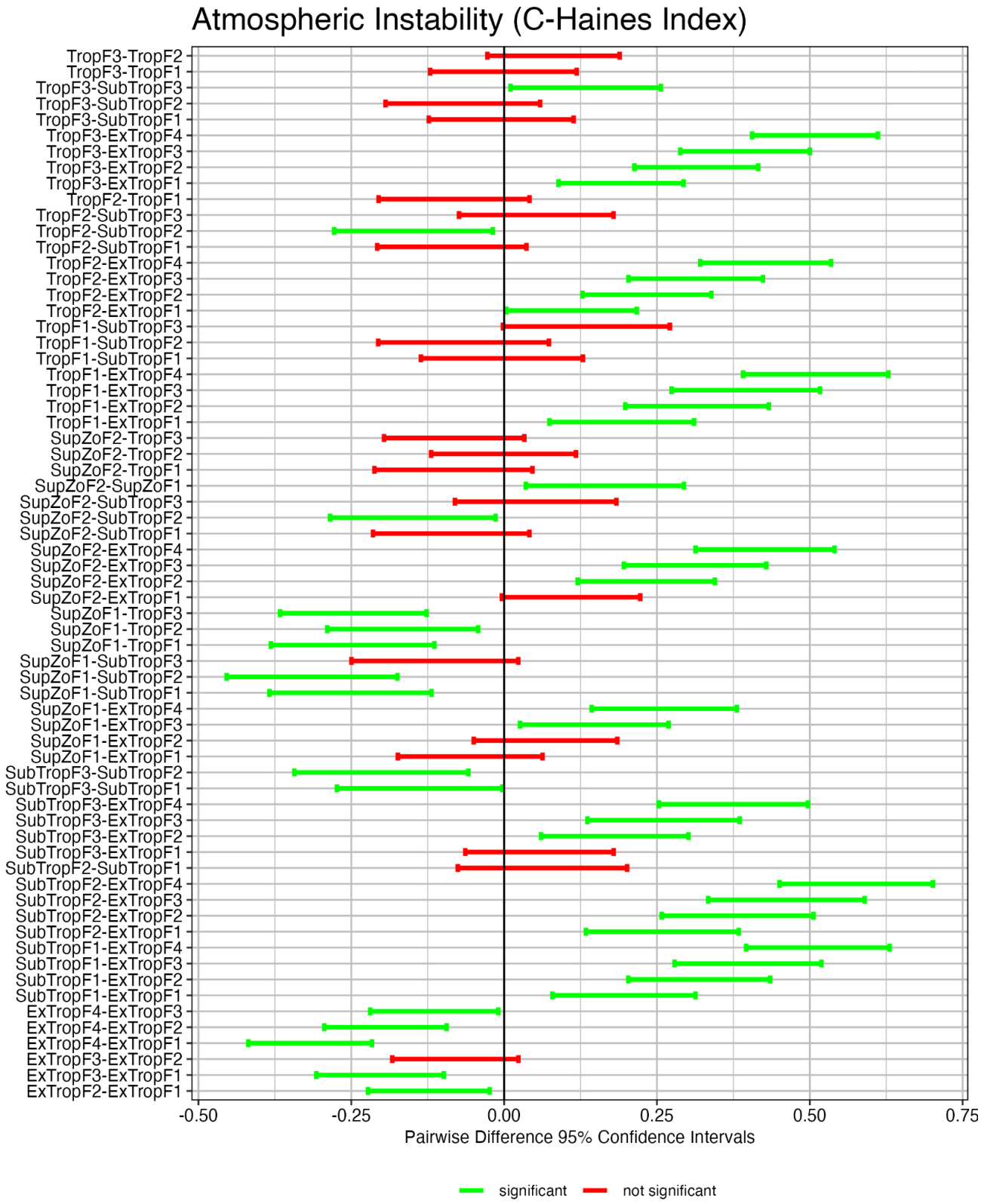

Figure S19 (cont).

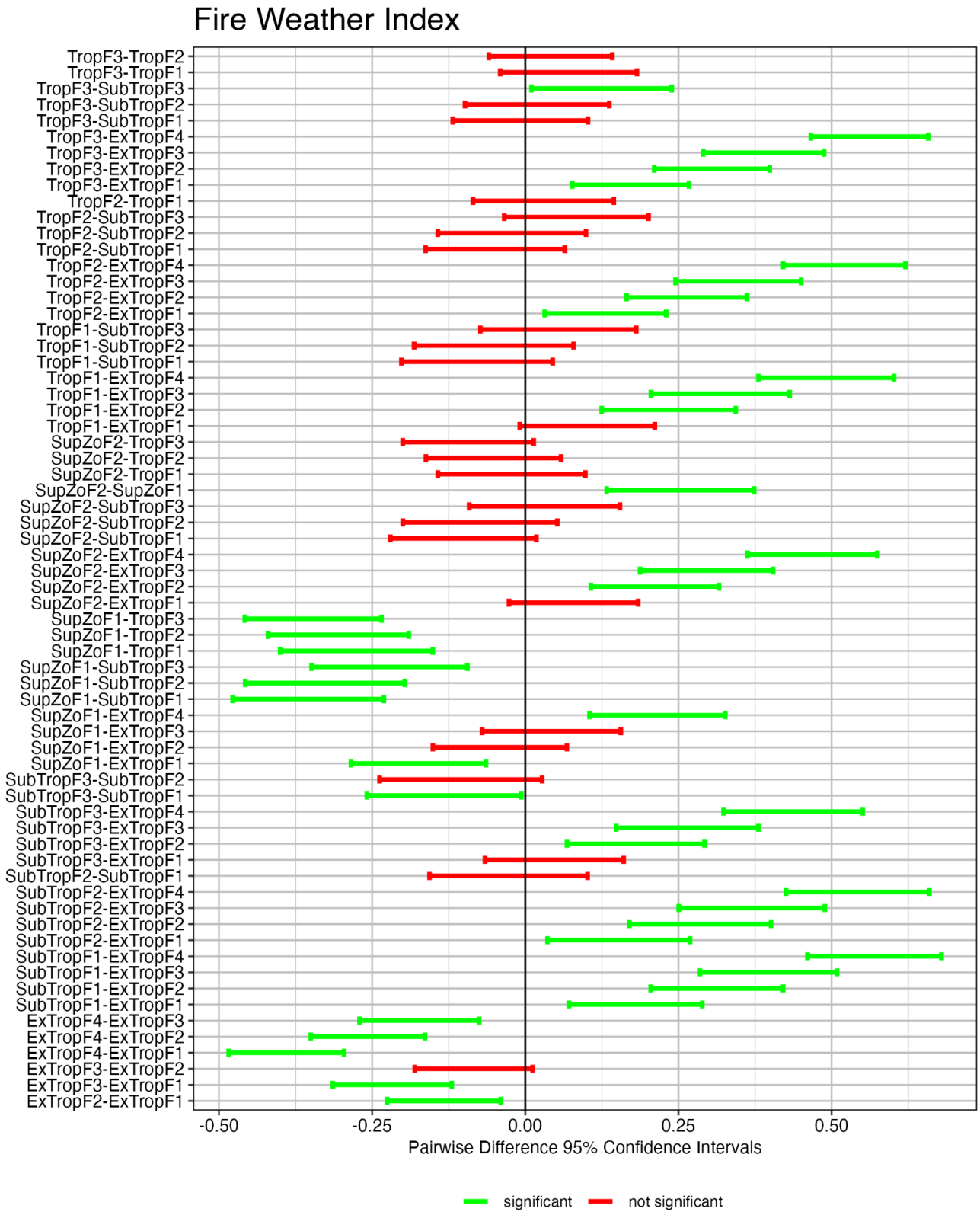

Figure S19 (cont).

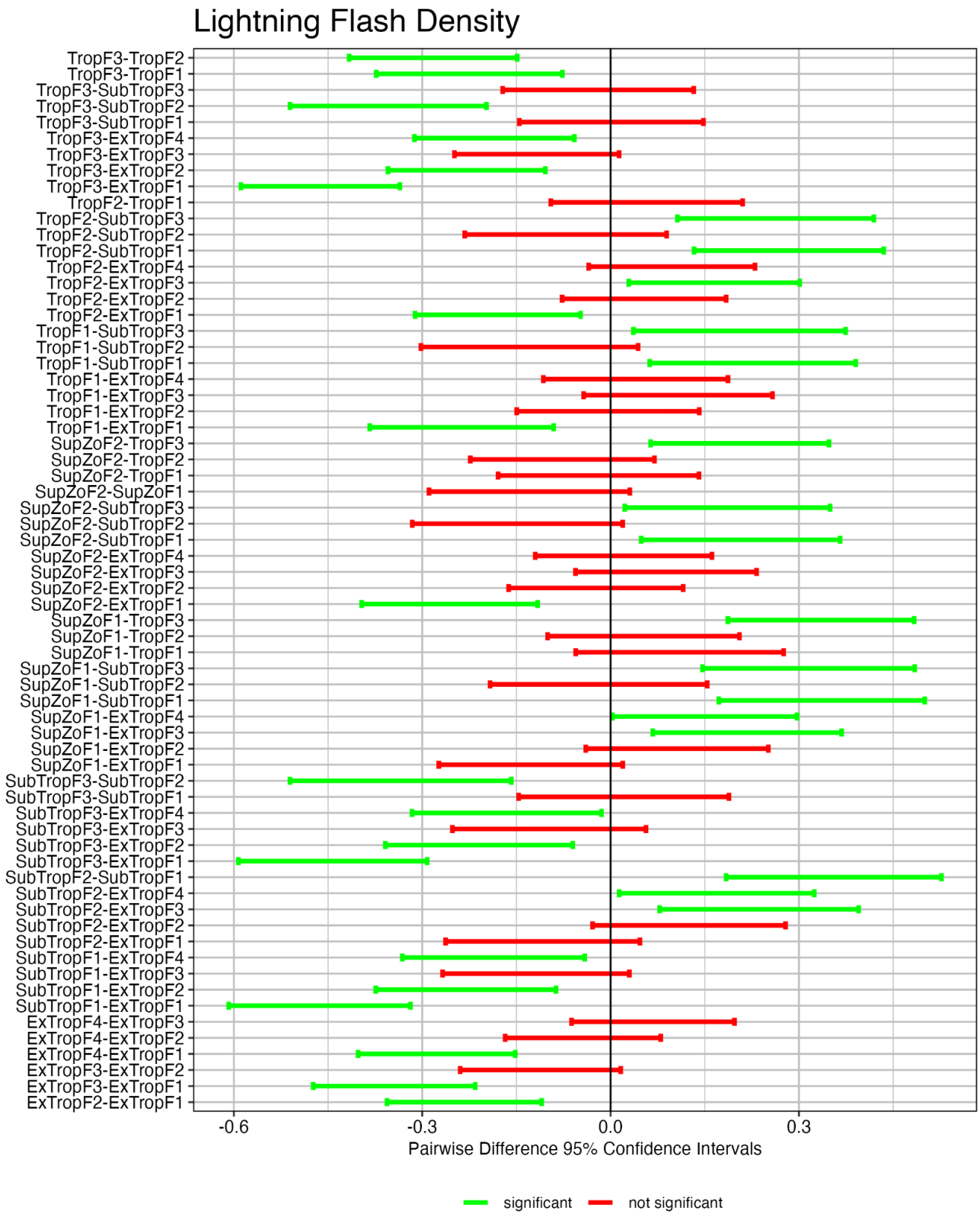

Figure S19 (cont).

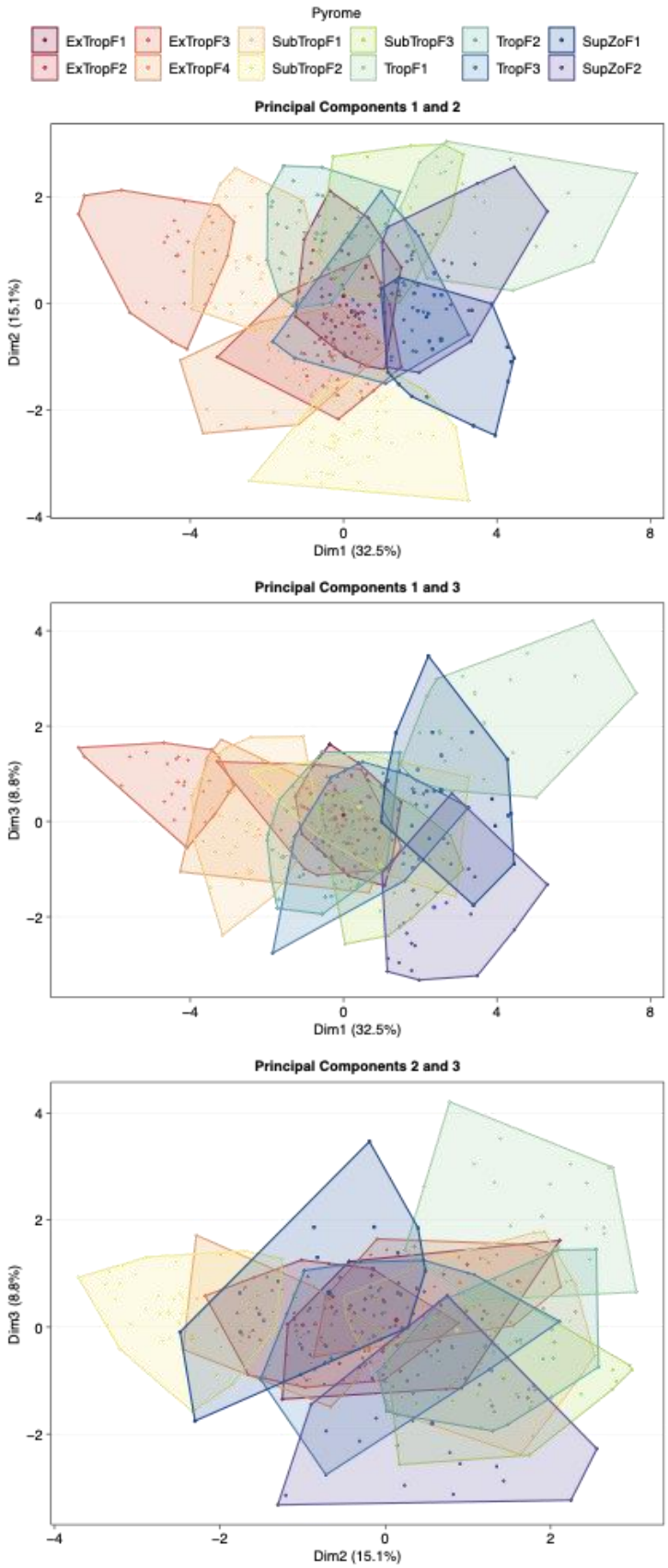

Figure S20: Separation of the pyromes along three components explaining the majority of the hyperdimensional variance in the input data, based on principal component analysis.

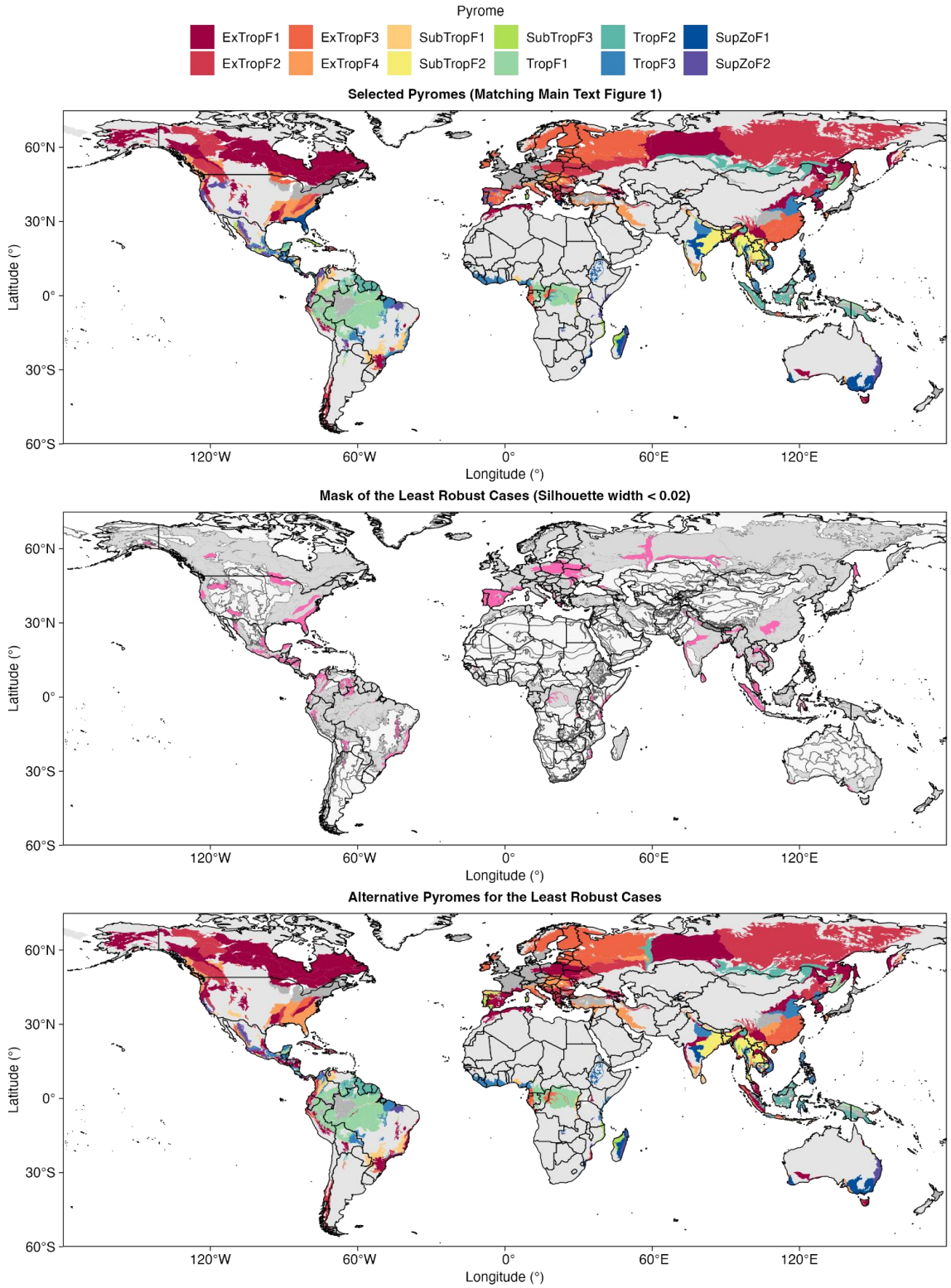

Figure S21: Map showing an alternative mapping of the pyromes for the 20% of ecoregions that were clustered least robustly (i.e. the ecoregions whose affinity to their alternative cluster is most similar to that of their selected cluster, and thus where their fit to the selected cluster is most ambiguous). **(a)** shows a replica of **Fig. 1** from the main text. **(b)** shows a mask of the ecoregions that were clustered least robustly (highlighted in pink). **(c)** shows the effect of replacing the selected pyromes with the best alternative pyrome. **Fig. S22** shows a summary of the confusion between selected pyromes and alternative pyromes for the least robust cases.

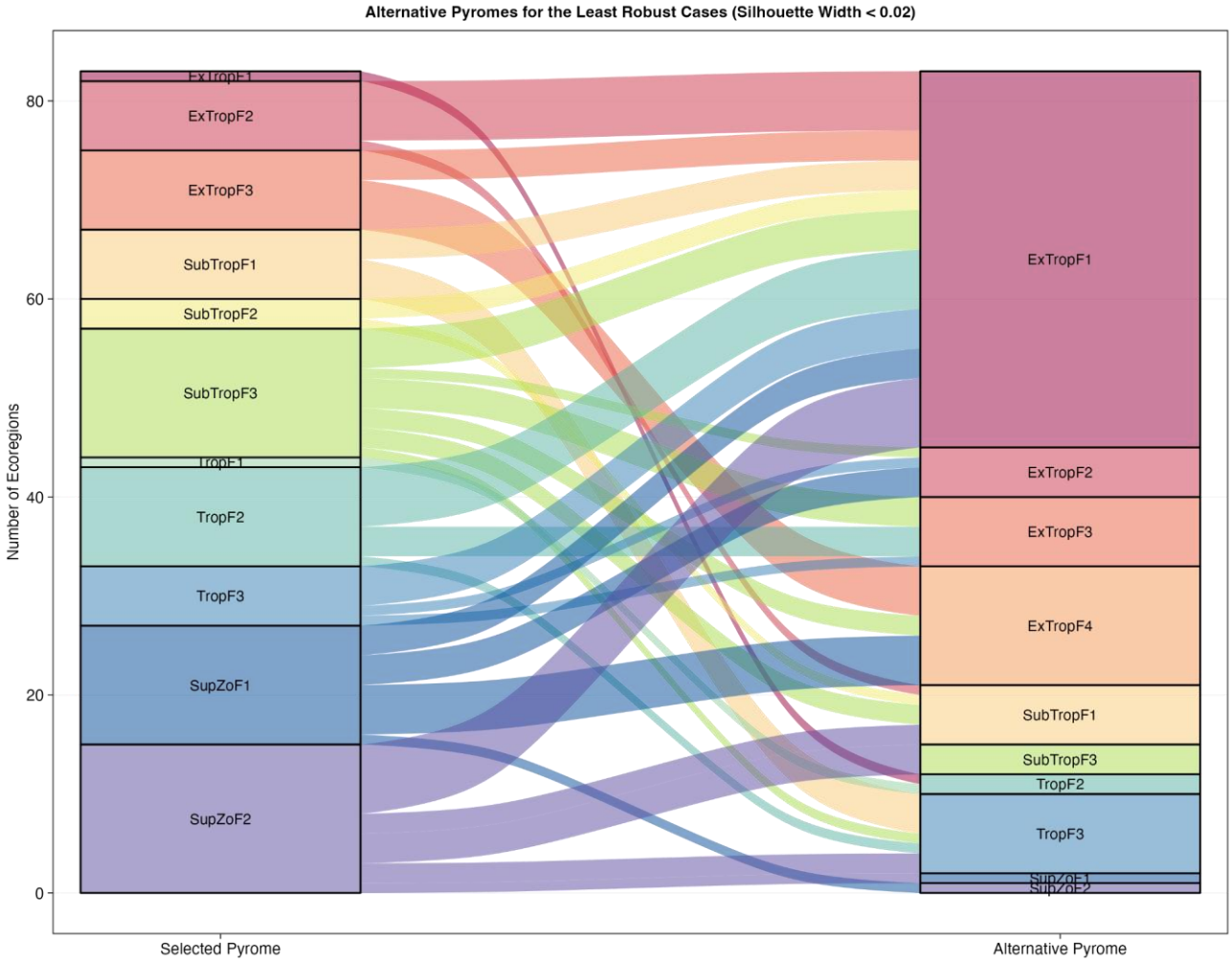

Figure S22: Confusion plot showing the association between the pyromes selected for each ecoregions and the best alternative pyrome, according to the k-means clustering algorithm. The plot includes the 20% of ecoregions that were clustered least robustly (i.e. the ecoregions whose affinity to their alternative pyrome is most similar to that of their selected pyrome, and thus where their fit to the selected pyrome is most ambiguous).

Supplementary Tables

Table S1: Summary statistics for a range of variables related to burnable area, burned area (BA), burned area fraction (BAF), fire return interval (FRI), fire C emissions, and fire C combustion rate (C emissions per unit BA).

Variable	ExTropF1	ExTropF2	ExTrop3	ExTropF4	SubTropF1	SubTropF2	SubTropF3	TropF1	TropF2	TropF3	SupZoF1	SupZoF2	ALL FOREST ECOREGIONS
Ecoregion Count													
# Ecoregions	46	48	40	45	27	22	24	26	37	43	25	31	414
Total Burnable Area													
Total Burnable Area (thousand km^2 year^{-1})	9106	9109	5540	2552	1259	2125	757	5281	3020	3052	1920	1690	45411
Fraction of Global Forest Ecoregion Area in Pyrome (%)	20	20	12	6	3	5	2	12	7	7	4	4	
Forest Burnable Area													
Mean Forest Burnable Area (thousand km^2)	4652	3528	3345	977	508	751	138	4681	2376	1286	464	595	23302
Absolute Change in Forest Burnable Area (thousand km^2)	867	1042	505	76	40	42	5	-118	210	20	5	-15	2547
Relative Change in Forest Burnable Area (%)	19	30	15	8	8	6	4	-3	9	2	1	-2	11
Significance of Change in Forest Burnable Area	***	***	***	***	***	***		***	***	*		*	***
Pyrome Fraction of Global Forest Burnable Area (%)	20	15	14	4	2	3	1	20	10	6	2	3	
# Ecoregions of Pyrome with Increased Forest Burnable Area	42	39	35	33	20	13	14	7	24	27	18	14	
of which significant	37	36	30	33	14	9	10	6	22	18	11	10	
# Ecoregions of Pyrome with Decreased Forest Burnable Area	4	6	5	10	6	7	10	19	11	16	8	13	
of which significant	2	4	3	5	4	6	3	14	8	10	6	9	
Forest Cover Fraction													
Mean Forest Cover Fraction in Pyrome (%)	51	39	60	38	40	35	18	89	79	42	24	35	51
Relative Change in Forest Cover Fraction (%)	19	30	15	8	8	6	4	-3	9	2	1	-2	11
Significance of Change in Forest Cover Fraction	***	***	***	***	***	***		***	***	*		*	***
Total Burned Area													
Mean Annual Total BA (thousand km^2 year^{-1})	41	72	13	12	20	61	54	71	30	73	56	32	536
Absolute Change in Total BA (thousand km^2 year^{-1})	-12	43	-12	3	-4	1	-13	4	-23	-44	-12	-2	-90
Relative Change in Total BA (%)	-28	60	-86	27	-22	1	-25	5	-76	-61	-20	-8	-17
Significance of Change in Total BA		***	***	*	***		***		***	***	***		***
Pyrome Fraction of Global Total BA (%)	8	13	3	2	4	11	10	13	6	14	11	6	
Pyrome Fraction of Global Gross Increases in Total BA (%)		85		6		2		8					
Pyrome Fraction of Global Gross Decreases in Total BA (%)	10		10		4		11		19	36	9	2	
# Ecoregions of Pyrome with Increased Total BA	19	28	5	18	8	14	8	12	7	16	13	14	
of which significant	11	20	2	7	5	5	5	5	4	8	5	3	
# Ecoregions of Pyrome with Decreased Total BA	25	16	25	21	18	8	16	13	28	26	12	16	
of which significant	12	10	18	10	13	5	14	8	22	19	5	11	
Forest Burned Area													
Mean Annual Forest BA (thousand km^2 year^{-1})	19	21	3	1	4	23	10	22	13	20	7	12	156
Absolute Change in Forest BA (thousand km^2 year^{-1})	6	35	-2	1	-1	-6	-3	4	-7	-10	1	2	19
Relative Change in Forest BA (%)	30	167	-46	40	-32	-25	-26	19	-56	-50	8	18	12
Significance of Change in Forest BA	***	***	**	***	***		**	*	***	***		.	*

Variable	ExTropF1	ExTropF2	ExTrop3	ExTropF4	SubTropF1	SubTropF2	SubTropF3	TropF1	TropF2	TropF3	SupZoF1	SupZoF2	ALL FOREST ECOREGIONS
Pyrome Fraction of Global Forest BA (%)	12	13	2	1	3	15	6	14	8	13	4	8	
Pyrome Fraction of Global Gross Increases in Forest BA (%)	12	72		1				9			1	5	
Pyrome Fraction of Global Gross Decreases in Forest BA (%)			5		5	20	9		26	35			
# Ecoregions of Pyrome with Increased Forest BA	25	29	9	16	10	12	9	17	6	17	12	19	
of which significant	17	26	2	8	4	5	5	7	4	8	8	10	
# Ecoregions of Pyrome with Decreased Forest BA	19	9	17	9	15	10	13	8	29	22	10	10	
of which significant	7	2	10	1	12	2	11	4	13	13	4	4	
Forest Fraction of Total Burned Area													
Forest Fraction of Total BA in Pyrome (%)	45	27	25	12	20	36	18	31	43	27	12	39	29
Absolute Change in Forest Fraction of Total BA in Pyrome (%)	26	32	10	5	-5	-5	0	4	0	3	2	12	9
Relative Change in Forest Fraction of Total BA in Pyrome (%)	58	117	39	42	-24	-13	1	14	0	9	20	30	30
Significance of Change in Forest Fraction of Total BA in Pyrome	***	***	***	***	**			***			*	***	***
# Ecoregions of Pyrome with Increased Forest Fraction of Total Burned Area	33	32	18	20	14	9	11	17	20	26	11	22	
of which significant	23	27	13	13	8	8	6	12	16	17	8	16	
# Ecoregions of Pyrome with Decreased Forest Fraction of Total Burned Area	10	7	8	5	10	13	11	8	14	14	14	7	
of which significant	4	4	2	1	5	8	6	2	9	7	6	2	
Total Burned Area Fraction													
Mean Annual Total BAF (%)	0.45	0.79	0.24	0.46	1.61	2.89	7.10	1.35	0.99	2.38	2.94	1.88	1.18
Relative Change in Total BAF (%)	-28	60	-86	27	-22	1	-25	5	-76	-61	-20	-8	-17
Significance of Change in Total BAF		***	***	*	***		***		***	***	***		***
Mean Total BAF in Ecoregions of Pyrome (%)	0.73	1.17	0.41	0.43	1.34	2.67	4.58	1.09	1.29	2.62	2.89	3.18	
Median Total BAF in Ecoregions of Pyrome (%)	0.29	0.45	0.14	0.11	0.63	1.66	2.04	0.76	0.36	1.52	1.17	1.27	
Mean Relative Change in Total BAF in Ecoregions of Pyrome (%)	-8	10	-47	-9	-22	11	-33	0	-31	-20	7	-14	
Median Relative Change in Total BAF in Ecoregions of Pyrome (%)	-2	12	-19	0	-20	11	-24	0	-24	-16	1	-20	
# Ecoregions of Pyrome with Increased Total BAF	19	28	5	18	8	14	8	12	7	16	13	14	
of which significant	11	20	2	7	5	5	5	5	4	8	5	3	
# Ecoregions of Pyrome with Decreased Total BAF	25	16	25	21	18	8	16	13	28	26	12	16	
of which significant	12	10	18	10	13	5	14	8	22	19	5	11	
Forest Burned Area Fraction													
Mean Annual Forest BAF (%)	0.40	0.56	0.10	0.14	0.81	3.03	7.02	0.48	0.55	1.56	1.49	2.10	0.67
Relative Change in Forest BAF (%)	9	158	-56	33	-39	-26	-28	20	-63	-48	9	21	-2
Significance of Change in Forest BAF	*	***	***	***	***	*	***	*	***	***		*	
Mean Forest BAF in Ecoregions of Pyrome (%)	0.57	0.96	0.23	0.26	1.01	2.74	3.57	0.43	0.81	1.72	1.92	3.24	
Median Forest BAF in Ecoregions of Pyrome (%)	0.26	0.24	0.11	0.09	0.56	2.24	1.61	0.37	0.16	0.63	1.41	1.20	
Mean Relative Change in Forest BAF in Ecoregions of Pyrome (%)	4	22	-25	8	-13	2	-20	15	-21	-9	0	11	
Median Relative Change in Forest BAF in Ecoregions of Pyrome (%)	2	15	-1	0	-18	9	-4	10	-18	-5	0	8	
# Ecoregions of Pyrome with Increased Forest BAF	24	29	7	18	10	12	9	17	7	16	12	17	
of which significant	15	23	1	8	3	3	3	7	3	9	7	10	

Variable	ExTropF1	ExTropF2	ExTrop3	ExTropF4	SubTropF1	SubTropF2	SubTropF3	TropF1	TropF2	TropF3	SupZoF1	SupZoF2	ALL FOREST ECOREGIONS
# Ecoregions of Pyrome with Decreased Forest BAF	19	9	19	11	17	10	13	8	30	24	11	12	
of which significant	7	3	10	1	12	5	8	3	16	13	4	4	
Total Fire Return Interval													
Mean Total FRI of Pyrome (years)	222	127	411	218	62	35	14	74	101	42	34	53	
Mean Total FRI of ecoregions in pyrome (years)	433	580	1012	1357	289	108	176	318	349	241	189	112	
Median Total FRI of ecoregions in pyrome (years)	341	223	694	870	159	60	50	131	277	66	86	79	
Forest Fire Return Interval													
Mean Forest FRI of Pyrome (years)	249	177	997	717	123	33	14	209	182	64	67	48	
Mean Forest FRI of ecoregions in pyrome (years)	683	857	1563	1356	407	82	263	576	701	514	163	123	
Median Forest FRI of ecoregions in pyrome (years)	378	417	951	1070	178	45	63	270	620	159	72	85	
Total Fire C Emissions													
Mean Total Fire C Emissions (Tg C $year^{-1}$)	91	129	6	4	14	37	23	67	52	47	27	27	524
Absolute Change in Total Fire C Emissions (Tg C $year^{-1}$)	-16	155	-4	1	-6	-3	-4	9	-53	-14	6	10	94
Relative Change in Total Fire C Emissions (%)	-18	120	-67	29	-43	-7	-17	13	-102	-31	21	36	18
Significance of Change in Total Fire C Emissions		***	***	***	***		***		***	*	***	***	*
Pyrome Fraction of Global Total Fire C Emissions (%)	17	25	1	1	3	7	4	13	10	9	5	5	
Pyrome Fraction of Global Gross Increases in Total Fire C Emissions (%)		86		1				5			3	5	
Pyrome Fraction of Global Gross Decreases in Total Fire C Emissions (%)	16		4		6	3	4		53	14			
# Ecoregions of Pyrome with Increased Total C Emissions	17	30	5	14	8	9	9	12	6	15	16	17	
of which significant	5	20	0	7	3	3	4	7	3	8	8	3	
# Ecoregions of Pyrome with Decreased Total C Emissions	27	14	26	26	19	13	15	14	31	27	10	13	
of which significant	13	4	21	9	12	9	11	8	21	13	5	6	
Forest Fire C Emissions													
Mean Forest Fire C Emissions (Tg C $year^{-1}$)	47	60	2	1	6	20	7	43	28	24	9	16	263
Absolute Change in Forest Fire C Emissions (Tg C $year^{-1}$)	30	116	-1	1	-3	0	-2	24	-26	-5	4	7	157
Relative Change in Forest Fire C Emissions (%)	65	194	-26	76	-52	-2	-25	56	-96	-19	44	43	60
Significance of Change in Forest Fire C Emissions	***	***		***	**		***	***	***		***	***	***
Pyrome Fraction of Global Forest Fire C Emissions (%)	18	23	1	0	2	7	3	16	10	9	4	6	
Pyrome Fraction of Global Gross Increases in Forest Fire C Emissions (%)	17	64		1				13			2	4	
Pyrome Fraction of Global Gross Decreases in Forest Fire C Emissions (%)			2		9	1	5		71	13			
# Ecoregions of Pyrome with Increased Forest C Emissions	20	30	7	16	10	10	7	12	6	17	13	18	
of which significant	11	25	2	9	4	1	3	7	4	7	9	9	
# Ecoregions of Pyrome with Decreased Forest C Emissions	23	9	19	13	17	12	15	13	31	25	11	12	
of which significant	8	2	12	2	10	9	11	6	22	13	4	2	
Forest Fraction of Fire C Emissions													
Forest Fraction of Total C Emissions in Pyrome (%)	51	41	40	27	44	51	32	62	55	50	31	57	49
Absolute Change in Forest Fraction of Total C Emissions in Pyrome (%)	43	44	15	21	-11	-7	-4	21	15	8	13	11	24
Relative Change in Forest Fraction of Total C Emissions in Pyrome (%)	84	107	38	79	-25	-13	-13	34	28	16	42	19	49

Variable	ExTropF1	ExTropF2	ExTrop3	ExTropF4	SubTropF1	SubTropF2	SubTropF3	TropF1	TropF2	TropF3	SupZoF1	SupZoF2	ALL FOREST ECOREGIONS
Significance of Change in Forest Fraction of Total C Emissions in Pyrome	***	***	***	***	*			***	***	*	***	***	***
# Ecoregions of Pyrome with Increased Forest Fraction of Total C Emissions	33	34	14	22	17	10	9	17	14	25	11	18	
of which significant	22	25	8	15	5	5	4	11	9	17	5	10	
# Ecoregions of Pyrome with Decreased Forest Fraction of Total C Emissions	10	7	11	7	10	12	13	9	20	17	12	11	
of which significant	5	2	5	1	8	8	5	2	9	9	4	3	
Total Fire C Combustion Rate													
Mean Total Fire C Emissions per unit BA (g C m^{-2})	2174	1694	448	378	693	598	427	923	1650	641	479	814	979
Absolute Change in Total Fire C Emissions per unit BA (g C m^{-2})	3	992	55	40	-54	-34	28	140	-934	109	145	363	327
Relative Change in Total Fire C Emissions per unit BA (%)	0	59	12	11	-8	-6	7	15	-57	17	30	45	33
Significance of Change in Total Fire C Emissions per unit BA		***	***	.			***	*	***	***	***	***	***
Mean Total Fire C Emissions per Unit BA in Ecoregions of Pyrome (g C m^{-2})	1429	852	610	544	1016	628	419	1008	1529	631	790	752	
Median Total Fire C Emissions per Unit BA in Ecoregions of Pyrome (g C m^{-2})	987	457	396	405	627	585	378	975	989	475	682	689	
Mean Relative Change in Total Fire C Emissions per Unit BA in Ecoregions of Pyrome (%)	9	28	-2	10	-2	-8	10	16	-4	6	13	27	
Median Relative Change in Total Fire C Emissions per Unit BA in Ecoregions of Pyrome (%)	10	20	0	5	6	-3	10	6	-4	8	4	22	
# Ecoregions of Pyrome with Increased Total Fire C Emissions per Unit BA	26	33	17	26	17	10	14	19	14	27	15	23	
of which significant	14	28	9	15	6	5	11	11	8	17	11	20	
# Ecoregions of Pyrome with Decreased Total Fire C Emissions per Unit BA	18	12	16	14	9	12	10	6	21	15	11	7	
of which significant	9	7	6	7	4	6	6	5	12	9	3	4	
Forest Fire C Combustion Rate													
Mean Forest Fire C Emissions per unit BA (g C m^{-2})	2390	2586	738	849	1523	856	749	1846	2055	1193	1238	1176	1663
Absolute Change in Forest Fire C Emissions per unit BA (g C m^{-2})	810	1510	30	371	9	11	-49	584	-936	317	978	436	775
Relative Change in Forest Fire C Emissions per unit BA (%)	34	58	4	44	1	1	-7	32	-46	27	79	37	47
Significance of Change in Forest Fire C Emissions per unit BA	***	***	.	***			.	***	***	***	***	***	***
Mean Forest Fire C Emissions per Unit BA in Ecoregions of Pyrome (g C m^{-2})	1587	962	705	603	1273	888	659	1521	1801	941	1090	1092	
Median Forest Fire C Emissions per Unit BA in Ecoregions of Pyrome (g C m^{-2})	1204	604	504	446	895	870	612	1461	1295	767	876	970	
Mean Relative Change in Forest Fire C Emissions per Unit BA in Ecoregions of Pyrome (%)	12	30	-10	15	-7	-7	10	23	-12	7	17	20	
Median Relative Change in Forest Fire C Emissions per Unit BA in Ecoregions of Pyrome (%)	10	20	0	0	-10	0	0	16	-13	5	8	22	
# Ecoregions of Pyrome with Increased Forest Fire C Emissions per Unit BA	25	31	10	19	10	11	11	21	10	25	17	21	
of which significant	14	23	6	11	8	4	9	16	7	17	11	17	
# Ecoregions of Pyrome with Decreased Forest Fire C Emissions per Unit BA	18	8	17	12	17	11	11	4	26	17	5	8	
of which significant	7	5	8	0	9	5	8	3	13	9	2	5	

Table S2: Summary statistics describing the mean annual values of several climate variables for each pyrome and their change during the period 2001-2023 (2010-2021 for lightning density). The values shown are the mean or median values of the stated variable across all constituent ecoregions of each pyrome, as indicated in the square parentheses. The number of ecoregions with increasing or decreasing trends are also shown for each variable. The distributions of values across ecoregions for each pyrome are shown in **Fig. S13-S17**.

Variable	Statistic	ExTropF1	ExTropF2	ExTrop3	ExTropF4	SubTropF1	SubTropF2	SubTropF3	TropF1	TropF2	TropF3	SupZoF1	SupZoF2
Ecoregion Count													
# Ecoregions	Count of ecoregions	46	48	40	45	27	22	24	26	37	43	25	31
Extreme Fire Weather Days (FWI95d) during the Fire Season (95th Percentile Days)													
Mean Annual FWI95d (days year^{-1})	Mean across ecoregions	18	18	13	14	16	14	16	25	16	18	15	21
Mean Annual FWI95d (days year^{-1})	Median across ecoregions	18	19	12	11	17	14	16	24	14	19	14	20
Absolute Change in Annual FWI95d (days year^{-1})	Mean across ecoregions	2	5	1	4	2	-4	2	15	2	5	2	7
Absolute Change in Annual FWI95d (days year^{-1})	Median across ecoregions	2	6	-1	1	0	-4	-2	12	-1	2	0	5
Relative Change in Annual FWI95d (%)	Mean across ecoregions	9	26	-3	15	2	-25	-6	47	-4	19	2	23
Relative Change in Annual FWI95d (%)	Median across ecoregions	12	31	-12	13	-1	-26	-13	60	-10	11	3	26
# Ecoregions of Pyrome with Increased FWI95d	Count of ecoregions	24	30	16	25	10	4	10	18	13	24	13	21
of which significant	Count of ecoregions	16	20	10	15	6	0	5	17	6	12	6	12
# Ecoregions of Pyrome with Decreased FWI95d	Count of ecoregions	21	16	19	16	10	18	12	7	17	15	12	9
of which significant	Count of ecoregions	7	6	7	5	5	8	7	1	9	4	6	3
Normalised Difference Vegetation Index during the Growing Season													
Mean Annual NDVI (unitless)	Mean across ecoregions	0.64	0.60	0.65	0.61	0.68	0.65	0.63	0.76	0.72	0.68	0.62	0.62
Mean Annual NDVI (unitless)	Median across ecoregions	0.65	0.61	0.67	0.63	0.68	0.65	0.65	0.76	0.74	0.70	0.62	0.64
Absolute Change in Annual NDVI (unitless)	Mean across ecoregions	0.03	0.03	0.04	0.04	0.02	0.05	0.03	0.01	0.02	0.02	0.04	0.02
Absolute Change in Annual NDVI (unitless)	Median across ecoregions	0.03	0.02	0.04	0.04	0.02	0.05	0.02	0.01	0.02	0.02	0.03	0.02
Relative Change in Annual NDVI (%)	Mean across ecoregions	4.7	4.5	5.7	6.7	2.9	8.3	4.5	1.1	2.7	2.9	6.1	4.2
Relative Change in Annual NDVI (%)	Median across ecoregions	3.8	3.9	5.4	5.8	2.7	8.2	3.2	1.1	2.4	2.5	5.0	2.9
# Ecoregions of Pyrome with Increased NDVI	Count of ecoregions	45	44	37	42	21	22	21	20	34	39	23	26
of which significant	Count of ecoregions	44	43	35	39	19	22	20	19	31	38	23	24
# Ecoregions of Pyrome with Decreased NDVI	Count of ecoregions	1	3	3	3	6	0	3	6	3	4	3	4
of which significant	Count of ecoregions	0	0	1	0	0	0	0	1	1	0	1	2
Soil Moisture Content during the Fire Season													
Mean Annual Soil Moisture (m^3 water m^{-3} soil)	Mean across ecoregions	0.319	0.310	0.331	0.300	0.313	0.280	0.265	0.364	0.365	0.320	0.235	0.258
Mean Annual Soil Moisture (m^3 water m^{-3} soil)	Median across ecoregions	0.303	0.306	0.341	0.326	0.326	0.279	0.260	0.367	0.370	0.320	0.222	0.257
Absolute Change in Annual Soil Moisture (m^3 water m^{-3} soil)	Mean across ecoregions	-0.001	-0.009	0.009	0.000	0.009	0.001	0.000	-0.018	0.008	-0.001	0.003	-0.004
Absolute Change in Annual Soil Moisture (m^3 water m^{-3} soil)	Median across ecoregions	0.000	-0.005	0.005	0.000	0.007	0.000	0.003	-0.015	0.010	-0.001	-0.001	-0.005
Relative Change in Annual Soil Moisture (%)	Mean across ecoregions	-0.3	-2.8	2.5	-0.5	3.3	0.5	0.4	-5.2	2.1	-0.3	1.0	-1.5
Relative Change in Annual Soil Moisture (%)	Median across ecoregions	0.1	-1.7	1.5	-0.2	2.9	0.0	1.1	-3.7	3.1	-0.4	0.0	-2.1
# Ecoregions of Pyrome with Increased Soil Moisture	Count of ecoregions	24	15	28	21	17	11	14	6	22	19	13	10

Variable	Statistic	ExTropF1	ExTropF2	ExTrop3	ExTropF4	SubTropF1	SubTropF2	SubTropF3	TropF1	TropF2	TropF3	SupZoF1	SupZoF2
of which significant	Count of ecoregions	8	3	13	9	10	3	5	1	18	6	6	1
# Ecoregions of Pyrome with Decreased Soil Moisture	Count of ecoregions	22	33	12	24	10	11	10	20	15	24	13	20
of which significant	Count of ecoregions	8	20	5	11	5	2	5	17	7	11	6	7
Lightning Density during the Fire Season (2010-2021 only)													
Mean Annual Lightning Density (flashes km^{-2} $year^{-1}$)	Mean across ecoregions	0.204	0.185	0.248	0.165	1.086	0.371	0.478	0.478	0.688	0.729	0.347	0.905
Mean Annual Lightning Density (flashes km^{-2} $year^{-1}$)	Median across ecoregions	0.064	0.061	0.087	0.028	0.802	0.324	0.200	0.432	0.342	0.552	0.107	0.324
Absolute Change in Annual Lightning Density (flashes km^{-2} $year^{-1}$)	Mean across ecoregions	0.052	0.083	0.019	0.046	-0.077	-0.004	0.141	0.118	-0.129	0.074	0.050	-0.001
Absolute Change in Annual Lightning Density (flashes km^{-2} $year^{-1}$)	Median across ecoregions	0.019	0.012	0.007	0.002	-0.056	0.055	0.019	0.093	-0.021	0.002	0.011	0.031
Relative Change in Annual Lightning Density (%)	Mean across ecoregions	53.9	39.3	38.4	32.9	-17.2	15.9	11.8	18.0	-3.7	7.1	10.9	15.4
Relative Change in Annual Lightning Density (%)	Median across ecoregions	64.9	43.3	56.7	27.9	-17.8	11.4	12.3	18.8	-10.3	2.4	17.8	12.3
# Ecoregions of Pyrome with Increased Lightning Density	Count of ecoregions	36	35	25	27	11	14	17	20	15	23	16	19
of which significant	Count of ecoregions	25	22	18	14	3	7	3	8	6	7	7	3
# Ecoregions of Pyrome with Decreased Lightning Density	Count of ecoregions	10	12	15	16	16	8	7	6	22	20	10	11
of which significant	Count of ecoregions	3	5	4	2	9	4	2	3	7	5	4	3

References and Notes

1. L. T. Kelly, K. M. Giljohann, A. Duane, N. Aquilué, S. Archibald, E. Batllori, A. F. Bennett, S. T. Buckland, Q. Canelles, M. F. Clarke, M.-J. Fortin, V. Hermoso, S. Herrando, R. E. Keane, F. K. Lake, M. A. McCarthy, A. Morán-Ordóñez, C. L. Parr, J. G. Pausas, T. D. Penman, A. Regos, L. Rumpff, J. L. Santos, A. L. Smith, A. D. Syphard, M. W. Tingley, L. Brotons, Fire and biodiversity in the Anthropocene. *Science* **370**, eabb0355 (2020). doi:10.1126/science.abb0355 Medline

2. D. M. J. S. Bowman, J. K. Balch, P. Artaxo, W. J. Bond, J. M. Carlson, M. A. Cochrane, C. M. D'Antonio, R. S. Defries, J. C. Doyle, S. P. Harrison, F. H. Johnston, J. E. Keeley, M. A. Krawchuk, C. A. Kull, J. B. Marston, M. A. Moritz, I. C. Prentice, C. I. Roos, A. C. Scott, T. W. Swetnam, G. R. van der Werf, S. J. Pyne, Fire in the Earth system. *Science* **324**, 481–484 (2009). doi:10.1126/science.1163886 Medline

3. G. Lasslop, S. Hantson, S. P. Harrison, D. Bachelet, C. Burton, M. Forkel, M. Forrest, F. Li, J. R. Melton, C. Yue, S. Archibald, S. Scheiter, A. Arneth, T. Hickler, S. Sitch, Global ecosystems and fire: Multi-model assessment of fire-induced tree-cover and carbon storage reduction. *Glob. Change Biol.* **26**, 5027–5041 (2020). doi:10.1111/gcb.15160 Medline

4. W. M. Jolly, M. A. Cochrane, P. H. Freeborn, Z. A. Holden, T. J. Brown, G. J. Williamson, D. M. J. S. Bowman, Climate-induced variations in global wildfire danger from 1979 to 2013. *Nat. Commun.* **6**, 7537 (2015). doi:10.1038/ncomms8537 Medline

5. J. T. Abatzoglou, A. P. Williams, Impact of anthropogenic climate change on wildfire across western US forests. *Proc. Natl. Acad. Sci. U.S.A.* **113**, 11770–11775 (2016). doi:10.1073/pnas.1607171113 Medline

6. M. W. Jones, J. T. Abatzoglou, S. Veraverbeke, N. Andela, G. Lasslop, M. Forkel, A. J. P. Smith, C. Burton, R. A. Betts, G. R. van der Werf, S. Sitch, J. G. Canadell, C. Santín, C. Kolden, S. H. Doerr, C. L. Quéré, Global and Regional Trends and Drivers of Fire Under Climate Change. *Reviews of Geophysics* **60**, e2020RG000726 (2022). doi:10.1029/2020RG000726

7. United Nations Environment Programme, "Spreading like Wildfire – The Rising Threat of Extraordinary Landscape Fires" (UNEP, 2022); https://www.unep.org/resources/report/spreading-wildfire-rising-threat-extraordinary-landscape-fires.

8. B. Zheng, P. Ciais, F. Chevallier, E. Chuvieco, Y. Chen, H. Yang, Increasing forest fire emissions despite the decline in global burned area. *Sci. Adv.* **7**, eabh2646 (2021). doi:10.1126/sciadv.abh2646 Medline

9. J. G. Canadell, C. P. M. Meyer, G. D. Cook, A. Dowdy, P. R. Briggs, J. Knauer, A. Pepler, V. Haverd, Multi-decadal increase of forest burned area in Australia is linked to climate change. *Nat. Commun.* **12**, 6921 (2021). doi:10.1038/s41467-021-27225-4 Medline

10. A. P. Williams, J. T. Abatzoglou, A. Gershunov, J. Guzman-Morales, D. A. Bishop, J. K. Balch, D. P. Lettenmaier, Observed Impacts of Anthropogenic Climate Change on Wildfire in California. *Earths Futur.* **7**, 892–910 (2019). doi:10.1029/2019EF001210

11. E. Ponomarev, N. Yakimov, T. Ponomareva, O. Yakubailik, S. G. Conard, Current Trend of Carbon Emissions from Wildfires in Siberia. *Atmosphere* **12**, 559 (2021). doi:10.3390/atmos12050559

12. S. A. Parks, J. T. Abatzoglou, Warmer and Drier Fire Seasons Contribute to Increases in Area Burned at High Severity in Western US Forests From 1985 to 2017. *Geophys. Res. Lett.* **47**, e2020GL089858 (2020). doi:10.1029/2020GL089858

13. L. V. Gatti, L. S. Basso, J. B. Miller, M. Gloor, L. Gatti Domingues, H. L. G. Cassol, G. Tejada, L. E. O. C. Aragão, C. Nobre, W. Peters, L. Marani, E. Arai, A. H. Sanches, S. M. Corrêa, L. Anderson, C. Von Randow, C. S. C. Correia, S. P. Crispim, R. A. L. Neves, Amazonia as a carbon source linked to deforestation and climate change. *Nature* **595**, 388–393 (2021). doi:10.1038/s41586-021-03629-6 Medline

14. J. R. Marlon, P. J. Bartlein, D. G. Gavin, C. J. Long, R. S. Anderson, C. E. Briles, K. J. Brown, D. Colombaroli, D. J. Hallett, M. J. Power, E. A. Scharf, M. K. Walsh, Long-term perspective on wildfires in the western USA. *Proc. Natl. Acad. Sci. U.S.A.* **109**, E535–E543 (2012). doi:10.1073/pnas.1112839109 Medline

15. N. Andela, D. C. Morton, L. Giglio, Y. Chen, G. R. van der Werf, P. S. Kasibhatla, R. S. DeFries, G. J. Collatz, S. Hantson, S. Kloster, D. Bachelet, M. Forrest, G. Lasslop, F. Li, S. Mangeon, J. R. Melton, C. Yue, J. T. Randerson, A human-driven decline in global burned area. *Science* **356**, 1356–1362 (2017). doi:10.1126/science.aal4108 Medline

16. B. Zheng, P. Ciais, F. Chevallier, H. Yang, J. G. Canadell, Y. Chen, I. R. van der Velde, I. Aben, E. Chuvieco, S. J. Davis, M. Deeter, C. Hong, Y. Kong, H. Li, H. Li, X. Lin, K. He, Q. Zhang, Record-high CO_2 emissions from boreal fires in 2021. *Science* **379**, 912–917 (2023). doi:10.1126/science.ade0805 Medline

17. I. R. van der Velde, G. R. van der Werf, S. Houweling, J. D. Maasakkers, T. Borsdorff, J. Landgraf, P. Tol, T. A. van Kempen, R. van Hees, R. Hoogeveen, J. P. Veefkind, I. Aben, Vast CO_2 release from Australian fires in 2019-2020 constrained by satellite. *Nature* **597**, 366–369 (2021). doi:10.1038/s41586-021-03712-y Medline

18. P. E. Higuera, J. T. Abatzoglou, Record-setting climate enabled the extraordinary 2020 fire season in the western United States. *Glob. Change Biol.* **27**, 1–2 (2021). doi:10.1111/gcb.15388 Medline

19. M. W. Jones, D. I. Kelley, C. A. Burton, F. Di Giuseppe, M. L. F. Barbosa, E. Brambleby, A. J. Hartley, A. Lombardi, G. Mataveli, J. R. McNorton, F. R. Spuler, J. B. Wessel, J. T. Abatzoglou, L. O. Anderson, N. Andela, S. Archibald, D. Armenteras, E. Burke, R. Carmenta, E. Chuvieco, H. Clarke, S. H. Doerr, P. M. Fernandes, L. Giglio, D. S. Hamilton, S. Hantson, S. Harris, P. Jain, C. A. Kolden, T. Kurvits, S. Lampe, S. Meier, S. New, M. Parrington, M. M. G. Perron, Y. Qu, N. S. Ribeiro, B. H. Saharjo, J. San-Miguel-Ayanz, J. K. Shuman, V. Tanpipat, G. R. van der Werf, S. Veraverbeke, G. Xanthopoulos, State of Wildfires 2023–2024. *Earth Syst. Sci. Data* **16**, 3601–3685 (2024). doi:10.5194/essd-16-3601-2024

20. M. Ward, A. I. T. Tulloch, J. Q. Radford, B. A. Williams, A. E. Reside, S. L. Macdonald, H. J. Mayfield, M. Maron, H. P. Possingham, S. J. Vine, J. L. O'Connor, E. J. Massingham, A. C. Greenville, J. C. Z. Woinarski, S. T. Garnett, M. Lintermans, B. C. Scheele, J. Carwardine, D. G. Nimmo, D. B. Lindenmayer, R. M. Kooyman, J. S. Simmonds, L. J.

Sonter, J. E. M. Watson, Impact of 2019-2020 mega-fires on Australian fauna habitat. *Nat. Ecol. Evol.* **4**, 1321–1326 (2020). doi:10.1038/s41559-020-1251-1 Medline

21. D. B. Lindenmayer, C. Taylor, New spatial analyses of Australian wildfires highlight the need for new fire, resource, and conservation policies. *Proc. Natl. Acad. Sci. U.S.A.* **117**, 12481–12485 (2020). doi:10.1073/pnas.2002269117 Medline

22. C. Yue, P. Ciais, D. Zhu, T. Wang, S. S. Peng, S. L. Piao, How have past fire disturbances contributed to the current carbon balance of boreal ecosystems? *Biogeosciences* **13**, 675–690 (2016). doi:10.5194/bg-13-675-2016

23. S. P. Harrison, P. J. Bartlein, V. Brovkin, S. Houweling, S. Kloster, I. C. Prentice, The biomass burning contribution to climate–carbon-cycle feedback. *Earth Syst. Dyn.* **9**, 663–677 (2018). doi:10.5194/esd-9-663-2018

24. D. M. J. S. Bowman, G. J. Williamson, O. F. Price, M. N. Ndalila, R. A. Bradstock, Australian forests, megafires and the risk of dwindling carbon stocks. *Plant Cell Environ.* **44**, 347–355 (2021). doi:10.1111/pce.13916 Medline

25. C. A. Phillips, B. M. Rogers, M. Elder, S. Cooperdock, M. Moubarak, J. T. Randerson, P. C. Frumhoff, Escalating carbon emissions from North American boreal forest wildfires and the climate mitigation potential of fire management. *Sci. Adv.* **8**, eabl7161 (2022). doi:10.1126/sciadv.abl7161 Medline

26. D. M. J. S. Bowman, G. J. Williamson, J. T. Abatzoglou, C. A. Kolden, M. A. Cochrane, A. M. S. Smith, Human exposure and sensitivity to globally extreme wildfire events. *Nat Ecol Evol* **1**, 0058 (2017). doi:10.1038/s41559-016-0058

27. D. Wang, D. Guan, S. Zhu, M. M. Kinnon, G. Geng, Q. Zhang, H. Zheng, T. Lei, S. Shao, P. Gong, S. J. Davis, Economic footprint of California wildfires in 2018. *Nat. Sustain.* **4**, 252–260 (2021). doi:10.1038/s41893-020-00646-7

28. F. H. Johnston, N. Borchers-Arriagada, G. G. Morgan, B. Jalaludin, A. J. Palmer, G. J. Williamson, D. M. J. S. Bowman, Unprecedented health costs of smoke-related PM2.5 from the 2019–20 Australian megafires. *Nat. Sustain.* **4**, 42–47 (2021). doi:10.1038/s41893-020-00610-5

29. H. Clarke, R. H. Nolan, V. R. De Dios, R. Bradstock, A. Griebel, S. Khanal, M. M. Boer, Forest fire threatens global carbon sinks and population centres under rising atmospheric water demand. *Nat. Commun.* **13**, 7161 (2022). doi:10.1038/s41467-022-34966-3 Medline

30. World Bank Group, "World Bank Policy Note: Managing Wildfires in a Changing Climate" (WBG, 2020); https://www.profor.info/sites/default/files/PROFOR_ManagingWildfires_2020_final.pdf

31. J. T. Abatzoglou, A. P. Williams, R. Barbero, Global Emergence of Anthropogenic Climate Change in Fire Weather Indices. *Geophys. Res. Lett.* **46**, 326–336 (2019). doi:10.1029/2018GL080959

32. J. T. Abatzoglou, C. A. Kolden, J. K. Balch, B. A. Bradley, Controls on interannual variability in lightning-caused fire activity in the western US. *Environ. Res. Lett.* **11**, 045005 (2016). doi:10.1088/1748-9326/11/4/045005

33. S. Veraverbeke, B. M. Rogers, M. L. Goulden, R. R. Jandt, C. E. Miller, E. B. Wiggins, J. T. Randerson, Lightning as a major driver of recent large fire years in North American boreal forests. *Nat. Clim. Chang.* **7**, 529–534 (2017). doi:10.1038/nclimate3329

34. T. A. J. Janssen, M. W. Jones, D. Finney, G. R. van der Werf, D. van Wees, W. Xu, S. Veraverbeke, Extratropical forests increasingly at risk due to lightning fires. *Nat. Geosci.* **16**, 1136–1144 (2023). doi:10.1038/s41561-023-01322-z

35. G. A. Mills, W. L. McCaw, Centre for Australian Weather and Climate Research, "Atmospheric Stability Environments and Fire Weather in Australia: Extending the Haines Index" (CAWCR Technical report no. 20, 2010).

36. G. Di Virgilio, J. P. Evans, S. A. P. Blake, M. Armstrong, A. J. Dowdy, J. Sharples, R. McRae, Climate Change Increases the Potential for Extreme Wildfires. *Geophys. Res. Lett.* **46**, 8517–8526 (2019). doi:10.1029/2019GL083699

37. G. J. van Oldenborgh, F. Krikken, S. Lewis, N. J. Leach, F. Lehner, K. R. Saunders, M. van Weele, K. Haustein, S. Li, D. Wallom, S. Sparrow, J. Arrighi, R. K. Singh, M. K. van Aalst, S. Y. Philip, R. Vautard, F. E. L. Otto, Attribution of the Australian bushfire risk to anthropogenic climate change. *Nat. Hazards Earth Syst. Sci.* **21**, 941–960 (2021). doi:10.5194/nhess-21-941-2021

38. M. C. Kirchmeier-Young, F. W. Zwiers, N. P. Gillett, A. J. Cannon, Attributing extreme fire risk in Western Canada to human emissions. *Clim. Change* **144**, 365–379 (2017). doi:10.1007/s10584-017-2030-0 Medline

39. J. G. Pausas, J. E. Keeley, Wildfires and global change. *Front. Ecol. Environ.* **19**, 387–395 (2021). doi:10.1002/fee.2359

40. D. I. Kelley, I. Bistinas, R. Whitley, C. Burton, T. R. Marthews, N. Dong, How contemporary bioclimatic and human controls change global fire regimes. *Nat. Clim. Chang.* **9**, 690–696 (2019). doi:10.1038/s41558-019-0540-7

41. D. M. J. S. Bowman, C. A. Kolden, J. T. Abatzoglou, F. H. Johnston, G. R. van der Werf, M. Flannigan, Vegetation fires in the Anthropocene. *Nat. Rev. Earth Environ.* **1**, 500–515 (2020). doi:10.1038/s43017-020-0085-3

42. N. J. Abram, B. J. Henley, A. Sen Gupta, T. J. R. Lippmann, H. Clarke, A. J. Dowdy, J. J. Sharples, R. H. Nolan, T. Zhang, M. J. Wooster, J. B. Wurtzel, K. J. Meissner, A. J. Pitman, A. M. Ukkola, B. P. Murphy, N. J. Tapper, M. M. Boer, Connections of climate change and variability to large and extreme forest fires in southeast Australia. *Commun. Earth Environ.* **2**, 8 (2021). doi:10.1038/s43247-020-00065-8

43. L. E. O. C. Aragão, L. O. Anderson, M. G. Fonseca, T. M. Rosan, L. B. Vedovato, F. H. Wagner, C. V. J. Silva, C. H. L. Silva Junior, E. Arai, A. P. Aguiar, J. Barlow, E. Berenguer, M. N. Deeter, L. G. Domingues, L. Gatti, M. Gloor, Y. Malhi, J. A. Marengo, J. B. Miller, O. L. Phillips, S. Saatchi, 21st Century drought-related fires counteract the decline of Amazon deforestation carbon emissions. *Nat. Commun.* **9**, 536 (2018). doi:10.1038/s41467-017-02771-y Medline

44. J. K. Balch, B. A. Bradley, J. T. Abatzoglou, R. C. Nagy, E. J. Fusco, A. L. Mahood, Human-started wildfires expand the fire niche across the United States. *Proc. Natl. Acad. Sci. U.S.A.* **114**, 2946–2951 (2017). doi:10.1073/pnas.1617394114 Medline

45. P. M. Fernandes, A. P. Pacheco, R. Almeida, J. Claro, The role of fire-suppression force in limiting the spread of extremely large forest fires in Portugal. *Eur. J. For. Res.* **135**, 253–262 (2016). doi:10.1007/s10342-015-0933-8

46. F. Moreira, D. Ascoli, H. Safford, M. A. Adams, J. M. Moreno, J. M. C. Pereira, F. X. Catry, J. Armesto, W. Bond, M. E. González, T. Curt, N. Koutsias, L. McCaw, O. Price, J. G. Pausas, E. Rigolot, S. Stephens, C. Tavsanoglu, V. R. Vallejo, B. W. Van Wilgen, G. Xanthopoulos, P. M. Fernandes, Wildfire management in Mediterranean-type regions: Paradigm change needed. *Environ. Res. Lett.* **15**, 011001 (2020). doi:10.1088/1748-9326/ab541e

47. R. A. Bradstock, M. M. Boer, G. J. Cary, O. F. Price, R. J. Williams, D. Barrett, G. Cook, A. M. Gill, L. B. W. Hutley, H. Keith, S. W. Maier, M. Meyer, S. H. Roxburgh, J. Russell-Smith, Modelling the potential for prescribed burning to mitigate carbon emissions from wildfires in fire-prone forests of Australia. *Int. J. Wildland Fire* **21**, 629–639 (2012). doi:10.1071/WF11023

48. C. H. L. Silva Junior, L. E. O. C. Aragão, L. O. Anderson, M. G. Fonseca, Y. E. Shimabukuro, C. Vancutsem, F. Achard, R. Beuchle, I. Numata, C. A. Silva, E. E. Maeda, M. Longo, S. S. Saatchi, Persistent collapse of biomass in Amazonian forest edges following deforestation leads to unaccounted carbon losses. *Sci. Adv.* **6**, eaaz8360 (2020). doi:10.1126/sciadv.aaz8360 Medline

49. T. M. Rosan, S. Sitch, L. M. Mercado, V. Heinrich, P. Friedlingstein, L. E. O. C. Aragão, Fragmentation-Driven Divergent Trends in Burned Area in Amazonia and Cerrado. *Front. For. Glob. Change* **5**, 801408 (2022). doi:10.3389/ffgc.2022.801408

50. M.-A. Parisien, Q. E. Barber, K. G. Hirsch, C. A. Stockdale, S. Erni, X. Wang, D. Arseneault, S. A. Parks, Fire deficit increases wildfire risk for many communities in the Canadian boreal forest. *Nat. Commun.* **11**, 2121 (2020). doi:10.1038/s41467-020-15961-y Medline

51. B. M. Rogers, A. J. Soja, M. L. Goulden, J. T. Randerson, Influence of tree species on continental differences in boreal fires and climate feedbacks. *Nat. Geosci.* **8**, 228–234 (2015). doi:10.1038/ngeo2352

52. M. L. Pettinari, E. Chuvieco, Generation of a global fuel data set using the Fuel Characteristic Classification System. *Biogeosciences* **13**, 2061–2076 (2016). doi:10.5194/bg-13-2061-2016

53. M. Forkel, N. Andela, S. P. Harrison, G. Lasslop, M. van Marle, E. Chuvieco, W. Dorigo, M. Forrest, S. Hantson, A. Heil, F. Li, J. Melton, S. Sitch, C. Yue, A. Arneth, Emergent relationships with respect to burned area in global satellite observations and fire-enabled vegetation models. *Biogeosciences* **16**, 57–76 (2019). doi:10.5194/bg-16-57-2019

54. J. T. Abatzoglou, A. P. Williams, L. Boschetti, M. Zubkova, C. A. Kolden, Global patterns of interannual climate-fire relationships. *Glob. Change Biol.* **24**, 5164–5175 (2018). doi:10.1111/gcb.14405 Medline

55. M. Forkel, W. Dorigo, G. Lasslop, I. Teubner, E. Chuvieco, K. Thonicke, A data-driven approach to identify controls on global fire activity from satellite and climate

observations (SOFIA V1). *Geosci. Model Dev.* **10**, 4443–4476 (2017). doi:10.5194/gmd-10-4443-2017

56. E. Chuvieco, M. L. Pettinari, N. Koutsias, M. Forkel, S. Hantson, M. Turco, Human and climate drivers of global biomass burning variability. *Sci. Total Environ.* **779**, 146361 (2021). doi:10.1016/j.scitotenv.2021.146361 Medline

57. D. M. Olson, E. Dinerstein, E. D. Wikramanayake, N. D. Burgess, G. V. N. Powell, E. C. Underwood, J. A. D'amico, I. Itoua, H. E. Strand, J. C. Morrison, C. J. Loucks, T. F. Allnutt, T. H. Ricketts, Y. Kura, J. F. Lamoreux, W. W. Wettengel, P. Hedao, K. R. Kassem, Terrestrial Ecoregions of the World: A New Map of Life on Earth. *Bioscience* **51**, 933 (2001). doi:10.1641/0006-3568(2001)051[0933:TEOTWA]2.0.CO;2

58. L. Giglio, L. Boschetti, D. P. Roy, M. L. Humber, C. O. Justice, The Collection 6 MODIS burned area mapping algorithm and product. *Remote Sens. Environ.* **217**, 72–85 (2018). doi:10.1016/j.rse.2018.08.005 Medline

59. D. van Wees, G. R. van der Werf, J. T. Randerson, B. M. Rogers, Y. Chen, S. Veraverbeke, L. Giglio, D. C. Morton, Global biomass burning fuel consumption and emissions at 500 m spatial resolution based on the Global Fire Emissions Database (GFED). *Geosci. Model Dev.* **15**, 8411–8437 (2022). doi:10.5194/gmd-15-8411-2022

60. C. E. Van Wagner, "Development and Structure of the Canadian Forest Fire Weather Index System" (Canadian Forestry Service, Forestry Technical Report 351987, 1987); https://cfs.nrcan.gc.ca:443/publications?id=19927.

61. C. Vitolo, F. Di Giuseppe, C. Barnard, R. Coughlan, J. San-Miguel-Ayanz, G. Libertá, B. Krzeminski, ERA5-based global meteorological wildfire danger maps. *Sci. Data* **7**, 216 (2020). doi:10.1038/s41597-020-0554-z Medline

62. J. Muñoz-Sabater, E. Dutra, A. Agustí-Panareda, C. Albergel, G. Arduini, G. Balsamo, S. Boussetta, M. Choulga, S. Harrigan, H. Hersbach, B. Martens, D. G. Miralles, M. Piles, N. J. Rodríguez-Fernández, E. Zsoter, C. Buontempo, J.-N. Thépaut, ERA5-Land: A state-of-the-art global reanalysis dataset for land applications. *Earth Syst. Sci. Data* **13**, 4349–4383 (2021). doi:10.5194/essd-13-4349-2021

63. R. H. Holzworth, J. B. Brundell, M. P. McCarthy, A. R. Jacobson, C. J. Rodger, T. S. Anderson, Lightning in the Arctic. *Geophys. Res. Lett.* **48**, e2020GL091366 (2021). doi:10.1029/2020GL091366

64. A. Huete, K. Didan, T. Miura, E. P. Rodriguez, X. Gao, L. G. Ferreira, Overview of the radiometric and biophysical performance of the MODros. Inf. Serv. vegetation indices. *Remote Sens. Environ.* **83**, 195–213 (2002). doi:10.1016/S0034-4257(02)00096-2

65. K. Didan, MOD13A3 - MODIS/Terra Vegetation Indices Monthly L3 Global 1km SIN Grid, NASA LP DAAC (2021); http://doi.org/10.5067/MODIS/MOD13A3.006.

66. J. E. Dobson, E. A. Bright, P. R. Coleman, R. C. Durfee, B. A. Worley, LandScan: A global population database for estimating populations at risk. *Photogramm. Eng. Remote Sensing* **66**, 849–857 (2000).

67. M. Friedl, D. Sulla-Menashe, MCD12Q1 - MODIS/Terra+Aqua Land Cover Type Yearly L3 Global 500m SIN Grid, NASA LP DAAC (2019); http://doi.org/10.5067/MODIS/MCD12Q1.006.

68. T. P. Robinson, G. R. W. Wint, G. Conchedda, T. P. Van Boeckel, V. Ercoli, E. Palamara, G. Cinardi, L. D'Aietti, S. I. Hay, M. Gilbert, Mapping the global distribution of livestock. *PLOS ONE* **9**, e96084 (2014). doi:10.1371/journal.pone.0096084 Medline

69. J. R. Meijer, M. A. J. Huijbregts, K. C. G. J. Schotten, A. M. Schipper, Global patterns of current and future road infrastructure. *Environ. Res. Lett.* **13**, 064006 (2018). doi:10.1088/1748-9326/aabd42

70. G. Amatulli, D. McInerney, T. Sethi, P. Strobl, S. Domisch, Geomorpho90m, empirical evaluation and accuracy assessment of global high-resolution geomorphometric layers. *Sci. Data* **7**, 162 (2020). doi:10.1038/s41597-020-0479-6 Medline

71. S. Archibald, C. E. R. Lehmann, J. L. Gómez-Dans, R. A. Bradstock, Defining pyromes and global syndromes of fire regimes. *Proc. Natl. Acad. Sci. U.S.A.* **110**, 6442–6447 (2013). doi:10.1073/pnas.1211466110 Medline

72. M. E. Cattau, A. L. Mahood, J. K. Balch, C. A. Wessman, Modern Pyromes: Biogeographical Patterns of Fire Characteristics across the Contiguous United States. *Fire* **5**, 95 (2022). doi:10.3390/fire5040095

73. M. García, M. L. Pettinari, E. Chuvieco, J. Salas, F. Mouillot, W. Chen, I. Aguado, Characterizing Global Fire Regimes from Satellite-Derived Products. *Forests* **13**, 699 (2022). doi:10.3390/f13050699

74. C. X. Cunningham, G. J. Williamson, R. H. Nolan, L. Teckentrup, M. M. Boer, D. M. J. S. Bowman, Pyrogeography in flux: Reorganization of Australian fire regimes in a hotter world. *Glob. Change Biol.* **30**, e17130 (2024). doi:10.1111/gcb.17130 Medline

75. M. Forkel, K. Thonicke, C. Beer, W. Cramer, S. Bartalev, C. Schmullius, Extreme fire events are related to previous-year surface moisture conditions in permafrost-underlain larch forests of Siberia. *Environ. Res. Lett.* **7**, 044021 (2012). doi:10.1088/1748-9326/7/4/044021

76. V. I. Kharuk, M. L. Dvinskaya, S. T. Im, A. S. Golyukov, K. T. Smith, Wildfires in the Siberian Arctic. *Fire (Basel)* **5**, 106 (2022). doi:10.3390/fire5040106

77. P. M. Brando, L. Paolucci, C. C. Ummenhofer, E. M. Ordway, H. Hartmann, M. E. Cattau, L. Rattis, V. Medjibe, M. T. Coe, J. Balch, Droughts, Wildfires, and Forest Carbon Cycling: A Pantropical Synthesis. *Annu. Rev. Earth Planet. Sci.* **47**, 555–581 (2019). doi:10.1146/annurev-earth-082517-010235

78. T. Nikonovas, A. Spessa, S. H. Doerr, G. D. Clay, S. Mezbahuddin, Near-complete loss of fire-resistant primary tropical forest cover in Sumatra and Kalimantan. *Commun. Earth Environ.* **1**, 1–8 (2020). doi:10.1038/s43247-020-00069-4

79. J. Barlow, E. Berenguer, R. Carmenta, F. França, Clarifying Amazonia's burning crisis. *Glob. Change Biol.* **26**, 319–321 (2020). doi:10.1111/gcb.14872 Medline

80. V. R. Pivello, The Use of Fire in the Cerrado and Amazonian Rainforests of Brazil: Past and Present. *Fire Ecol* **7**, 24–39 (2011). doi:10.4996/fireecology.0701024

81. R. D. Field, G. R. van der Werf, S. S. P. Shen, Human amplification of drought-induced biomass burning in Indonesia since 1960. *Nat. Geosci.* **2**, 185–188 (2009). doi:10.1038/ngeo443

82. P. G. Curtis, C. M. Slay, N. L. Harris, A. Tyukavina, M. C. Hansen, Classifying drivers of global forest loss. *Science* **361**, 1108–1111 (2018). doi:10.1126/science.aau3445 Medline

83. M. R. Rosa, P. H. S. Brancalion, R. Crouzeilles, L. R. Tambosi, P. R. Piffer, F. E. B. Lenti, M. Hirota, E. Santiami, J. P. Metzger, Hidden destruction of older forests threatens Brazil's Atlantic Forest and challenges restoration programs. *Sci. Adv.* **7**, eabc4547 (2021). doi:10.1126/sciadv.abc4547 Medline

84. J. C. Aleman, M. A. Jarzyna, A. C. Staver, Forest extent and deforestation in tropical Africa since 1900. *Nat. Ecol. Evol.* **2**, 26–33 (2018). doi:10.1038/s41559-017-0406-1 Medline

85. Y. Le Page, D. Oom, J. M. N. Silva, P. Jönsson, J. M. C. Pereira, Seasonality of vegetation fires as modified by human action: Observing the deviation from eco-climatic fire regimes. *Glob. Ecol. Biogeogr.* **19**, 575–588 (2010). doi:10.1111/j.1466-8238.2010.00525.x

86. M. Castellnou, N. Prat-Guitart, E. Arilla, A. Larrañaga, E. Nebot, X. Castellarnau, Empowering strategic decision-making for wildfire management: avoiding the fear trap and creating a resilient landscape. *Fire Ecol* **15**, 31 (2019). doi:10.1186/s42408-019-0048-6

87. H. Hesseln, Wildland Fire Prevention: A Review. *Curr. For. Rep.* **4**, 178–190 (2018). doi:10.1007/s40725-018-0083-6

88. J. T. Abatzoglou, D. S. Battisti, A. P. Williams, W. D. Hansen, B. J. Harvey, C. A. Kolden, Projected increases in western US forest fire despite growing fuel constraints. *Commun. Earth Environ.* **2**, 1–8 (2021). doi:10.1038/s43247-021-00299-0

89. H. Clarke, R. Gibson, B. Cirulis, R. A. Bradstock, T. D. Penman, Developing and testing models of the drivers of anthropogenic and lightning-caused wildfire ignitions in south-eastern Australia. *J. Environ. Manage.* **235**, 34–41 (2019). doi:10.1016/j.jenvman.2019.01.055 Medline

90. R. A. Bradstock, A biogeographic model of fire regimes in Australia: current and future implications: A biogeographic model of fire in Australia. *Glob. Ecol. Biogeogr.* **19**, 145–158 (2010). doi:10.1111/j.1466-8238.2009.00512.x

91. R. Rotbarth, E. H. Van Nes, M. Scheffer, J. U. Jepsen, O. P. L. Vindstad, C. Xu, M. Holmgren, Northern expansion is not compensating for southern declines in North American boreal forests. *Nat. Commun.* **14**, 3373 (2023). doi:10.1038/s41467-023-39092-2 Medline

92. L. T. Berner, S. J. Goetz, Satellite observations document trends consistent with a boreal forest biome shift. *Glob. Change Biol.* **28**, 3275–3292 (2022). doi:10.1111/gcb.16121 Medline

93. H. Yang, P. Ciais, F. Frappart, X. Li, M. Brandt, R. Fensholt, L. Fan, S. Saatchi, S. Besnard, Z. Deng, S. Bowring, J.-P. Wigneron, Global increase in biomass carbon stock dominated

by growth of northern young forests over past decade. *Nat. Geosci.* **16**, 886–892 (2023). doi:10.1038/s41561-023-01274-4

94. Y. Li, D. Sulla-Menashe, S. Motesharrei, X.-P. Song, E. Kalnay, Q. Ying, S. Li, Z. Ma, Inconsistent estimates of forest cover change in China between 2000 and 2013 from multiple datasets: Differences in parameters, spatial resolution, and definitions. *Sci. Rep.* **7**, 8748 (2017). doi:10.1038/s41598-017-07732-5 Medline

95. H. Yin, A. Khamzina, D. Pflugmacher, C. Martius, Forest cover mapping in post-Soviet Central Asia using multi-resolution remote sensing imagery. *Sci. Rep.* **7**, 1375 (2017). doi:10.1038/s41598-017-01582-x Medline

96. X. Wei, Y. Liu, L. Qi, J. Chen, G. Wang, L. Zhang, R. Liu, Monitoring forest dynamics in Africa during 2000–2020 using a remotely sensed fractional tree cover dataset. *Int. J. Digit. Earth* **16**, 2212–2232 (2023). doi:10.1080/17538947.2023.2220613

97. S. Piao, X. Wang, T. Park, C. Chen, X. Lian, Y. He, J. W. Bjerke, A. Chen, P. Ciais, H. Tømmervik, R. R. Nemani, R. B. Myneni, Characteristics, drivers and feedbacks of global greening. *Nat. Rev. Earth Environ.* **1**, 14–27 (2020). doi:10.1038/s43017-019-0001-x

98. Y. He, Y. Liu, L. Lei, C. Terrer, C. Huntingford, J. Peñuelas, H. Xu, S. Piao, CO_2 fertilization contributed more than half of the observed forest biomass increase in northern extra-tropical land. *Glob. Change Biol.* **29**, 4313–4326 (2023). doi:10.1111/gcb.16806 Medline

99. S. L. Lewis, D. P. Edwards, D. Galbraith, Increasing human dominance of tropical forests. *Science* **349**, 827–832 (2015). doi:10.1126/science.aaa9932 Medline

100. S. Archibald, Managing the human component of fire regimes: Lessons from Africa. *Philos. Trans. R. Soc. Lond. B Biol. Sci.* **371**, 20150346 (2016). doi:10.1098/rstb.2015.0346 Medline

101. Q. Xu, A. L. R. Westerling, A. Notohamiprodjo, C. Wiedinmyer, J. J. Picotte, S. A. Parks, M. D. Hurteau, M. E. Marlier, C. A. Kolden, J. A. Sam, W. J. Baldwin, C. Ade, Wildfire burn severity and emissions inventory: An example implementation over California. *Environ. Res. Lett.* **17**, 085008 (2022). doi:10.1088/1748-9326/ac80d0

102. E. A. Kukavskaya, E. G. Shvetsov, L. V. Buryak, P. D. Tretyakov, P. Y. Groisman, Increasing Fuel Loads, Fire Hazard, and Carbon Emissions from Fires in Central Siberia. *Fire (Basel)* **6**, 63 (2023). doi:10.3390/fire6020063

103. R. C. Scholten, D. Coumou, F. Luo, S. Veraverbeke, Early snowmelt and polar jet dynamics co-influence recent extreme Siberian fire seasons. *Science* **378**, 1005–1009 (2022). doi:10.1126/science.abn4419 Medline

104. E. I. Ponomarev, A. N. Zabrodin, E. G. Shvetsov, T. V. Ponomareva, Wildfire Intensity and Fire Emissions in Siberia. *Fire (Basel)* **6**, 246 (2023). doi:10.3390/fire6070246

105. T. D. Hessilt, J. T. Abatzoglou, Y. Chen, J. T. Randerson, R. C. Scholten, G. van der Werf, S. Veraverbeke, Future increases in lightning ignition efficiency and wildfire occurrence expected from drier fuels in boreal forest ecosystems of western North America. *Environ. Res. Lett.* **17**, 054008 (2022). doi:10.1088/1748-9326/ac6311

106. J. K. Shuman, J. K. Balch, R. T. Barnes, P. E. Higuera, C. I. Roos, D. W. Schwilk, E. N. Stavros, T. Banerjee, M. M. Bela, J. Bendix, S. Bertolino, S. Bililign, K. D. Bladon, P. Brando, R. E. Breidenthal, B. Buma, D. Calhoun, L. M. V. Carvalho, M. E. Cattau, K. M. Cawley, S. Chandra, M. L. Chipman, J. Cobian-Iñiguez, E. Conlisk, J. D. Coop, Al. Cullen, K. T. Davis, A. Dayalu, F. De Sales, M. Dolman, L. M. Ellsworth, S. Franklin, C. H. Guiterman, M. Hamilton, E. J. Hanan, W. D. Hansen, S. Hantson, B. J. Harvey, A. Holz, T. Huang, M. D. Hurteau, N. T. Ilangakoon, M. Jennings, C. Jones, A. Klimaszewski-Patterson, L. N. Kobziar, J. Kominoski, B. Kosovic, M. A. Krawchuk, P. Laris, J. Leonard, S. M. Loria-Salazar, M. Lucash, H. Mahmoud, E. Margolis, T. Maxwell, J. L. McCarty, D. B. McWethy, R. S. Meyer, J. R. Miesel, W. K. Moser, R. C. Nagy, D. Niyogi, H. M. Palmer, A. Pellegrini, B. Poulter, K. Robertson, A. V. Rocha, M. Sadegh, F. Santos, F. Scordo, J. O. Sexton, A. S. Sharma, A. M. S. Smith, A. J. Soja, C. Still, T. Swetnam, A. D. Syphard, M. W. Tingley, A. Tohidi, A. T. Trugman, M. Turetsky, J. M. Varner, Y. Wang, T. Whitman, S. Yelenik, X. Zhang,Reimagine fire science for the anthropocene. *PNAS Nexus*, **1** pgac115 (2022). doi:10.1093/pnasnexus/pgac115 Medline

107. M. A. Cochrane, D. M. J. S. Bowman, Manage fire regimes, not fires. *Nat. Geosci.* **14**, 455–457 (2021). doi:10.1038/s41561-021-00791-4

108. S. Bloem, A. C. Cullen, L. O. Mearns, J. T. Abatzoglou, The Role of International Resource Sharing Arrangements in Managing Fire in the Face of Climate Change. *Fire* **5**, 88 (2022). doi:10.3390/fire5040088

109. C. F. Starrs, V. Butsic, C. Stephens, W. Stewart, The impact of land ownership, firefighting, and reserve status on fire probability in California. *Environ. Res. Lett.* **13**, 034025 (2018). doi:10.1088/1748-9326/aaaad1

110. A. C. M. Pessôa, T. F. Morello, C. H. L. Silva-Junior, J. Doblas, N. S. Carvalho, L. E. O. C. Aragão, L. O. Anderson, Protected areas are effective on curbing fires in the Amazon. *Ecol. Econ.* **214**, 107983 (2023). doi:10.1016/j.ecolecon.2023.107983

111. C. C. Hanes, X. Wang, P. Jain, M.-A. Parisien, J. M. Little, M. D. Flannigan, Fire-regime changes in Canada over the last half century. *Can. J. For. Res.* **49**, 256–269 (2019). doi:10.1139/cjfr-2018-0293

112. P. Friedlingstein, M. O'Sullivan, M. W. Jones, R. M. Andrew, D. C. E. Bakker, J. Hauck, P. Landschützer, C. Le Quéré, I. T. Luijkx, G. P. Peters, W. Peters, J. Pongratz, C. Schwingshackl, S. Sitch, J. G. Canadell, P. Ciais, R. B. Jackson, S. R. Alin, P. Anthoni, L. Barbero, N. R. Bates, M. Becker, N. Bellouin, B. Decharme, L. Bopp, I. B. M. Brasika, P. Cadule, M. A. Chamberlain, N. Chandra, T.-T.-T. Chau, F. Chevallier, L. P. Chini, M. Cronin, X. Dou, K. Enyo, W. Evans, S. Falk, R. A. Feely, L. Feng, D. J. Ford, T. Gasser, J. Ghattas, T. Gkritzalis, G. Grassi, L. Gregor, N. Gruber, Ö. Gürses, I. Harris, M. Hefner, J. Heinke, R. A. Houghton, G. C. Hurtt, Y. Iida, T. Ilyina, A. R. Jacobson, A. Jain, T. Jarníková, A. Jersild, F. Jiang, Z. Jin, F. Joos, E. Kato, R. F. Keeling, D. Kennedy, K. Klein Goldewijk, J. Knauer, J. I. Korsbakken, A. Körtzinger, X. Lan, N. Lefèvre, H. Li, J. Liu, Z. Liu, L. Ma, G. Marland, N. Mayot, P. C. McGuire, G. A. McKinley, G. Meyer, E. J. Morgan, D. R. Munro, S.-I. Nakaoka, Y. Niwa, K. M. O'Brien, A. Olsen, A. M. Omar, T. Ono, M. Paulsen, D. Pierrot, K. Pocock, B. Poulter, C. M. Powis, G. Rehder, L. Resplandy, E. Robertson, C. Rödenbeck, T. M. Rosan, J.

Schwinger, R. Séférian, T. L. Smallman, S. M. Smith, R. Sospedra-Alfonso, Q. Sun, A. J. Sutton, C. Sweeney, S. Takao, P. P. Tans, H. Tian, B. Tilbrook, H. Tsujino, F. Tubiello, G. R. van der Werf, E. van Ooijen, R. Wanninkhof, M. Watanabe, C. Wimart-Rousseau, D. Yang, X. Yang, W. Yuan, X. Yue, S. Zaehle, J. Zeng, B. Zheng, Global Carbon Budget 2023. *Earth Syst. Sci. Data* **15**, 5301–5369 (2023). doi:10.5194/essd-15-5301-2023

113. S. Sitch, C. Huntingford, N. Gedney, P. E. Levy, M. Lomas, S. L. Piao, R. Betts, P. Ciais, P. Cox, P. Friedlingstein, C. D. Jones, I. C. Prentice, F. I. Woodward, Evaluation of the terrestrial carbon cycle, future plant geography and climate-carbon cycle feedbacks using five Dynamic Global Vegetation Models (DGVMs). *Glob. Change Biol.* **14**, 2015–2039 (2008). doi:10.1111/j.1365-2486.2008.01626.x

114. C.-E. Yang, J. Mao, F. M. Hoffman, D. M. Ricciuto, J. S. Fu, C. D. Jones, M. Thurner, Uncertainty Quantification of Extratropical Forest Biomass in CMIP5 Models over the Northern Hemisphere. *Sci. Rep.* **8**, 10962 (2018). doi:10.1038/s41598-018-29227-7 Medline

115. S. Kloster, G. Lasslop, Historical and future fire occurrence (1850 to 2100) simulated in CMIP5 Earth System Models. *Global Planet. Change* **150**, 58–69 (2017). doi:10.1016/j.gloplacha.2016.12.017

116. M. C. Mack, X. J. Walker, J. F. Johnstone, H. D. Alexander, A. M. Melvin, M. Jean, S. N. Miller, Carbon loss from boreal forest wildfires offset by increased dominance of deciduous trees. *Science* **372**, 280–283 (2021). doi:10.1126/science.abf3903 Medline

117. J. L. Baltzer, N. J. Day, X. J. Walker, D. Greene, M. C. Mack, H. D. Alexander, D. Arseneault, J. Barnes, Y. Bergeron, Y. Boucher, L. Bourgeau-Chavez, C. D. Brown, S. Carrière, B. K. Howard, S. Gauthier, M.-A. Parisien, K. A. Reid, B. M. Rogers, C. Roland, L. Sirois, S. Stehn, D. K. Thompson, M. R. Turetsky, S. Veraverbeke, E. Whitman, J. Yang, J. F. Johnstone, Increasing fire and the decline of fire adapted black spruce in the boreal forest. *Proc. Natl. Acad. Sci. U.S.A.* **118**, e2024872118 (2021). doi:10.1073/pnas.2024872118 Medline

118. M. S. Balshi, A. D. Mcguire, P. Duffy, M. Flannigan, D. W. Kicklighter, J. Melillo, Vulnerability of carbon storage in North American boreal forests to wildfires during the 21st century. *Glob. Change Biol.* **15**, 1491–1510 (2009). doi:10.1111/j.1365-2486.2009.01877.x

119. S. Schaphoff, C. P. O. Reyer, D. Schepaschenko, D. Gerten, A. Shvidenko, Tamm Review: Observed and projected climate change impacts on Russia's forests and its carbon balance. *For. Ecol. Manage.* **361**, 432–444 (2016). doi:10.1016/j.foreco.2015.11.043

120. M. R. Turetsky, E. S. Kane, J. W. Harden, R. D. Ottmar, K. L. Manies, E. Hoy, E. S. Kasischke, Recent acceleration of biomass burning and carbon losses in Alaskan forests and peatlands. *Nat. Geosci.* **4**, 27–31 (2011). doi:10.1038/ngeo1027

121. J. MacCarthy, A. Tyukavina, M. J. Weisse, N. Harris, E. Glen, Extreme wildfires in Canada and their contribution to global loss in tree cover and carbon emissions in 2023. *Glob. Change Biol.* **30**, e17392 (2024). doi:10.1111/gcb.17392 Medline

122. Government of Canada, “National inventory report: greenhouse gas sources and sinks in Canada” (2024); publications.gc.ca/pub?id=9.506002&sl=0

123. B. W. Griscom, J. Adams, P. W. Ellis, R. A. Houghton, G. Lomax, D. A. Miteva, W. H. Schlesinger, D. Shoch, J. V. Siikamäki, P. Smith, P. Woodbury, C. Zganjar, A. Blackman, J. Campari, R. T. Conant, C. Delgado, P. Elias, T. Gopalakrishna, M. R. Hamsik, M. Herrero, J. Kiesecker, E. Landis, L. Laestadius, S. M. Leavitt, S. Minnemeyer, S. Polasky, P. Potapov, F. E. Putz, J. Sanderman, M. Silvius, E. Wollenberg, J. Fargione, Natural climate solutions. *Proc. Natl. Acad. Sci. U.S.A.* **114**, 11645–11650 (2017). doi:10.1073/pnas.1710465114 Medline

124. H. B. Smith, N. E. Vaughan, J. Forster, Long-term national climate strategies bet on forests and soils to reach net-zero. *Commun. Earth Environ.* **3**, 1–12 (2022). doi:10.1038/s43247-022-00636-x

125. W. S. Walker, S. R. Gorelik, S. C. Cook-Patton, A. Baccini, M. K. Farina, K. K. Solvik, P. W. Ellis, J. Sanderman, R. A. Houghton, S. M. Leavitt, C. R. Schwalm, B. W. Griscom, The global potential for increased storage of carbon on land. *Proc. Natl. Acad. Sci. U.S.A.* **119**, e2111312119 (2022). doi:10.1073/pnas.2111312119 Medline

126. B. K. Haya, S. Evans, L. Brown, J. Bukoski, V. Butsic, B. Cabiyo, R. Jacobson, A. Kerr, M. Potts, D. L. Sanchez, Comprehensive review of carbon quantification by improved forest management offset protocols. *Front. For. Glob. Change* **6**, 2023 | (2023). doi:10.3389/ffgc.2023.958879

127. IPCC, “Summary for Policymakers” in Climate Change 2021: The Physical Science Basis. Contribution of Working Group I to the Sixth Assessment Report of the Intergovernmental Panel on Climate Change, V. Masson-Delmotte, P. Zhai, A. Pirani, S. L. Connors, C. Péan, S. Berger, N. Caud, Y. Chen, L. Goldfarb, M. I. Gomis, M. Huang, K. Leitzell, E. Lonnoy, J. B. R. Matthews, T. K. Maycock, T. Waterfield, O. Yelekçi, R. Yu, B. Zhou, Eds. (Cambridge Univ. Press, 2021), pp. 3–32.

128. S. Smith, O. Geden, G. F. Nemet, M. Gidden, W. F. Lamb, C. Powis, R. Bellamy, M. Callaghan, A. Cowie, E. Cox, S. Fuss, T. Gasser, G. Grassi, J. Greene, S. Lueck, A. Mohan, F. Müller-Hansen, G. Peters, Y. Pratama, T. Repke, K. Riahi, F. Schenuit, J. Steinhauser, J. Strefler, J. M. Valenzuela, J. Minx “The state of carbon dioxide removal” (University of Oxford’s Smith School of Enterprise and the Environment, 2024); https://osf.io/w3b4z/

129. J. Barlow, L. Parry, T. A. Gardner, J. Ferreira, L. E. O. C. Aragão, R. Carmenta, E. Berenguer, I. C. G. Vieira, C. Souza, M. A. Cochrane, The critical importance of considering fire in REDD+ programs. *Biol. Conserv.* **154**, 1–8 (2012). doi:10.1016/j.biocon.2012.03.034

130 Organisation for Economic Cooperation and Development (OECD), “Taming Wildfires in the Context of Climate Change” (OECD, 2023); https://www.oecd-ilibrary.org/environment/taming-wildfires-in-the-context-of-climate-change_dd00c367-en.

131. M. W. Jones, Supplementary Data: Global rise in forest fire emissions linked to climate change in the extratropics, Zenodo (2024); https://doi.org/10.5281/zenodo.10036942.

132. D. van Wees, G. R. van der Werf, J. T. Randerson, B. M. Rogers, Y. Chen, S. Veraverbeke, L. Giglio, D. C. Morton, Model data for "Global biomass burning fuel consumption and emissions at 500-m spatial resolution based on the Global Fire Emissions Database (GFED)," version v2, Zenodo (2024); https://doi.org/10.5281/zenodo.12670427.

133. G. R. van der Werf, J. T. Randerson, L. Giglio, T. T. van Leeuwen, Y. Chen, B. M. Rogers, M. Mu, M. J. E. van Marle, D. C. Morton, G. J. Collatz, R. J. Yokelson, P. S. Kasibhatla, Global fire emissions estimates during 1997–2016. *Earth Syst. Sci. Data* **9**, 697–720 (2017). doi:10.5194/essd-9-697-2017

134. C. DiMiceli, J. Townshend, M. Carroll, R. Sohlberg, Evolution of the representation of global vegetation by vegetation continuous fields. *Remote Sens. Environ.* **254**, 112271 (2021). doi:10.1016/j.rse.2020.112271

135. C. DiMiceli, M. Carroll, R. Sohlberg, D.-H. Kim, M. Kelly, J. Townshend, MOD44B - MODIS/Terra Vegetation Continuous Fields Yearly L3 Global 250m SIN Grid, NASA LP DAAC (2015); http://doi.org/10.5067/MODIS/MOD44B.006.

136. T. Majasalmi, M. Rautiainen, Representation of tree cover in global land cover products: Finland as a case study area. *Environ. Monit. Assess.* **193**, 121 (2021). doi:10.1007/s10661-021-08898-2 Medline

137. P. Potapov, M. C. Hansen, A. Pickens, A. Hernandez-Serna, A. Tyukavina, S. Turubanova, V. Zalles, X. Li, A. Khan, F. Stolle, N. Harris, X.-P. Song, A. Baggett, I. Kommareddy, A. Kommareddy, The Global 2000-2020 Land Cover and Land Use Change Dataset Derived From the Landsat Archive: First Results. *Front. remote sens.* **3** 856903 (2022). doi:10.1016/j.rse.2017.06.027

138. T. J. Hawbaker, M. K. Vanderhoof, Y.-J. Beal, J. D. Takacs, G. L. Schmidt, J. T. Falgout, B. Williams, N. M. Fairaux, M. K. Caldwell, J. J. Picotte, S. M. Howard, S. Stitt, J. L. Dwyer, Mapping burned areas using dense time-series of Landsat data. *Remote Sens. Environ.* **198**, 504–522 (2017). doi:10.1016/j.rse.2017.06.027

139. H. Tatli, M. Türkeş, Climatological evaluation of Haines forest fire weather index over the Mediterranean Basin. *Meteorol. Appl.* **21**, 545–552 (2014). doi:10.1002/met.1367

140. B. E. Potter, Quantitative Evaluation of the Haines Index's Ability to Predict Fire Growth Events. *Atmosphere* **9**, 177 (2018). doi:10.3390/atmos9050177

141. M. N. Ndalila, G. J. Williamson, P. Fox-Hughes, J. Sharples, D. M. J. S. Bowman, Evolution of a pyrocumulonimbus event associated with an extreme wildfire in Tasmania, Australia. *Nat. Hazards Earth Syst. Sci.* **20**, 1497–1511 (2020). doi:10.5194/nhess-20-1497-2020

142. H. Hersbach, B. Bell, P. Berrisford, S. Hirahara, A. Horányi, J. Muñoz-Sabater, J. Nicolas, C. Peubey, R. Radu, D. Schepers, A. Simmons, C. Soci, S. Abdalla, X. Abellan, G. Balsamo, P. Bechtold, G. Biavati, J. Bidlot, M. Bonavita, G. De Chiara, P. Dahlgren, D. Dee, M. Diamantakis, R. Dragani, J. Flemming, R. Forbes, M. Fuentes, A. Geer, L. Haimberger, S. Healy, R. J. Hogan, E. Hólm, M. Janisková, S. Keeley, P. Laloyaux, P. Lopez, C. Lupu, G. Radnoti, P. de Rosnay, I. Rozum, F. Vamborg, S. Villaume, J.-N. Thépaut, The ERA5 global reanalysis. *Q. J. R. Meteorol. Soc.* **146**, 1999–2049 (2020). doi:10.1002/qj.3803

143. Y. Chen, D. M. Romps, J. T. Seeley, S. Veraverbeke, W. J. Riley, Z. A. Mekonnen, J. T. Randerson, Future increases in Arctic lightning and fire risk for permafrost carbon. *Nat. Clim. Chang.* **11**, 404–410 (2021). doi:10.1038/s41558-021-01011-y

144. M. Hutchins, "Worldwide Lightning Location Network 1° Detection Efficiency Maps" (2023); http://wwlln.net/deMaps/.

145. M. Zubkova, L. Boschetti, J. T. Abatzoglou, L. Giglio, , Changes in Fire Activity in Africa from 2002 to 2016 and Their Potential Drivers. *Geophys. Res. Lett.* **46**, 7643–7653 (2019). doi:10.1029/2019GL083469 Medline

146. T. Kitzberger, T. W. Swetnam, T. T. Veblen, Inter-hemispheric synchrony of forest fires and the El Niño-Southern Oscillation. *Glob. Ecol. Biogeogr.* **10**, 315–326 (2001). doi:10.1046/j.1466-822X.2001.00234.x

147. Y. Chen, D. C. Morton, N. Andela, G. R. van der Werf, L. Giglio, J. T. Randerson, A pan-tropical cascade of fire driven by El Niño/Southern Oscillation. *Nat. Clim. Chang.* **7**, 906–911 (2017). doi:10.1038/s41558-017-0014-8

148. R. de Jong, S. de Bruin, A. de Wit, M. E. Schaepman, D. L. Dent, Analysis of monotonic greening and browning trends from global NDVI time-series. *Remote Sens. Environ.* **115**, 692–702 (2011). doi:10.1016/j.rse.2010.10.011

149. R. D. Ottmar, D. V. Sandberg, C. L. Riccardi, S. J. Prichard, An overview of the Fuel Characteristic Classification System — Quantifying, classifying, and creating fuelbeds for resource planning. *Can. J. For. Res.* **37**, 2383–2393 (2007). doi:10.1139/X07-077

150. T. A. P. West, P. M. Fearnside, Brazil's conservation reform and the reduction of deforestation in Amazonia. *Land Use Policy* **100**, 105072 (2021). doi:10.1016/j.landusepol.2020.105072

151. S. Pais, N. Aquilué, J. Campos, Â. Sil, B. Marcos, F. Martínez-Freiría, J. Domínguez, L. Brotons, J. P. Honrado, A. Regos, Mountain farmland protection and fire-smart management jointly reduce fire hazard and enhance biodiversity and carbon sequestration. *Ecosyst. Serv.* **44**, 101143 (2020). doi:10.1016/j.ecoser.2020.101143

152. D. M. J. S. Bowman, J. Balch, P. Artaxo, W. J. Bond, M. A. Cochrane, C. M. D'Antonio, R. Defries, F. H. Johnston, J. E. Keeley, M. A. Krawchuk, C. A. Kull, M. Mack, M. A. Moritz, S. Pyne, C. I. Roos, A. C. Scott, N. S. Sodhi, T. W. Swetnam, R. Whittaker, The human dimension of fire regimes on Earth. *J. Biogeogr.* **38**, 2223–2236 (2011). doi:10.1111/j.1365-2699.2011.02595.x Medline

153. M. Gilbert, G. Nicolas, G. Cinardi, T. P. Van Boeckel, S. O. Vanwambeke, G. R. W. Wint, T. P. Robinson, Global distribution data for cattle, buffaloes, horses, sheep, goats, pigs, chickens and ducks in 2010. *Sci. Data* **5**, 180227 (2018). doi:10.1038/sdata.2018.227 Medline

154. Eurostat, "Glossary: Livestock unit (LSU)" (2023); https://ec.europa.eu/eurostat/statistics-explained/index.php?title=Glossary:Livestock_unit_(LSU).

155. P. Vogt, K. Riitters, P. Rambaud, R. d'Annunzio, E. Lindquist, A. Pekkarinen, GuidosToolbox Workbench: Spatial analysis of raster maps for ecological applications. *Ecography* **2022**, e05864 (2022). doi:10.1111/ecog.05864

156. Joint Research Centre (European Commission), P. Vogt, K. Riitters, G. Caudullo, B. Eckhardt, “FAO, State of the World’s Forests” (EU Publications Office, 2019); https://data.europa.eu/doi/10.2760/145325.

157. L. Teckentrup, S. P. Harrison, S. Hantson, A. Heil, J. R. Melton, M. Forrest, F. Li, C. Yue, A. Arneth, T. Hickler, S. Sitch, G. Lasslop, Response of simulated burned area to historical changes in environmental and anthropogenic factors: A comparison of seven fire models. *Biogeosciences* **16**, 3883–3910 (2019). doi:10.5194/bg-16-3883-2019

158. E. Doxsey-Whitfield, K. MacManus, S. B. Adamo, L. Pistolesi, J. Squires, O. Borkovska, S. R. Baptista, Taking Advantage of the Improved Availability of Census Data: A First Look at the Gridded Population of the World, Version 4. *Pap. Appl. Geogr.* **1**, 226–234 (2015). doi:10.1080/23754931.2015.1014272

159. D. Nepstad, G. Carvalho, A. Cristina Barros, A. Alencar, J. Paulo Capobianco, J. Bishop, P. Moutinho, P. Lefebvre, U. Lopes Silva Jr., E. Prins, Road paving, fire regime feedbacks, and the future of Amazon forests. *For. Ecol. Manage.* **154**, 395–407 (2001). doi:10.1016/S0378-1127(01)00511-4

160. F. X. Catry, F. C. Rego, F. L. Bação, F. Moreira, Modeling and mapping wildfire ignition risk in Portugal. *Int. J. Wildland Fire* **18**, 921–931 (2009). doi:10.1071/WF07123

161. G. Narayanaraj, M. C. Wimberly, Influences of forest roads on the spatial pattern of wildfire boundaries. *Int. J. Wildland Fire* **20**, 792 (2011). doi:10.1071/WF10032

162. R. A. Bradstock, K. A. Hammill, L. Collins, O. Price, Effects of weather, fuel and terrain on fire severity in topographically diverse landscapes of south-eastern Australia. *Landsc. Ecol.* **25**, 607–619 (2010). doi:10.1007/s10980-009-9443-8

163. G. J. Cary, R. E. Keane, R. H. Gardner, S. Lavorel, M. D. Flannigan, I. D. Davies, C. Li, J. M. Lenihan, T. S. Rupp, F. Mouillot, Comparison of the Sensitivity of Landscape-fire-succession Models to Variation in Terrain, Fuel Pattern, Climate and Weather. *Landsc. Ecol.* **21**, 121–137 (2006). doi:10.1007/s10980-005-7302-9

164. J. J. Sharples, R. H. D. McRae, S. R. Wilkes, Wind–terrain effects on the propagation of wildfires in rugged terrain: Fire channelling. *Int. J. Wildland Fire* **21**, 282–296 (2012). doi:10.1071/WF10055

165. R. Durão, C. Alonso, C. Gouveia, The Performance of ECMWF Ensemble Prediction System for European Extreme Fires: Portugal/Monchique in 2018. *Atmosphere* **13**, 1239 (2022). doi:10.3390/atmos13081239

166. A. Huete, C. Justice, W. Van Leeuwen, “MODIS VEGETATION INDEX (MOD 13) ALGORITHM THEORETICAL BASIS DOCUMENT”, version 3, (1999); https://modis.gsfc.nasa.gov/data/atbd/atbd_mod13.pdf.

167. M. L. Hutchins, R. H. Holzworth, C. J. Rodger, J. B. Brundell, Far-Field Power of Lightning Strokes as Measured by the World Wide Lightning Location Network. *AMS* **29**, 1102–1110 (2012). doi:10.1175/JTECH-D-11-00174.1.

168. J. O. Kaplan, K. H.-K. Lau, The WGLC global gridded lightning climatology and time series. *Earth Syst. Sci. Data* **13**, 3219–3237 (2021). doi:10.5194/essd-13-3219-2021

169. M. Li, P. Wu, Z. Ma, A comprehensive evaluation of soil moisture and soil temperature from third-generation atmospheric and land reanalysis data sets. *RMetS* **40**, 5744–5766 (2020). doi:10.1002/joc.6549

170. A. Strahler, D. Muchoney, J. Borak, M. Friedl, S. Gopal, E. Lambin, A. Moody, MODIS Land Cover Product, Algorithm Theoretical Basis, Document (ATBD), Version 5.0, NASA (1999); https://modis.gsfc.nasa.gov/data/atbd/atbd_mod12.pdf.

171. E. Chuvieco, F. Mouillot, G. R. van der Werf, J. San Miguel, M. Tanase, N. Koutsias, M. García, M. Yebra, M. Padilla, I. Gitas, A. Heil, T. J. Hawbaker, L. Giglio, Historical background and current developments for mapping burned area from satellite Earth observation. *Remote Sens. Environ.* **225**, 45–64 (2019). doi:10.1016/j.rse.2019.02.013

172. G. R. van der Werf, J. T. Randerson, L. Giglio, G. J. Collatz, M. Mu, P. S. Kasibhatla, D. C. Morton, R. S. DeFries, Y. Jin, T. T. van Leeuwen, Global fire emissions and the contribution of deforestation, savanna, forest, agricultural, and peat fires (1997–2009). *Atmos. Chem. Phys.* **10**, 11707–11735 (2010). doi:10.5194/acp-10-11707-2010

173. T. T. van Leeuwen, G. R. van der Werf, A. A. Hoffmann, R. G. Detmers, G. Rücker, N. H. F. French, S. Archibald, J. A. Carvalho Jr., G. D. Cook, W. J. de Groot, C. Hély, E. S. Kasischke, S. Kloster, J. L. McCarty, M. L. Pettinari, P. Savadogo, E. C. Alvarado, L. Boschetti, S. Manuri, C. P. Meyer, F. Siegert, L. A. Trollope, W. S. W. Trollope, Biomass burning fuel consumption rates: A field measurement database. *Biogeosciences* **11**, 7305–7329 (2014). doi:10.5194/bg-11-7305-2014

174. J. T. Randerson, Y. Chen, G. R. van der Werf, B. M. Rogers, D. C. Morton, Global burned area and biomass burning emissions from small fires: BURNED AREA FROM SMALL FIRES. *J. Geophys. Res.* **117**, G04012 (2012). doi:10.1029/2012JG002128

175. D. van Wees, G. R. van der Werf, Modelling biomass burning emissions and the effect of spatial resolution: A case study for Africa based on the Global Fire Emissions Database (GFED). *Geosci. Model Dev.* **12**, 4681–4703 (2019). doi:10.5194/gmd-12-4681-2019

176. S. Veraverbeke, B. M. Rogers, J. T. Randerson, Daily burned area and carbon emissions from boreal fires in Alaska. *Biogeosciences* **12**, 3579–3601 (2015). doi:10.5194/bg-12-3579-2015

177. N. Andela, G. R. van der Werf, J. W. Kaiser, T. T. van Leeuwen, M. J. Wooster, C. E. R. Lehmann, Biomass burning fuel consumption dynamics in the tropics and subtropics assessed from satellite. *Biogeosciences* **13**, 3717–3734 (2016). doi:10.5194/bg-13-3717-2016

178. M. Charrad, N. Ghazzali, V. Boiteau, A. Niknafs, NbClust: An R Package for Determining the Relevant Number of Clusters in a Data Set. *J. Stat. Softw.* **61**, 1–36 (2014). doi:10.18637/jss.v061.i06

179. J. Lizundia-Loiola, M. L. Pettinari, E. Chuvieco, Temporal Anomalies in Burned Area Trends: Satellite Estimations of the Amazonian 2019 Fire Crisis. *Remote Sens. (Basel)* **12**, 151 (2020). doi:10.3390/rs12010151

180. M. Tabarelli, L. P. Pinto, J. M. C. Silva, M. Hirota, L. Bede, Challenges and Opportunities for Biodiversity Conservation in the Brazilian Atlantic Forest. *Conserv. Biol.* **19**, 695–700 (2005). doi:10.1111/j.1523-1739.2005.00694.x